MAGMATIC EVOLUTION OF THE WESTERN PANAMANIAN ARC

By

Paulo Hidalgo

A DISSERTATION

Submitted to
Michigan State University
in partial fulfillment of the requirements
for the degree of

DOCTOR OF PHILOSOPHY

Geological Sciences

2012

ABSTRACT

MaGMATIC EVOLUTION OF THE WESTERN PANAMANIAN ARC

By

Paulo Hidalgo

The Panamanian arc exhibits a swift transition from calc-alkaline to adakitic magmatism during the Quaternary. This transition has important implications for magma generation processes in the region. Specifically, are adakite magmas derived from slab melting during subduction, or to volatile fluxing of the mantle wedge? At Baru and El Valle volcanoes, we have used a robust geochronological and geochemical dataset to examine processes that are responsible for the generation of magmas from the Miocene to present. Our results show that both of these volcanic edifices were constructed over timescales consistent with typical arc volcanoes - much faster than slab melt derived volcanic edifices. The magma production rates necessary to account for Quaternary magmatism in Panama are difficult to achieve via slab melting processes alone. Here we present a model whereby typical calc-alkaline magmas can acquire an adakitic signal through crystal fractionation processes in the lithosphere. The water content of arc magmas is a critical control of the fractionating assemblage. At moderate pressures, high magmatic water contents promote amphibole stability and fractionation paths that yield normal island arc magmas. With decreasing water contents garnet becomes stable at the expense

of amphibole, yielding an adakitic magmatic signature. We have recorded such a drop in water content by using mass balance calculations and forward modeling of our geochemical dataset. Despite the lower modeled water contents of magmas during the Quaternary adakitic phase, these magma water contents are significantly elevated in comparison to magmas generated by slab melting processes. Our results support previous studies suggesting that some adakites may be produced by fractional crystallization of amphibole and garnet. This model is consistent with amphibole-rich cumulates observed in lavas throughout the region. We show that in arcs with moderate crustal thicknesses, variations in magma water content may be the primary variable controlling shifts in magma composition from typical calc-alkaline towards adakitic.

to Nidal and Zaila my strengths

ACKNOWLEDGEMENTS

I will like to thank my advisor Dr. Tyrone Rooney for his advice and guidance throughout program. I will also thank Lina Patino and Tom Vogel for their advice and patient revisions. Special gratitude to Lepolt Linkimer and Ryan Currier for being an important friends and colleagues who played an important role during my graduate studies. Collaboration during the laboratory work given by Carl Henderson, Dave Szymanski and Chris Hall was invaluable. Eternal gratitude goes to Angel Rodriguez and Carla Black for their inconditional support during the field season.

TABLE OF CONTENTS

LIST OF TABLES

LIST OF FIGURES

CHAPTER 2:

CHAPTER 3:

CHAPTER 4:

CHAPTER ONE INTRODUCTION

Subduction zones constitute environments where the exchange of mantle and crustal material is possible. This exchange plays a central role in the evolution of the continental crust and the Earth's mantle. The mantle and crustal components of this exchange are the subducting oceanic crust (and overlying sediment) along with the peridiotites within the mantle wedge. This process initiates when fluids from the dewatering subducted sediments and hydrothermally metamorphosed crustal materials are fluxed in to mantle rocks triggering melting (Davies and Stevenson 1992; Forneris and Holloway 2003; Grove, et al. 2002; Schmidt and Poli 1998; Tatsumi and Eggins 1995; Ulmer 2001). This process may be aided by mantle decompression from subduction induced corner flow in the mantle wedge (Elkins-Tanton, et al. 2001; Hasegawa and Nakajima 2004; Sisson and Bronto 1998). The resulting primary magmas are subsequently transferred in to the overlying crust where AFC (Assimilation, Fractional Crystallization) (DePaolo 1981) and mixing processes are responsible for the chemical variety observed on island arcs. AFC and mixing processes can take place in a variety of settings:

- Crystallization in shallow crustal magma chambers (e.g. Grove, et al. 1997; Pichavant, et al. 2002; Sisson and Grove 1993).
- Crystallization in the deep arc crust close to the Moho (e.g. Annen and Sparks 2002; Müntener, et al. 2001; Prouteau and Scaillet 2003).

- Crustal assimilation (cumulates) during fractionation (e.g. Jackson, et al. 2003; Petford and Atherton 1996; Smith and Leeman 1987b).

While the mantle melting model is broadly successful in accounting for most of the observed variety in island arcs, it has been suggested that melting of a subducting slab might be an important magma source (Clark 1989; de Boer, et al. 1991; Defant, et al. 2002; Defant 1990; Defant, et al. 1991a; Defant, et al. 1991b; Drummond and Defant 1989; Drummond and Defant 1990). Melting of the subducted slab in subduction zones will imprint the resulting magma (termed adakites) with high SiO_2 (>56 wt.%), high Al_2O_3 (>15%), low MgO (<3%), high Sr (>300 ppm), no Eu anomaly, Low Y(<15 ppm), high Sr/Y (>20), low Yb (<1.9 ppm), high La/Yb (>20), low HFSEs (Nb, Ta), and isotopic signatures similar to MORBS (Castillo 2006; Defant 1990). These chemical signatures (specially heavy rare element depletions) are closely associated with garnet fractionation in the deep in the arc crust, within the garnet stability field. The term adakite has been controversial as this geochemically defined rock type was also synonymous with a particular petrogenetic process – namely melting of the subducting slab. Subsequent studies have shown that adakitic signature may be derived from numerous processes:

- Partial melting of the underplated basaltic lower crust (Rapp, et al. 2002) or delaminated lower crust (Macpherson 2008; Xu, et al. 2002).
- Melting of underplated basalt at the base of a tectonically thickened crust (Atherton and Petford 1993; Kay and Kay 2002).

- Assimilation and crystallization processes of basaltic magma under high pressure (Castillo, et al. 1999).
- Transport of elements not typically thought of as fluid-mobile by super-critical fluids may yield adakite-like trace-element patterns (Kessel, et al. 2005).

In some island arcs (e.g. East Phillipines Arc, Eastern Central American arc, Izu-Bonin, Aleutian, etc), periods of “typical” calc-alkaline arc magmatism swiftly transition to periods of adakitic volcanism (Defant, Clark, Stewart, Drummond, de Boer, Maury, Bellon, Jackson and Restrepo 1991a; Defant, Richerson, Deboer, Stewart, Maury, Bellon, Drummond, Feigenson and Jackson 1991b; Drummond, et al. 1995; Hidalgo, et al. 2012.; Macpherson 2008; Macpherson, et al. 2006; Pearce, et al. 1992; Yogodzinski and Kelemen 1998). The transition between periods of typical island arc and adakitic volcanism is an important observation that has significant consequences for the thermal state of subduction zones and it needs to be addressed when modeling magmatic fluxes on any island arc.

The central hypothesis of my project was that fluctuations in the thickness of the Panamanian arc lithosphere throughout the history of the margin, might be controlling the spatial and temporal variation in magma fluxes in to the arc crust and hence, the chemical composition of the resulting magmas. In other words, the transition from “typical” arc to adakitic magmatism would be an important indicator of lithosphere thickening and may not relate to melting in the subducted slab. In the case that the hypothesis is correct, the occurrence of adakites would be correlated to intermediate to mature stages in the island arc development, where high pressure fractionation processes are possible (i.e. within the garnet stability field) either on the lower lithosphere or as described by Stratford and Stern (2004) on the upper mantle.

The hypothesis stated that melting of the subducting oceanic crust is not responsible for the generation of the adakite signature in the Panamanian arc. We hypothesize that the adakitic signature is derived from garnet fractionation in the lower crust. However, most models for the origin of adakites in southern Central America have invocated slab-melting processes (Abratis and Worner 2001; Defant, et al. 1992). Hoernle et al. (2008a) has explained the transport of the Galapagos plume signature from Southern Costa Rica to Southern Nicaragua by invoking a ‘melt-like slab component’ from the Galapagos track. This ‘melt-like slab component’ has reacted with overlying peridiotite forming pyroxenites that are later transported northwards beneath the arc by mantle flow. One of the seminal papers for adakite generation by Drummond and Defant (1989) explains that the adakite signature is derived from residual garnet in the subducting slab. These authors inferred that the Panamanian crust will be too thin for garnet to be a stable fractionating phase, and the only other possibility is that garnet conforms a restite in the subducting eclogitized oceanic crust. Recent experimental work has substantially revised the estimates for garnet stability; water saturated melts may now produce and fractionate igneous garnet at pressure and temperature ranges expected in the Panama arc (e.g. Alonso-Perez, et al. 2009), removing the requirement that the garnet signature must have been derived from the eclogitized subducting slab.

The main goal of my research project is to determine the circumstances that allow for a transition from typical arc magmas to the adakitic signature, at Baru volcano.

With this goal in mind my dissertation addresses three key questions about the magma generation processes in the region:

1. What is the roll of the ubiquitous crustal cumulates nodules found at Baru volcano?

The second chapter of this dissertation explores the roll of crustal cumulate nodules in the magmatic evolution of Baru volcano. Quaternary magmas at Baru volcano in Panama contain ubiquitous amphibole-bearing cumulates that provide an opportunity to probe the magma plumbing system of an active arc volcano. We have determined that these cumulates are related to their host magmas by crystal fractionation processes. Pressure and temperature estimates for amphiboles within these cumulates and the host rock are consistent with sampling of mush/magma zones from throughout the arc crust. Our results highlight the importance of amphibole fractionation in the differentiation sequence of island arcs.

2. Can the rates of magma formation, transfer, storage and eruption beneath arc volcanoes place constrains on the physical processes responsible for the generation of adakites?

In chapter 3, we combine detailed stratigraphy, $^{40}Ar/^{39}Ar$ dating , and geochemistry and we show that the entire volcanic edifice at Baru volcano is constructed from magmas with adakite-like compositions. In addition, the volume of volcanism at Baru is substantial (~450 km^3) and comparable to other arc volcanoes such as Mt. Shasta or Irazu. We also have determined that most of the volcanic edifice of Baru volcano was constructed extremely rapidly (less than ~213 k.a.) in comparison to other typical adakitic volcanoes (Adagdak and Cook), but in time frames that have been observed in typical arc volcanoes. All of these observations are hard to reconcile with the lower volumes expected to be derived from slab melting alone. Our approach provides a method to discriminate melting of the subducting slab adakites from adakites that have been generated by high-pressure fractionation processes.

3. Can the nature of the mantle and the fluid component provide insights into the generation of adakites?

In the fourth chapter of this dissertation, I combine the observations and the knowledge that I have gain in previous chapters with new geochemical and geochronological analyses of the Miocene- Quaternary transition at Baru volcano. I show that (1) the mantle source that generated the Miocene to Quaternary magmas has been modified throughout this temporal transition (2) that the Miocene rocks from the 10-9 Ma period at Baru volcano were derived from water rich basalts produced by large degrees of melting (3) that the abundant melts from this transitional period may have stalled at the Panamanian lower crust to form abundant amphibole rich cumulates (4) that the transition from typical arc volcanism (10-9 Ma) to adakite volcanism (Quaternary) is the product of reduced hydrous fluids andcrustal thickening processes that allowed for garnet to be a stable phase in the Panamanian sub arc lithosphere.

This contribution will add vital temporal and geochemical components to the existing debate over the generation of adakites, question the proposed models of magmatic evolution for the region and provide a model of adakite generation that might be widely applicable.

CHAPTER TWO CRYSTAL FRACTIONATION PROCESSES AT BARU VOLCANO FROM THE DEEP TO SHALLOW CRUST

1. INTRODUCTION

The study of magmatic processes is generally constrained to the shallowest parts of the plumbing system of any given arc volcano, with only few studies that address mid- to lower crustal processes (e.g. Beard, 1986; Cigolini et al., 2008; DeBari and Coleman, 1989). Correlating shallow, deep, and upper mantle processes at volcanic arcs has been an important goal for generating a fuller understanding of the growth and evolution of the continental crust (Davidson et al., 2005). *Rudnick and Fountain* (1995) and *Rudnick and Gao* (2005) estimated that the average composition of the continental crust is andesitic to dacitic, emphasizing that the crust is stratified: mafic rocks (or melts) at the base of the crust and andesitic or dacitic-like rocks concentrated in the upper crust. This crustal stratification has been supported by geological evidence observed in arc terranes where mafic rocks are abundant in exposed lower crustal sections (Dhuime et al., 2007; Jagoutz et al., 2006).

Crystal cumulates are compelling evidence of fractionation processes at active arcs (e.g. Chiaradia et al., 2009). The importance of these cumulates cannot be underestimated, as mass balance models predict that their volume should be roughly twice the volume of derivative intermediate to silicic magmas that are either erupted or stall on their path to the surface (Foden and Green, 1992; Müntener, 2001). Hence, several authors have proposed that crystal ‘mushes’ at the roots of an arc volcano are the magmatic reservoirs responsible for the generation of large volumes of evolved magmas (Bachmann and Bergantz, 2004; Deering et al., 2010; Sisson and Bacon, 1999). Such crystal ‘mushes’ are rarely erupted. However, in unusual circumstances they may be transported as cumulates to shallow crustal levels. Commonly in arcs, these cumulates are best represented by two major groups: gabbroic cumulates or olivine gabbros (calcic plagioclase and Fe-rich olivine) and amphibole rich cumulates (hornblende gabbros). The occurrence of these cumulates and their mafic assemblage is the most solid evidence supporting crystal fractionation as a major process contributing to the generation of intermediate to silicic magmas at arcs (DeBari and Coleman, 1989; Müntener, 2001). Olivine gabbros and gabbronorites are by far the most common types of arc cumulates, and are observed in a great number of oceanic arcs from Japan (Aoki and Kuno, 1972; Yamamoto, 1988), Lesser Antilles (Arculus and Wills, 1980), Izu-Bonin (Tatsumi et al., 2008), Philippines (Newhall, 1979), Aleutians (Kay and Kay, 1985), Central America (Walker, 1984), to New Guinea (Gust and Johnson, 1981). Amphibole-rich cumulates (amphibole gabbros), are less common and have been described only at a limited number of active oceanic arc localities in New Guinea (Gust and Johnson, 1981), Aleutians (Debari et al., 1987), and Panama (Hidalgo, 2007; Rooney et al., 2010a).

The role of a mid- to lower crustal amphibole fractionation from hydrous magmas has been recognized by some researchers as an important component in the evolution of magmatism and recycling in volcanic arcs (Allen and Boettcher, 1983; Boettcher, 1973, 1977; Davidson et al., 2007). Despite being generally absent as a phenocryst phase in arc-related volcanic rocks, the geochemical signature of amphibole fractionation is pervasive in most arcs (decreasing Dy/Yb with fractionation indices, Davidson et al., 2007). Arc terranes that have been exhumed (e.g., Alaska, Kohistan arc, Bonanza arc) commonly contain amphibole-bearing cumulates and these illustrate the important role of amphibole in the sub-arc crust. Amphibole in these hydrous cumulates is typically reported as an intercumulus phase that developed as magma conditions evolved towards lower temperature and higher water content (Bachmann et al., 2002). Most studies in these terranes have concluded that the intercumulus crystallization of amphibole from hydrous magmas has controlled the compositions of derivative liquids until the onset of plagioclase crystallization (DeBari and Coleman, 1989; Greene et al., 2006; Jagoutz, 2010; Jan and Howie, 1981). In active arcs, amphibole-bearing cumulate xenoliths may be the only available window into mid- to lower crustal processes.

The Quaternary magmas at Baru volcano in Panama contain ubiquitous amphibole-bearing cumulates that provide an opportunity to probe the magma plumbing system of an active arc volcano. In this study, we use amphibole compositions from crystals hosted in the most recent products of Baru volcanism along with whole rock major and trace element analyses to evaluate Baru volcano magma differentiation processes. The advantage of using the amphibole chemistry is its sensitivity to both pressure and temperature. Moreover, amphibole is an ideal phase to study magmatic evolution due to its early appearance in the calc-alkaline liquidus in hydrous magmas

(Alonso-Perez et al., 2009; Carmichael, 2002). Our relative pressure and temperature estimates help to elucidate the nature of the Panamanian sub-arc crust and aid in the study of the magma plumbing system of Baru volcano showing that the magmatic evolution may be closely related to deep differentiation processes in hot zones within the sub-arc crust. Our detailed study may have broader application –in so far as these amphibole-rich cumulates are not exclusive to Baru volcano and have been identified in other regions of the Panamanian arc (e.g. Quaternary volcanism at El Valle, Oligocene sequence at the Panama Canal) (Hidalgo, 2007; Rooney et al., 2010a). The widespread presence of amphibole-rich cumulates in Panamanian magmas allows for the study of a regional amphibole rich layer within the arc crust that originated most likely by stalling and fractionating mantle derived water-rich magmas.

2. STUDY AREA AND TECTONIC SETTING

Baru volcano is located in Western Panama, 35 km east of the Costa Rica – Panama border at the terminus of the Talamanca Cordillera. The summit of the volcano at 3,374 m, overlooks populated valleys 2,000 m below (Figure 2.1). Despite being dormant for the last 400 years, Baru volcano is active, with at least four eruptive episodes in the last 1,600 years and several others in the prior 10,000 years (Sherrod et al., 2007). The volcanic edifice has been constructed by numerous eruptions. *Sherrod et al.* (2007) estimated that the last period of abundant lava flows (last 11,500 yr) is presumed to have formed the large andesitic-dacitic dome sequence located at the summit.

Tectonically, Baru volcano is situated at the southern end of the Central American Volcanic Arc (CAVA) (Figure 2.1). This section of crust was first described by *Kellogg et al.* (1995) as the Panama block and is moving northward relative to the Caribbean plate and eastward relative to the South American plate (Kellogg et al., 1985). The northern boundary of the Panama Block is the North Panama Deformed Belt (NPDB) characterized by the southward subduction of the Caribbean Plate (Camacho et al., 2010; Kellogg et al., 1985). The NPDB crosses Costa Rica on a westward trend to meet the Middle America Trench in a Caribbean Plate-Cocos Plate-Panama Block triple junction (Bird, 2003; Mann and Kolarsky, 1995). The eastern limit of the Panama Block is the Panama-Colombia suture zone (collision zone), and has been described extensively by *Mann and Kolarsky* (1995). The southern boundary of the Panama block is the Panamanian Trench (or Southern Panama Deformed Belt). This boundary is complex; it changes character eastward from oblique subduction (between 83˚W–80.5˚W) of the Nazca plate (V=5cm/yr, Jarrard, 1986; Trenkamp et al., 2002) to a sinistral strike-slip fault (80˚W to 78.8˚W, Westbrook et al., 1995). Volcanism at Baru is interpreted to result from the subduction of the Nazca Plate under the Panama Block (Figure 1.1).

The material entering the Middle America Trench outboard of Panama has been derived from diverse sources including: East Pacific Rise (Barckhausen et al., 2001; Meschede et al., 1998), Cocos Nazca spreading centers (Barckhausen et al., 2001), Sandra Rift (Lonsdale, 2005) and Galapagos hot spot tracks. The Galapagos hot spot tracks are perhaps the most conspicuous features on the subducting Cocos and Nazca plates, best represented by the aseismic Cocos and Coiba ridges. These ridges are over-thickened sections of oceanic crust, that stand ~2 km above the surrounding ocean floor (Walther, 2003) and are interpreted to be colliding with the Middle American Trench (Lonsdale and Klitgord, 1978). The existing evidence suggests that the interaction of the Cocos and Coiba ridges with the Middle America Trench has a profound impact on the overriding plate, yielding compressive crustal stress conditions quite different from regions of ‘normal’ subduction. The timing of the exact arrival of the Cocos and Coiba Ridges at the Middle America Trench remains highly controversial and ranges from ~8 ma to ~1 Ma (Abratis and Worner, 2001; Collins et al., 1995; de Boer et al., 1995; Gardner et al., 1992; Morell et al., 2008).

3. FIELD AND PETROGRAPHIC OBSERVATIONS

The regional basement in western Panama is commonly referred to as an over thickened section of the lithosphere composed of oceanic assemblages (21 Ma to 71 Ma, Hoernle et al., 2002). This local basement is part of the Caribbean Large Igneous Province (CLIP), which is related to Galapagos hot spot; these assemblages are referred to as the Azuero-Soná Complex. The CLIP is exposed in the Azuero and Soná peninsulas, and various islands of the Chiriquí and Montijo gulfs (Denyer et al., 2006). The thickness of crust is unknown in the mountainous region of western Panama, but is likely thicker than the crust in the Panama Canal region, estimated at ~25 km (Briceno-Guarupe, 1978).

In other sections of the Central American Arc, Oligocene and Miocene arc sequences lie behind the currently active arc front (i.e. Costa Rican arc) (Carr et al., 2003; Gazel et al., 2009). At Baru volcano, the Miocene and modern arc products largely overlap. This feature makes Baru volcano a key location to study the temporal evolution of the arc in order to understand the arc initiation and the closure of the Isthmus of Panama. The subdivision of magmatism into two temporal groups simplifies the discussion of the stratigraphy of Baru volcano. The first group constitutes most of the volcanic edifice and is composed of pyroclastic flows, lava flows and lahar deposits (Sherrod et al., 2007). This unit represents about 60-70% of the total erupted volume. None of the rocks in the lower part of the sequence have been dated, however these deposits are attributed to the voluminous effusive activity during the late Miocene (de Boer et al., 1991; Drummond et al., 1995) and are the subject of ongoing research. The second group (that is directly addressed here) is composed of the products of Quaternary volcanism at Baru and is represented by at least two sub-units. The first is the Summit Domes unit that is composed mainly of hornblende bearing andesites and dacites (Rausch, 2008; Sherrod et al., 2007). The second Quaternary unit at the top of the sequence is characterized by fallout tephras and pyroclastic flow deposits. Dated samples from this unit yielded an age of 950 yr B.P. and 855 yr B.P respectively (Sherrod et al., 2007). The pumice block chemistry indicates that the composition varies from andesitic to dacitic. The Quaternary units have textural characteristics that suggest magma mingling/mixing at macro scale, but routine microscope work revealed that these textures are produced by fined grained and coarse grained cumulates hosted within both of the Quaternary units (Figure 2.2).

The present study focuses on the Quaternary units that bear abundant hornblende gabbro cumulates. Petrographically, the host andesite that contains these cumulates is crystal rich in the Summit Dome unit (up to 55%), but crystal poor (15%) in the Ash Flow unit. The mineralogy of the host magmas is dominated by plagioclase and zoned amphiboles with small amounts of Fe-Ti oxides and trace contents of sphene. Some plagioclase crystals have nucleated on resorbed and small quartz crystals (~0.3 mm) and in some cases crystallites of amphibole are observed in the plagioclase cores. Furthermore, some plagioclase crystals have convoluted and irregular zoning patterns and resorbed cores, while some of the largest amphiboles have orthopyroxene cores.

Texturally, cumulates can be organized in two groups, Fine Grained cumulates (Figures 2.2A-C and 2.3A) and Coarse Grained cumulates (Figures 2.2D-F, 2.3B-D). These cumulates occur in both host units (Ash Flow unit and Summit Domes unit) but are better preserved in the Summit Domes unit. None of the cumulate groups present chilled margins at the contact with the andesitic host. Fine Grained cumulates generally form large nodules (5-10 cm) that are composed of variable proportions of amphibole (acicular in some instances) and plagioclase phenocrysts and microlites along with minor interstitial glass. Some of the Fine Grained cumulates are amphibole rich (80% amphibole, 5% plagioclase, Fe-Ti oxides and interstitial glass) while some of them are plagioclase rich with little amphibole (90% plagioclase, some amphibole, interstitial glass and Fe-Ti oxides) (Figure 2.3A). The larger size Coarse Grained cumulates are more complex and can be further subdivided in two groups. The most common group forms 2-5 cm nodules of amphibole megacrysts (3-6 mm) with minor (<2%) interstitial glass. In some cases these cumulates contain anhedral plagioclase and apatite phenocrysts (~0.5 mm) in the interstices (Figure 2.3B). Less widespread is the second group within the Coarse Grained cumulates. This group of cumulates are composed of orthopyroxene and olivine crystals (Fo~80) that are surrounded by amphibole-dominated reaction rims that in some cases extend through fractures inside the cumulates (Figure 2.3D). Olivine ghosts and orthopyroxene crystals that have almost completely reacted to form amphibole are also observed.

4. ANALYTICAL TECHNIQUES

Major and trace element concentrations for the host lavas and the cumulates were determined by X-ray fluorescence (XRF) and Laser Ablation Inductively Coupled Plasma Mass Spectrometry (LA-ICP-MS) analyses at Michigan State University using fused glass disks of previously powdered samples. The procedure followed the outline described in *Hannah et al.* (2002) and *Deering et al.* (2008) for the preparation of low-dilution fusion glass disks (LDF). The fused disks were analyzed using a Bruker Pioneer S4 X-Ray fluorescent spectrograph. XRF element analyses were reduced using Bruker Spectra Plus software®, which uses fundamental parameters (Criss, 1980).

For LA-ICP-MS trace element analyses, a Cetac+ LSX200 laser ablation system coupled with a Micromass Platform ICP-MS was used. The Cetac® LSX-200+ is a Nd:YAG laser with a frequency quadrupled to an UV wavelength of 266nm. The analyses involved continuous ablation (line scan) for approximately three minutes. Strontium, determined by XRF, was used as an internal standard to correct for variations in ablated sample volume and instrument response. Trace element data reduction was done using MassLynx® software. Prior to any calculations, the background signal from the argon plasma was subtracted from each of the standards and samples. Element concentrations in the samples were calculated based on a linear regression method using BHVO, W-2, JB-1, JB-2, JB-3, JA-2, JA-3, BIR, QLO-1, and RGM-1 standards. Only standards with calculated values within 15% of the preferred standard values were used in the final calibration line for samples. Precision and accuracy of both the XRF and LA-ICP-MS chemical analyses have been reported in *Vogel et al.* (2006). Trace element reproducibility based on standard analyses is typically better than 5%.

Hornblende and plagioclase compositions were determined using a Cameca SX100 electron microprobe at the University of Michigan equipped with five wavelength spectrometers, using an accelerating potential of 15 kV, a focused beam with a 10 μm spot size, counting time of ~3 min per mineral, and a 10 nA beam current. Standards used were natural fluor-topaz (FTOP), natural jadeite (JD-1), natural grossular, Quebec (GROS), natural adularia, St. Gothard, Switzerland (GKFS), synthetic apatite (BACL), synthetic Cr_2O_3, and synthetic $FeSiO_3$ (FESI). Amphiboles typically average ~2 wt.% of

(H_2O + F +Cl); therefore, only analyses with anhydrous totals (SiO_2, Al_2O_3, FeO_{tot}, MgO, CaO, Na_2O, K_2O, TiO_2, MnO) of 98±1 wt. % were retained. For glass analyses (intercumulate glass and pumice samples) a 10 µm defocused beam and 5 nA beam current was used. In order to minimize Na migration during glass analyses, the count rate of Na was scanned through time and corrected using a built-in procedure (Devine, 1995).

5. NATURE OF THE HOST AND CUMULATES

Average compositions and standard deviations of major- and trace-elements are provided in Table 2.1 for the host and the cumulates. The complete geochemical analyses are presented in the online supplementary material. Samples with totals lower than 96% are excluded from the discussion because it was assumed that these samples were altered. In the figures all the major elements have been normalized to 100%.

5.1 Host

The host magmas consist of the Ash Flow unit and the Summit Domes unit. These two units are metaluminous calcalkaline andesites, with a few samples extending in to the dacite field. The host units generally present little variation in most of the major and trace elements (Figures 2.4, 2.5 and 2.6). The Ash Flow unit is slightly less evolved than the Summit Domes unit and extends to lower SiO_2, K_2O, Na_2O and higher contents of MgO, CaO, TiO_2, Fe_2O_3T (Table 2.1, Figures 2.4 and 2.5). Despite these differences, trace element variation between these two units is negligible which is consistent with a similar source for both of these deposits (Table 2.1, Figures 2.6 and 2.7). The differences observed in major elements between these deposits can be explained by the inability during the sample preparation process to separate hornblende rich Fine Grained cumulates from Ash Flow unit pumice blocks (host), which overall made this unit more mafic. Detailed microscope work on the most evolved samples of the Ash Flow unit revealed that they are entirely free of entrained cumulate material, while the most mafic samples have incorporated portions of Fine Grained cumulates. In addition, Fine Grained cumulates and small Coarse Grained cumulates could not be separated from a small group of samples (8 samples) from the Summit dome unit. These samples are relatively more enriched in MREE and HREE than the typical host (Figure 2.7b).

The trace element trends observed in the Quaternary magmatism are typical of island-arcs with pronounced depletions in Nb and Ta and enrichment of large ion lithophile elements (LILE) over the more immobile high field strength elements (HFSE). The small variations observed in trace elements between the host units suggest a similar source (Figure 2.7). Both of the host magmas have depleted heavy rare earth elements (HREE), low Y, high Sr, high Sr/Y, low K_2O / Na_2O (Figure 2.7). These are typical of adakite-like volcanism (Figure 2.8). This type of volcanism has been identified in the Quaternary activity of Panamanian arc (e.g. La Yeguada volcano, El Valle Volcano and Cerro Colorado) (Defant et al., 1991; Hidalgo, 2007; Restrepo, 1987; Roy, 1988) and is a clear indication of active and important regional magmatic processes within the isthmus.

5.2 Cumulates

Bulk analyses of cumulates provide detailed geochemical constraints on their origin. However, these analyses are not representative of liquid compositions. We use these bulk analyses simply as a reference to infer relationships to the host magma.

Fine and Coarse Grained cumulates despite having similar mineralogy (dominantly amphibole) have important geochemical differences. Typically, the Coarse Grained cumulates have higher MgO, CaO, TiO_2, Fe_2O_3T and lower SiO_2, K_2O, Na_2O than the Fine Grained cumulates (Figure 2.4 and 2.5). In addition, Coarse Grained cumulates present some scatter in Al_2O_3, TiO_2, MgO, CaO, FeO* versus SiO_2 (Figure 2.5). The scatter might represent different source liquids within the cumulates or might just represent variation in the amphibole-plagioclase ratios in this group. Small changes in the amphibole-plagioclase ratios would greatly affect Al_2O_3 as well as most major element concentrations.

Fine Grained cumulates were more difficult to analyze chemically due to their low abundance, poor preservation, and the difficulties in obtaining a pure sample from the Ash Flow host. Nonetheless, three samples included in the Summit Domes unit were analyzed and indicate that these cumulates have SiO_2, MgO, Fe_2O_3T, and CaO intermediate between those of the Coarse Grained cumulates and the host units (Table 2.1, Figure 2.5). In addition, the interstitial glass found in both of these cumulates is clearly distinct (Figure 2.5). The glass contained in the Coarse Grained cumulates is more enriched in K_2O and more depleted in Na_2O than the glass found in the Fine Grained cumulates. This suggests that the magma that transported these cumulate nodules was not completely homogeneous, or that slightly different magmas were involved in the transport of these cumulate piles to more shallow levels. The Coarse Grained cumulates, despite their more primitive composition, were transported by a slightly more evolved magma than the Fine Grained cumulates. Such heterogeneity may reflect the complexity of the volcano plumbing system under Baru and will be evaluated in subsequent sections.

Trace element diagrams effectively describe the differences between the cumulate types and the host magmas (Figures 2.7 and 2.8). The Coarse Grained unit is more depleted than the Fine Grained cumulates in most of the LILE and HFSE except for the HREE that are more enriched in the Coarse Grained cumulates (Figure 2.7). Light rare earth elements (LREE) are commonly more enriched in the Fine Grained cumulates while middle rare earth elements (MREE) are slightly more enriched in the

Coarse Grained cumulates. Compared to the host magmas both cumulate groups are more depleted in LILE and LREE and are more enriched in most HREE and MREE.

5.3 Relationship between the Cumulates and the Host

The host magmas and the Fine Grained cumulates have similar patterns of REE despite the slight enrichment of the later in most trace elements. This implies that these units are consistent with having similar parental magmas despite the contrasting concentrations of major elements (e.g. MgO, SiO_2, Fe_2O_3T, CaO, etc) observed in these units (Figures 2.4 and 2.5).

The relationship between the Coarse Grained cumulates and the rest of the units is less clear. Both cumulate groups and the evolved host magmas share similar mineralogy except for the presence of minor olivine and enstatite with amphibole reaction rims in the Coarse Grained cumulates (Figures 2.2F and 2.3d). Nonetheless, occasional olivine ghosts and resorbed and embayed crystals of olivine and enstatite have been also observed in the ash flow unit (host) samples. Plagioclase and amphibole are pervasive in the Fine Grained cumulates, the host magmas, and the Coarse Grained cumulates (sometimes with little or no plagioclase) which is suggestive of a common origin. Furthermore, amphibole and plagioclase compositions (supplemental material) from the Coarse Grained cumulates and the host magmas partially overlap. This is consistent with these crystal populations being co-genetic.

These observations allow us to identify a possible fractionating assemblage that can be used to model the magmatic variation observed at Baru volcano.

Major element mass balance and trace element Rayleigh fractionation schemes were used to constrain the fractionating assemblages as well as the fractionating proportions. Only samples that were free of contamination with other units (i.e. host mixed with cumulate units) were used for the mass balance and Rayleigh fractionation models. We started by selecting one of the most primitive samples found at Baru volcano (CR1100747) and then subtracted the average compositions of the minerals in the cumulate units. To minimize the residuals from ~54-64% SiO_2, 40% extraction (by mass) of the assemblage found in the cumulates units was needed (Tables 2.2 and 2.3). A subtracted assemblage dominated by a high-Al-amphibole, effectively reproduces the variation observed in our major element data. Moreover, the cumulates are also successfully reproduced by the modeled solid residue left by the fractionating parental magmas (table 2.3 and Figures. 2.8a-d). Coarse Grained cumulates contain all the phases necessary to explain the major element evolution of the Baru volcano magmatic suites.

Trace element Rayleigh fractionation was modeled using the results provided in the major element mass balance (Table 2.3). Unpublished mineral-partition coefficients used for the trace element modeling were determined experimentally in water rich basalts (Melekhova and Blundy, 2008) (Table 2.4). The model mineral proportions, which are in agreement with observed mineral proportions, were used to calculate the trace element composition of a model-derived evolved liquid. If a magma with the composition of one of the most primitive Baru lavas were to crystallize an assemblage dominated by amphibole (~85%) and minor plagioclase, leaving a melt fraction of 60% of the initial magma, the resulting melt would reproduce much of the trace element variation observed in the host and Fine Grained cumulate samples (Table 2.5). This modeled evolved liquid effectively correlates to most of trace element abundance observed in the most evolved magmas at Baru volcano, except for the HREE (Figure 2.9).

In our modeled magmas HREE are too enriched when compared to the variation observed in the most evolved magmas at Baru volcano (Figure 2.9). Cryptic garnet fractionation (Larocque and Canil, 2010; Macpherson, 2008; Rodriguez et al., 2007) might be a possible solution for this discrepancy. Garnet is extremely rare as a phenocryst in volcanic rocks, and is not observed in the cumulates from Baru volcano. Nonetheless, its importance in fractionating HREE from parental magmas has been described and detailed in a number of studies (Alonso-Perez et al., 2009; Hattori et al., 2010; Hidalgo et al., 2007; Kratzmann et al., 2010; Larocque and Canil, 2010; Lee et al., 2006). It is worth noting that even the most primitive of the Coarse Grained cumulates already displays a depletion of the HREE that can only be reproduced if a mafic magma undergoes fractional crystallization within the garnet stability field or if it is derived from partial melts of a garnet bearing protolith (Figure 2.8). The HREE depletion observed in the cumulates would be consistent with early garnet removal or melt extraction from the parental water-rich basalts within the garnet stability field. For our modeling, in addition to the mineral phases that are observed in the cumulates, garnet was subtracted (2.4%) until the concentration of Lu in the model matched the concentration of the average Lu in the host samples, which recreated the HREE depletion pattern observed in the host magmas (Figure 2.9).

We recognize that the two models (major element mass balance and Rayleigh fractionation) are a simplification of the complex magmatic processes occurring at Baru volcano. Nonetheless, we believe that the evolutionary magmatic trend during the Quaternary can be explained by fractionation processes within the Panamanian crust, without the need for a more rigorous fractional crystallization model derived from experimental data with the specific magma compositions of Baru volcano primitive magmas.

6. AMPHIBOLE COMPOSITIONS AND GEOTHERMOBAROMETRY

6.1 Amphibole compositions

Around 81 representative phenocrysts of amphibole from the host units, Coarse Grained cumulate and Fined Grained cumulate units were analyzed for major element composition in core to rim data points. Full geochemical analyses, graphical representation of the chemical variation and calculations related to these amphiboles can be found in the online supplementary material. All of the analyzed amphiboles are calcic amphiboles (CaB≥1.5; Ti<0.5 atoms per formula unit: apfu) and also classify as magnesian amphiboles ($Mg/Mg+Fe^{2+}$ 0.5-0.75) (Figure 2.10). The structural formulae of all the amphiboles used in this study were calculated using cation distribution determined by the procedure of *Leake et al.* (1997) which estimates ferric iron based on the maximum stoichiometric limits (13 CNK).

6.2 Geothermobarometry

In this section we use amphibole compositions from crystals hosted in the most recent eruptives to evaluate the magma plumbing system of Baru volcano. The advantage of using the amphibole chemistry is its sensitivity to both pressure and temperature. In addition, amphibole is an ideal phase to study magmatic evolution due to its early appearance on the calc-alkaline liquidus (Deering, 2009).

6.2.1 Exchange Mechanisms

Several studies have addressed the effects of temperature, pressure and $f\,H_2O$ on the composition of amphiboles (Blundy and Holland, 1990; Johnson and Rutherford, 1989; Scaillet and Evans, 1999; Schmidt, 1992; Spear, 1981; Thomas and Ernst, 1990). These studies have agreed that the Al-Tschermak substitution ($Si_T + Mg_{M1\text{-}M3} = Al_T + Al_{M1\text{-}M3}$) is susceptible to variations in pressure. In contrast, *Spear* (1981) and later *Blundy and Holland* (1990) determined that temperature variations are marked by an increase in total Al through the edenite exchange ($Si_T + \square_A = Al_T + (Na+K)_A$) and an increase in Ti through the Ti-Tschermak exchange ($2Si_T + Mn_{M1\text{-}M3} = 2Al_T + Ti_{M1\text{-}M3}$). *Spear* (1981) also described that the Ti-content correlates positively with temperature in the presence of a Ti rich phase. Independently of pressure and temperature, $f\,H_2O$

appears to have an effect on the amphibole Al_{tot} - experiments on the Mount Pinatubo magmas have reported an Al_{tot} increase with increasing $f\ H_2O$ (Scaillet and Evans, 1999).

Most of the variation observed within the units sampled at Baru volcano can be explained by these exchange mechanisms as a derivative processes of pressure and temperature variation (Figure 2.11). Figure 2.11b displays good correlation of $(Na+K)_A$ with Al_T $(Na+K)_A$ also correlates with Ti, not shown in figure) which is consistent with edenite exchange and hence a variation in the temperature conditions. This is further supported by Ti-C vs Al_{IV} diagram (Figure 2.11E). Nonetheless, the influence of pressure is evident (despite some scatter) in the correlation of Al_{IV} with Al_{VI} and the positive correlation of Al_{Vi} with Al_T (not shown), all of which is consistent with Al-tschermak exchange mechanism (Figure 2.11a). On the basis of these results, the observed cation variation in the amphiboles from Baru volcano is consistent with amphibole crystallization at polybaric conditions over either a significant temperature range and/or significant $f\ H_2O$ range.

6.2.2 Relative Pressure and Temperature determinations

The buffering assemblage quartz+alkali feldspar +plagioclase+ hornblende+biotite+Fe-Ti oxides+titanite+melt+fluid frequently has been used to calibrate amphibole barometers (Anderson and Smith, 1994; Hammarstrom and Zen, 1986; Johnson and Rutherford, 1989; Schmidt, 1992). However, this assemblage is not found in any of the sampled units from quaternary Baru volcanism. Therefore, our pressure estimates should be used with caution and serve only as a relative indicator between the distinct populations of cumulates and the host. Due to the temperature dependence of some of the amphibole barometers (Anderson and Smith, 1994) we have used the formulation of *Holland and Blundy* (1994) to establish which of the barometers listed in the previous paragraph is more suitable for our suite of samples. The temperature estimates determined by the calibration of *Holland and Blundy* (1994) were in excess of 800 ºC (Figure 2.12) and generally agree (within error) with the calculations of temperature using the Ti solubility method of *Femenias et al.* (2006). Due to these high temperatures, using the *Anderson and Smith* (1994) experimental calibration can result in increased corrections that may lead to erroneous pressure estimates. For this reason, we have chosen to determine the pressure estimates using the higher-temperature experimental calibration of *Schmidt* (1992).

The results derived from the *Holland and Blundy* (1994) and *Schmidt* (1992) calibrations have allowed us to characterize our suite of samples and help constrain their origin. The magnesiohornblendes found within the Fine Grained cumulates record the lowest pressures and temperatures (Figure 2.12, P: 0.25-0.4±0.06 GPa and T: 800-850ºC) of our sample suite and display the narrowest range of variation in pressure and temperature. Temperature and pressure variation from core to rim in amphiboles from the Fine Grained unit are unsystematic.

The amphiboles from Coarse Grained cumulates and the amphiboles included within the host andesites-dacites have similar P-T characteristics (Figure 2.12). The Coarse Grained cumulates display significant variability in pressure and temperature (Figure 2.12, P: 0.3-0.8±0.06 GPa and T: up to 950ºC). In a similar fashion, the host amphiboles have recorded extremely variable pressures (0.25-0.8± 0.06 GPa) and temperatures (800-900 ºC) that might be a reflection of the mixed crystal population of this unit. The amphibole compositional variation and the pressure and temperature overlap between the host units and the Coarse Grained cumulates is consistent with the amphibole population in both these groups being co-genetic. It is likely that most cumulates suffered disaggregation during transport (forming the host amphibole phenocrysts), while some Coarse Grained cumulates survived unperturbed.

7. DISCUSSION

7.1 The Role of amphibole during magma differentiation

7.1.1 Amphibole dominated crystal "mush"

We have established that the cumulates and host magmas are likely derived from the same magmaticplumbing system, a statement supported by comparable REE patterns (Figure 2.7), similar mineralogy (Figure 2.2 and 2.3) and overlapping amphibole and plagioclase compositions (Figures 2.10, see supplementary material). This determination allowed us to test for crystal fractionation as the main process driving magmatic evolution at Baru volcano (see section 5). Diagnostic trace elements from the Quaternary volcanism at Baru volcano (Dy, Yb, La) are consistent with the fractionating assemblage being dominated by amphibole (Figure 2.13), as is the ubiquitous presence of amphibole as the sole ferromagnesian phase. Amphibole appears throughout the magmatic differentiation process – as evidenced by the wide compositional ranges observed (Ti magnesiohastingsite-Ti Tschermakite-Tschermakite-magnesio hornblende) and thus amphibole fractionation is the key component in our modeled crystal fractionation schemes (Figure 2.9). Specifically we have shown that amphibole dominated fractionation (~85% of the fractionating assemblage) can be linked to the magmatic evolution from basalt to dacite, and thus may represent a liquid line of descent.

Recent efforts to understand magma differentiation mechanisms at arcs have been centered on crystal mush models (e.g. Bachmann and Bergantz, 2004; Bachmann and Bergantz, 2008) that are hypothesized to be located in deep crustal 'hot zones' (e.g. Annen et al., 2006; Davidson et al., 2007)). In host and cumulate amphiboles from Baru volcano the complex and heterogeneous chemical composition and geothermobarometry results from the sampled crystals are consistent with a crystal mush model of magma evolution that was sampled by ascending magmas. In this model, hydrous magmas stall in the lower crust where after a period of incubation, melt extraction of more evolved magmas (andesite-rhyolite) from the resulting crystal mush (cumulates) is possible (Deering et al., 2008). This process is long-lived and new replenishments of primitive hot magmas will keep mush generation and melt segregation processes active (Bachmann and Bergantz, 2008). It is important to remember that local variations in the parental magmas composition or P, T, fO_2, fH_2O

conditions would greatly modify the composition and mode of the crystallizing assemblage.

Our barometric calculations using the amphiboles from the cumulate rocks of Baru volcano have allowed for general pressure estimates that may be consistent with an amphibole rich accumulation zone (crystal mush) in the Panamanian sub-arc lithosphere (Figure 2.12). Amphibole phenocrysts contained within the host units would also be part of this accumulation zone; given the overlapping amphibole compositions and similar P-T variation when compared to the Coarse Grained cumulate nodules (Figure 2.12). This is consistent with the host amphibole phenocrysts being recycled antecrysts from crustal amphibole rich accumulation zones (Coarse Grained cumulate unit). This amphibole rich accumulation zone has been previously described by Davidson et al. (2007) as the ‘amphibole sponge’, due to its importance as a filter for water in its transition from mantle to crust and as a way to recycle water and incompatible elements back in to the mantle (delamination). Furthermore, it is within this mid-lower crust amphibole rich layer that water rich magmas can become stalled during fractionation, driving the interstitial liquids to more evolved compositions.

7.1.2 Pressure and temperature conditions

Pressure and temperature estimates derived from amphibole compositions in monomineralic cumulates can give some insight in to the P-T and hydrous conditions of the parental magmas in the region. Experimental studies on water saturated andesitic magmas at moderate to high pressures have concluded that amphibole might be first and sole phase on the liquidus at depths exceeding ~ 7km (Alonso-Perez et al., 2009;

Carmichael, 2002). Nonetheless, Grove et al. (2003), using a more primitive starting composition (basaltic andesite), have demonstrated that the first phases on the liquidus of a water-saturated magma are olivine and orthopyroxene. This incongruity may be overcome by fractionation of these mafic phases at the upper mantle/lower crust boundary. Fractionation of olivine and pyroxene in the upper mantle/lower crust would produce a residual liquid which could then follow a fractionation path that would yield a monomineralic amphibole cumulate (Alonso-Perez et al., 2009). This also agrees with experiments performed by *Carmichael* (2002) in which he suggested that the andesitic starting compositions could be derived directly from the upper mantle, provided the magma was sufficiently hydrous. In Baru volcano, there is some evidence that fractionation of olivine and pyroxene might be occurring at the mantle/lower crust boundary as the first step in fractionation of water rich magmas. Coarse Grained cumulates often contain olivine and orthopyroxene (Figure 2.3). In most samples where olivine crystals are present, they have been reduced to ghosts. However, in some rare occurrences well preserved dunites (~5 cm diameter) surrounded by orthopyroxene coronas and interstitial amphibole are observed. In addition, orthopyroxenes commonly are present at the cores of amphibole crystals or they have developed amphibole coronas that in some cases extend in to the crystal network through fractures.

The mafic association in the cumulates described for Baru volcano supports early fractionation of orthopyroxene and olivine from water-saturated magmas, followed by amphibole-dominated fractionation in the mid-lower crustal regions The variation of Mg-number (100*(Mg/(Mg+Fe^{2+})) with increasing SiO_2 is an excellent indicator to test this hypothesis and has been used with great success to access direct mantle equilibration models (Grove et al., 2003). During fractionation Mg-numbers commonly decrease with increasing SiO_2, however andesitic melts in equilibrium with the mantle would have much higher Mg-number at the same value of SiO_2 (Grove et al., 2003). The effect of fractionation processes can be readily detected in the composition of the entrained cumulate material. The Mg-number of amphiboles during the fractionation process may record heterogeneities in their parental melts as it is closely related to the Fe-Mg exchange between amphibole and liquid ($K_d{}^{\sum Fe/Mg}$). Nonetheless, variables such as fO_2, fH_2O (Grove et al., 2003), and to a lesser extent temperature (Alonso-Perez et al., 2009) may also affect the Mg-number of the crystallizing amphiboles. Amphiboles derived as initial fractionating products of a high Mg andesite or a basaltic andesite typically have Mg numbers of ~79 (Grove et al., 2005; Grove et al., 2003; Moore and Carmichael, 1998). The monomineralic Coarse Grained cumulates from Baru volcano have lower Mg-numbers (~75) than would be expected for the direct fractionation products of a mantle-derived melt. However, the Mg-number of amphiboles in the monomineralic cumulates are elevated when compared to initial amphibole fractionation products of a less Mg-rich andesite (Alonso-Perez et al., 2009), and are directly comparable to the early fractionation products of an amphibole-dominated andesite from the Panama Canal Region (Rooney et al., 2010a). Grove et al (2003) noted that plagioclase was an important phase coexisting at low pressures with amphibole (Mg-number ~ 75). The absence of plagioclase in equilibrium with the monomineralic cumulates at Baru volcano supports that these cumulates do not represent an evolved portion of the fractionating assemblage described by Grove et al (2003). The most plausible model for the generation of the lower Mg-number (~75) in the amphiboles from the monomineralic cumulates, is that the parental magmas of Baru volcano fractionated mafic phases in the upper mantle/lower crust boundary (Rooney et al., 2010b). This is supported by the observation of remnants of these phases in the some of the Coarse Grained cumulates from Baru. After separation of these mafic phases, the slightly more-evolved melt would yield monomineralic amphibole cumulates at mid-lower crustal levels with the appropriate Mg-numbers of those observed at Baru.

To achieve rapid and extensive crystallization of amphibole rich cumulates from hydrous basalts decompression models have been proposed (Blundy et al., 2006; Tamura and Tatsumi, 2002). Nonetheless, cooling of water-rich magmas would also produce large volumes of amphibole over timescales that are more in accord with U-series temporal estimates of magmatic differentiation processes in arcs (Davidson et al., 2007). In the case of decompression driven amphibole crystallization, the increase of crystallinity in the magmas diminishes the potential of these magmas to reach the surface due to increasing viscosity with decreasing H_2O content (Barclay and Carmichael, 2004; Tamura and Tatsumi, 2002). The crystallizing assemblage preserved within the Coarse Grained cumulates at Baru volcano as well as the relative P, T estimates summarized in figure 2.12, are consistent with these cumulates being part of crustal 'hot zones' where large amounts of amphibole fractionate in response to decompression in water saturated magmas or to extensive cooling. Moreover, the host andesitic magmas at Baru volcano can effectively be correlated to the liquid residue derived from the fractionation of amphibole rich cumulates in crustal hot zones.

An important consequence of early removal of large quantities of amphibole from water-saturated magmas is that this process would rapidly increase the SiO_2 content of the residual magmas (Carmichael, 2002). In comparison with gabbroic assemblages (olivine+pyroxene+plagioclase), amphibole fractionation will rapidly elevate differentiation indices with relatively less mass removal. A geochemical consequence of these contrasting fractionation paths is that trace elements concentrations within a hydrous-magma increase far less than in a dry magma at similar SiO_2 due to the lower volume of mass removed from the hydrous magmas (Rooney et al., 2010a). Extensive amphibole fractionation may explain why samples from Baru volcano and other volcanic deposits in the Panamanian arc exhibit some of the most depleted REE patterns in the entire Central American Volcanic Front.

7.2 The role of garnet fractionation

In addition to amphibole fractionation, our model required that some garnet (1.4%) needed to be removed from the parental melts to reproduce the HREE and Y depletion observed at Baru magmas (Figure 2.9). Cryptic garnet fractionation is a viable process to generate HREE and Y depletion due to the high partition coefficients of these elements in garnet (Larocque and Canil, 2010; Macpherson, 2008; Rodriguez et al., 2007). In our trace element modeling (section 5) bulk partition coefficients for HREE and Y in garnet between 2.45 and 4.2 are needed to fully explain the observed HREE and Y depletions between 54 and 64 wt% SiO_2. These values are well within experimental and calculated bulk partition coefficient values on basaltic liquids (Hauri et al., 1994; Johnson, 1994, 1998; Mckenzie and O'nions, 1991; Melekhova and Blundy, 2008). On the other hand, if amphibole (~85 wt% of the fractionated assemblage) were the only phase to significantly retain HREE and Y, amphibole-melt partition coefficients of ~4.5-6.8 would be required. Experimentally determined partition coefficients for amphibole in basaltic to basaltic andesitic liquids are well below this range (0.2 to 2) (Dalpe and Baker, 2000; Melekhova and Blundy, 2008).

Cryptic garnet fractionation is also supported by the metaluminous character of the Quaternary volcanism at Baru (Figure 2.4B). High pressure fractionation of garnet inhibits the evolution towards peraluminous liquids which are produced at restricted pressure range (0.7-1.2 GPa) (Müntener, 2001; Sisson and Grove, 1993). At shallower depths the metaluminous character of the liquid is preserved by the crystallization of An-rich plagioclase (Alonso-Perez et al., 2009). In addition, the decreasing FeO*/MgO ratio with increasing SiO_2 (Figure 2.13C) is also consistent with garnet fractionation. Garnet has a high Fe/Mg solid/liquid partition coefficient and tends to produce liquids with high Mg contents, therefore during garnet fractionation FeO*/MgO decreases with increasing SiO_2. The stability of garnet in experiments on synthetic andesites have concluded that under water saturated conditions garnet is stable at pressures as low as ~0.8 GPa allowing for the garnet to be stable in lower crustal-upper mantle reservoirs (~25 km) in mature oceanic arcs (Alonso-Perez et al., 2009).

7.3 Magma ascent rates at Baru volcano

The textural evidence preserved within the cumulate groups suggests that the ascent of the Baru volcano magmas may be rapid. *Rutherford and Hill* (1993) studied the stability of hornblende under experimental conditions and estimated that during adiabatic ascent reaction rims will form around amphibole crystals in only 4 days after crossing the 0.160 GPa pressure boundary. At shallower depths amphibole is no longer stable. The reaction rim would typically have small plagioclase, pyroxene, Fe-Ti oxides and is a result of the decrease of H_2O content of coexisting melt during magma ascent (Garcia and Jacobson, 1979). No reaction rims are evident in any of the amphiboles of the Quaternary products of Baru volcano, supporting a rapid ascent hypothesis in terms of the shallower portion of the magmatic plumbing system.

7.4 Formation of amphibole cumulates and nature of the Panamanian crust

Amphibole rich cumulates such as those described from Baru volcano may provide a way to generate the evolved composition of the continental crust. Such cumulates, have been described by *Jull and Kelemen* (2001) and *Dufek and Bergantz* (2005) as key components of the continental crust cycle (instability and accretion). The importance of mafic cumulates, cannot be underestimated, as mass balance models predict that their volume should be roughly twice the volume of derivative intermediate to silicic magmas that are either erupted or stall on their path to the surface (Foden and Green, 1992). In order to generate the SiO_2-rich continental crust, these mafic cumulates must be removed from the island arc crust. Delamination and convective erosion, which rely upon density and strength instability in the arc lithosphere, have been invoked as potential mechanisms for the removal of sub-arc cumulates. In gabbroic cumulates the assemblage would not be dense enough to recycle into the mantle unless a partial melting event depletes the cumulate in the plagioclase component resulting in a higher density assemblage (*Dufek and Bergantz*, 2005). In contrast, amphibole-rich cumulates, which contain little or no plagioclase are ideal candidates to develop a density instability and be returned to the mantle (Davidson et al., 2007; Dufek and Bergantz, 2005; Müntener, 2001). Amphibole also plays a key role in models of convective erosion by promoting destabilization of the arc lithosphere (Arcay et al., 2006). Specifically, amphibole rich layers in the sub-arc lithosphere are ideal sites for shearing to occur due to an abrupt decrease in viscosity within the amphibole layer derived from increased water contents (Arcay et al., 2006). The ubiquitous presence of amphibole rich cumulates in the host magmas at Baru volcano enhances the importance of amphibole dominated fractionation as a dominant process for generating continental crust in mature island arcs.

Amphibole rich cumulates have been noted elsewhere along the Panamanian arc (El valle volcano - Hidalgo, 2007; and the Panama Canal Zone - Rooney et al., 2010b), indicating that magmatic plumbing systems in the region share some commonalities.

The widespread role of amphibole in the Panamanian lithosphere may have its origin in the prevalent tectonic conditions of the arc. The arrival of the Cocos and Coiba ridges to the Middle American Trench generated significant perturbations of the crustal and upper mantle structure of the region. Specifically, enhanced plate coupling, crustal shortening, changes in the stress conditions of the overlying plate, and arc-parallel movement of material have been invoked (Hoernle et al., 2008; LaFemina et al., 2009). Under these conditions rapid magma ascent would be impeded during the initial stages of the ridge collision due to the sealing of usual crustal transfer structures, causing stalling and differentiation of magmas at lower crustal levels e.g. (Chiaradia et al., 2009; Rooney et al., 2010b). Magma stalling impedes the crystallization of anhydrous phases, which are favored during decompression and degassing (Annen et al., 2006), and cooling promotes the widespread precipitation of amphibole in hydrated magmas (e.g. Carmichael, 2002). Furthermore, magma stalling and fractionation at deeper crustal levels within the garnet stability field successfully explains the origin of adakite-like volcanism in the Central American arc.

8. CONCLUSIONS

Quaternary magmas erupted at Baru volcano are a product of deep fractionation processes that probe an amphibole rich hot zone at mid-lower crustal depths. One variety of the ubiquitous cumulates sampled at Baru volcano records high temperatures and pressures while the other variety distinctively shows textures and barometric data consistent with rapid decompression that triggered crystallization processes. The most likely scenario is that an interstitial melt was separated from a mush/magma accumulation zone in the mid-lower crust, carrying with it Coarse Grained cumulates that either were disaggregated to become antecrysts within the host or were preserved as cumulates. Soon after, this mixture of melt + antecrysts + cumulates reached shallower levels where previous magma pulses had formed a Fined Grained cumulate layer by decompression induced crystallization. The Fined Grained cumulate layer was then eroded and brought to the surface rapidly.

This model for generating the chemical diversity observed in the erupted products of Baru volcano agrees with models that propose that the chemical diversity in arc magmas is largely acquired in the mid-lower crust, whereas textural diversity is related to shallow level processes (e.g. Annen et al., 2006; Davidson et al., 2007). Moreover, the present study succeeds in linking the chemical variation of large andesitic-dacitic volcanic eruptions to voluminous mafic cumulates. The existence of amphibole rich cumulates in the sub-arc lithosphere has been long predicted but proving their influence in the magmatic differentiation process on an active arc has been elusive.

The arrival of the Cocos and Coiba ridges to the Middle American Trench had significant implications for subduction zone magmas in the region. The absence of amphibole rich cumulates and evolved magma compositions in older western Panamanian volcanics (Neogene) and the recent appearance of amphibole rich magmas, might be an important indicator of an abrupt transition from to protracted storage in lower crustal levels. Protracted storage allowed for extensive amphibole crystallization that resulted in an amphibole rich layer in the Panamanian lithosphere. This process could be used to explain the appearance of more evolved magma sequences (dacites) that are not recorded in western Panama before the Quaternary. Moreover, parental water-rich basalts stored at deep crustal levels would allow for garnet to be a stable crystallizing phase, resulting in the production of adakite-like volcanism during the Quaternary in the Panamanian arc.

Acknowledgments

The authors wish to thank Angel Rodriguez and Karla Black for their invaluable help during the sample collection process, without their help and advice it would have been impossible to cover as much area as we did. We like to thank Eduardo Camacho for his contribution to the sample collection logistics and advice.   We wish to thank Tom Vogel, Dave Szymanski, Matt Parsons and Carl Henderson for sample preparation and analytical assistance. We are grateful to Jim Vallance and David Sherrod for their invaluable advice prior the field season. We wish to acknowledge the very constructive and detailed reviews of two anonymous referees and the careful editorial handling of Joel Baker.

9. APPENDICES

9.1 Appendix one: figure captions.

Figure 2.1: For interpretation of the references to color in this and all other figures, the reader is referred to the electronic version of this thesis (or dissertation).Location and tectonic map for this study. Dashed lines with teeth marks represent zones of convergence; zippered line is the Panama - Colombia suture zone as described by *Bird* (2003). Dashed line in the continental areas represent the approximate location of the Central American Volcanic Arc (CAVA). Oceanic ridges and plateaus are in dark grey. Ages indicated for the Coiba Plateau, Malpelo ridge, and the Cocos and Nazca Plates are derived from *Lonsdale* (2005). West of the Panama Fracture Zone the ages of the seafloor are from *Barckhausen et al.* (2001). Age for the Cocos ridge is from *Werner et al.* (2003), *Hey* (1977) and *Lonsdale and Klitgord* (1978). Subducting rates are from *Trenkamp et al.* (2002). Close to the trench in the Panama Basin between the Panama Fracture Zone and the Coiba Fracture zone the subducting crust is interpreted to be 10-20 Ma according to *Barckhausen et al.* (2001). The inset displays the dissected geomorphology of Baru volcano, which is a product of the overlapping recent (Quaternary) and older (Neogene?) volcanic products. In this inset the locations of the samples used on this study are indicated by black triangles

Figure 2.2: Cumulate textures observed in lavas and pumice fragments representative of the last period of activity on Baru volcano. (A) Schematic diagram of the Fine Grained cumulates. Usually these cumulates are composed of variable amounts of plagioclase and amphibole that are free of reaction rims or chilled margins. In this diagram only the amphibole rich variety is shown. Occasionally, these cumulates can be observed entraining large amphibole crystals similar to phenocrysts observed in the Coarse Grained cumulates, these too are free of reaction rims or chilled margins. (B) Pumice block with a darker portion that is composed of Fine Grained cumulates (C) Andesitic-Dacitic lavas on Baru volcano summit, the darker portions are related to Fine Grained cumulates. (D) Schematic Coarse Grained cumulate found in the Dome unit lavas. (E) Photograph of typical amphibole rich Coarse Grained cumulate hosted in the Dome unit lavas. (F) Photograph of Coarse Grained cumulates hosted in andesitic lavas. In this case some olivine and some orthopyroxene can still be indentifiedlavas. (F) Photograph of Coarse Grained cumulates hosted in andesitic lavas. In this case some olivine and some orthopyroxene can still be indentified.

Figure 2.3: Photomicrographs of andesitic host and cumulates. Upper two images are shown in cross-polarized light. Lower two images are shown in plane polarized light (A) Plagioclase rich Fine Grained cumulate with some amphibole and Fe-Ti oxides - note the bimodal size distribution of plagioclase crystals within the cumulate (B) Coarse Grained cumulate with amphibole megacrysts (more than 2000 μm across), interstitial plagioclase and glass on andesitic host. Note the high degree of crystallinity of the host andesite (C) Amphibole and Fe-Ti oxide Coarse Grained cumulate, plagioclase is absent (D) Amphibole corona on orthopyroxene and olivine crystals

Figure 2.4: (A) Alkalis versus silica *LeBas* (1986) on samples from Baru volcano. Samples from the Ash Flow unit come from pumice blocks within the ash flow while samples from other units come from lava samples (Pc= Alkali Basalt, B=Basalt, O1=Basaltic Andesite, O2= Andesite, O3=Dacite, S1=Trachybasalt, S2=Basaltic-Trachyandesite, S3=Trachyandesite, T=Trachyte, Trachydacite, R=Rhyolite, Ph=Phonolite, U1=Tephri-basanite, U2=Phono-tephrite, U3=Tephri-phonolite). (B) Alumina saturation discrimination diagram. A/NK (Al_2O_3/ Na_2O + K_2O), A/CNK (Al_2O_3/ CaO+ Na_2O + K_2O

Figure 2.5: Bulk rock geochemistry – major element variation diagrams shown versus SiO_2. The Ash Flow unit is slightly more primitive than the Summit Domes unit. Fine Grained cumulates exhibit chemical variation between of the Fined Grained cumulates and the host units. Data is presented in the supplementary material

Figure 2.6: Bulk rock geochemistry for selected trace elements. Variation diagrams shown versus SiO_2. Both of the host magmas have depleted HREE (heavy rare earth elements), low Y, and high Sr. Data is presented in the supplementary material

Figure 2.7:(A) Primitive mantle normalized (Sun and McDonough, 1989) spider diagrams for host samples. (B) Chondrite normalized (Sun and McDonough, 1989) for the host samples. (C) Primitive mantle normalized (Sun and McDonough, 1989) spider diagrams for the cumulate samples. (D) Chondrite normalized (Sun and McDonough, 1989) for the cumulate samples. Grey areas represent the range of variation observed in the host magmas. The Coarse Grained cumulates are more depleted than the Fine Grained cumulates in most of the LILE and HFSE except for the HREE that are more enriched on the Coarse Grained cumulate

Figure 2.8: (A) Chondrite normalized (Sun and McDonough, 1989) La/Yb vs. Yb diagram. The superimposed adakite and typical arc fields are after *Jahn et al.* (1981). Same symbols as in previous figures. All the sampled units plot within the adakite-like field. Even the most primitive of the Coarse Grained cumulates already display depletion of the HREE. (B) Plot of Sr/Y vs. Y

Figure 2.9: Variation of TiO_2, MgO, FeO, and CaO vs wt% SiO_2 showing the major element mass-balance model (panels A-D). Star represents the solid residue after separation, which is similar to the composition of the Coarse Grained cumulates. When the solid fraction reaches 40% the variation observed within the host (Ash Flow unit and Summit Dome unit) is duplicated by the model. Tick marks correspond to 5% fractionation increments. The effects of 1.4% garnet fractionation in the major element patterns will be negligible, thus this model does not include any garnet subtraction. (E) Trace element Rayleigh fractional crystallization model results compared with the

variation observed in natural samples. Grey field represents the variation observed in the andesitic-dacitic host. In a black dashed line the composition of the modeled end-product without including garnet removal is compared with the variation observed in the host. In a red dashed line the composition of the HREE modeled end-product with garnet fractionation is compared to host samples. Because the influence of garnet crystallization in other trace elements different than Y and the HREE is minimal and to avoid data clustering; only the HREE modeled data is included for the garnet fractionation model. Samples are normalized to primitive mantle (Sun and McDonough, 1989

Figure 2.10: Amphibole classification using structural formulae as recommended by *Leake et al.*, (1997) (13eCNK: 13 cations excluding Ca, Na, and K). (A) $(Na+K)_A$ vs. Si; (B) XMg vs.Si; and (C) Ti vs. Si. All of the analyzed amphiboles are calcic amphiboles (CaB≥1.5; Ti<0.5 atoms per formula unit: apfu) but also classify as magnesian amphiboles ($Mg/Mg+Fe^{2+}$ 0.5-0.65). All of the amphiboles from the Fine Grained cumulates are magnesiohornblendes, while amphiboles from the host units and the Coarse Grained \cumulate unit range from magnesiohastingsite-tschermakite-magnesiohornblende

Figure 2.11: Correlation charts relating pressure and temperature sensitive reactions and related substitution mechanisms. (A) Plot of Al_{IV} vs. Al_{VI}, Al- Tschermakite exchange evaluation. The influence of pressure is evident (despite some scatter) in the correlation of Al_{iv} with Al_{vi} and the positive correlation of Al_{vi} with Al_T (not shown), all of which is consistent with Al-tschermak exchange mechanism. (B) Edenite exchange (C) Mg substitution (D) Plagioclase exchange (E) Ti-Tschermak exchange. Values for Ti-C, $(Na+K)_A$, Mg-C, Al_{iv}, Alvi and Al_T are derived from the APMH-CLASS spreadsheet of *Esawi* (2004)

Figure 2.12: Symbols are the same as in previous Figure (A). Pressure and (B) temperature frequency histograms showing the distribution of P-T among the Quaternary units. (C) Temperature vs. pressure diagram. The pressure was calculated by the experimental calibration of *Schmidt* (1992). This calibration is the more reliable given the temperature range determined by the method of *Holland and Blundy* (1994). The magnesiohornblendes found within the Fine Grained cumulates record the lowest pressures and temperatures and display the shortest range of variation in pressure and temperature of the analyzed units. Amphiboles from Coarse Grained cumulates and those included within the host andesites-dacites have similar PT range. The Coarse Grained cumulates display ample variability in pressure and temperature. In a similar fashion, the host amphiboles have recorded extremely variable pressures and temperatures that might be a reflection of the mixed crystal population of this unit

Figure 2.13: La, Yb and Dy concentrations are normalized to chondrite concentrations of Sun and McDonough (1989) (A) Garnet vs amphibole crystallization; the diagram indicates that both phases might be responsible for the chemical variation. (B) Diagram clearly shows the dominant influence of amphibole fractionation. (C) This diagram is consistent with garnet fractionation producing enrichment of MgO in the resulting magmas. The tholeiitic-calcalkaline line is from Miyashiro (1974). The cumulates do not represent magma compositions but are presented here as a way to compare magma compositions with the solid residue (cumulates) that fractionated to produce the evolved andesite-dacite sequence. The symbols are the same as previous figures

9.2 Appendix two: Figures

Figure 2.1. For interpretation of the references to color in this and all other figures, the reader is referred to the electronic version of this thesis (or dissertation).

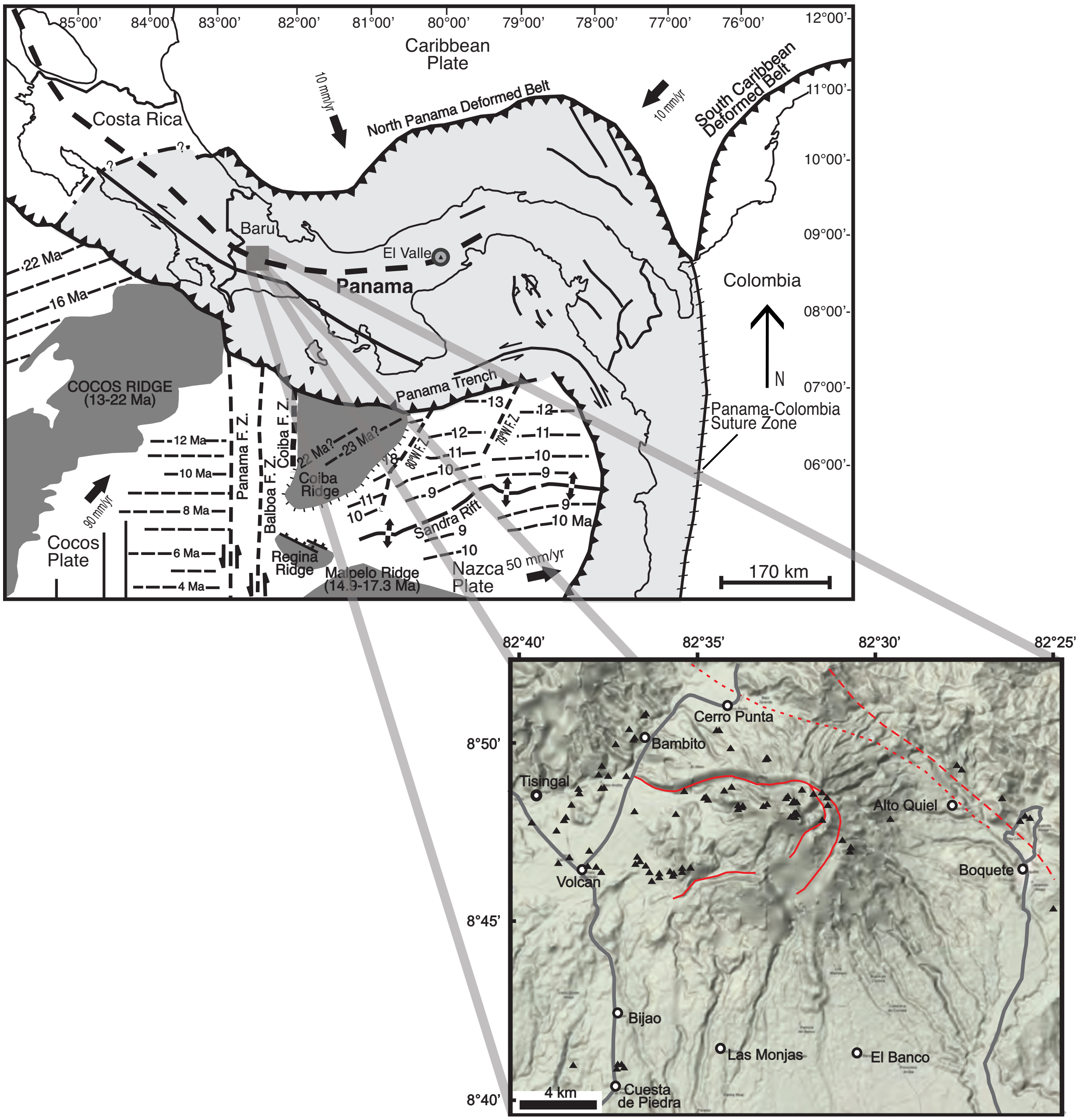

Figure 2.2

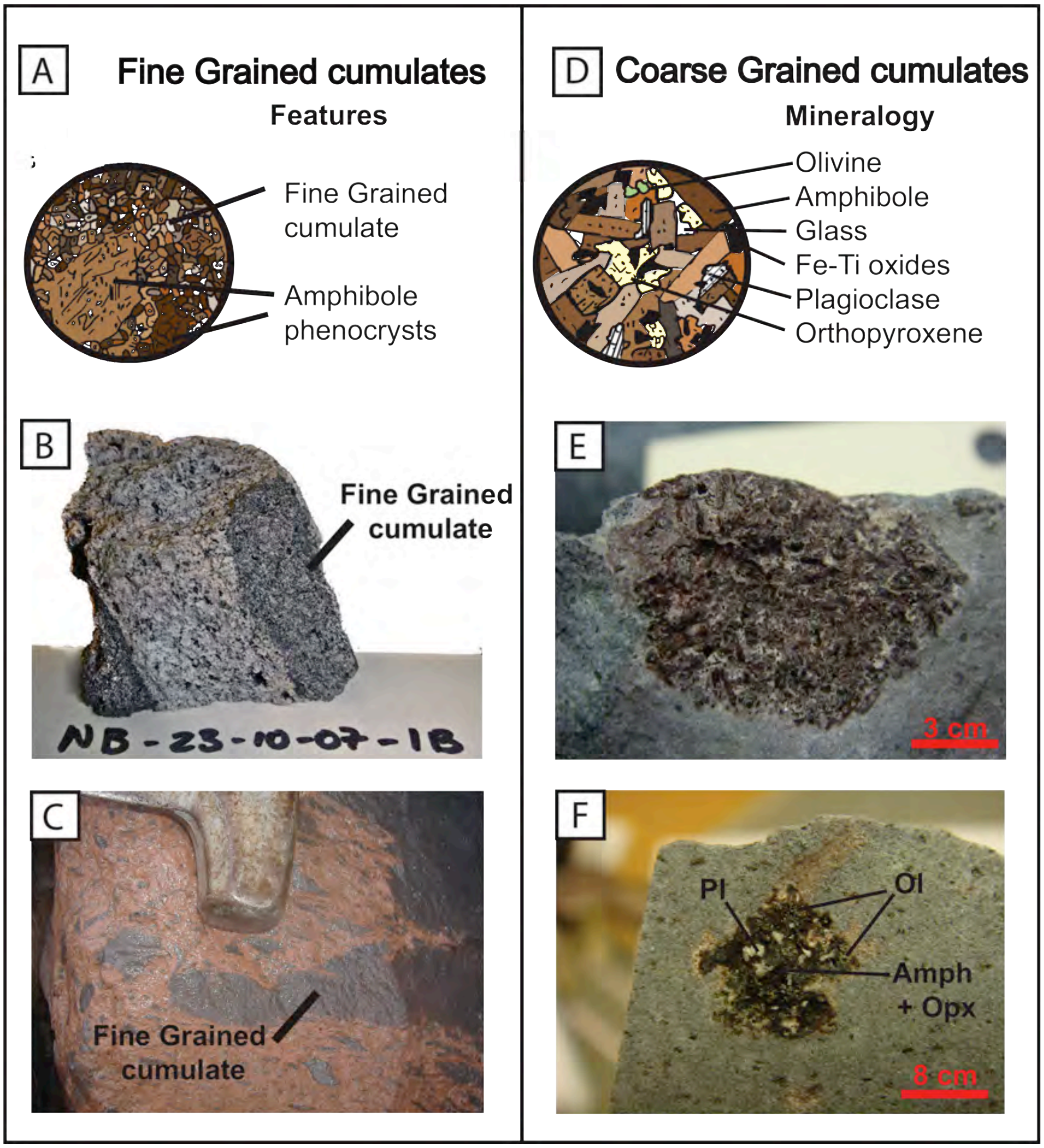
A
Fine Grained cumulates
Features
Fine Grained cumulate
Amphibole phenocrysts
D
Coarse Grained cumulates
Mineralogy
Olivine
Amphibole
Glass
Fe-Ti oxides
Plagioclase
Orthopyroxene
B
Fine Grained cumulate
NB-23-10-07-1B
E
3 cm
C
Fine Grained cumulate
F
Pl
Ol
Amph + Opx
8 cm

Figure 2.3

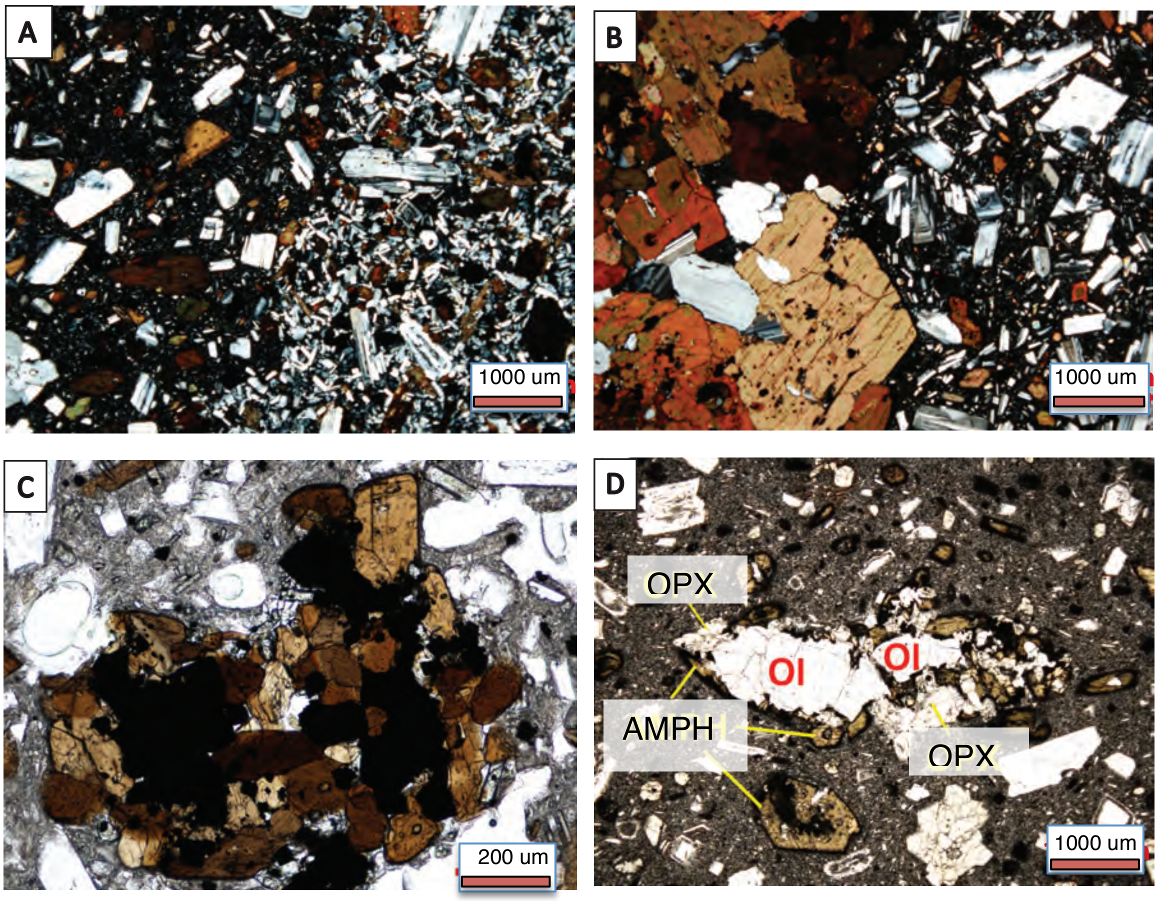

Figure 2.4

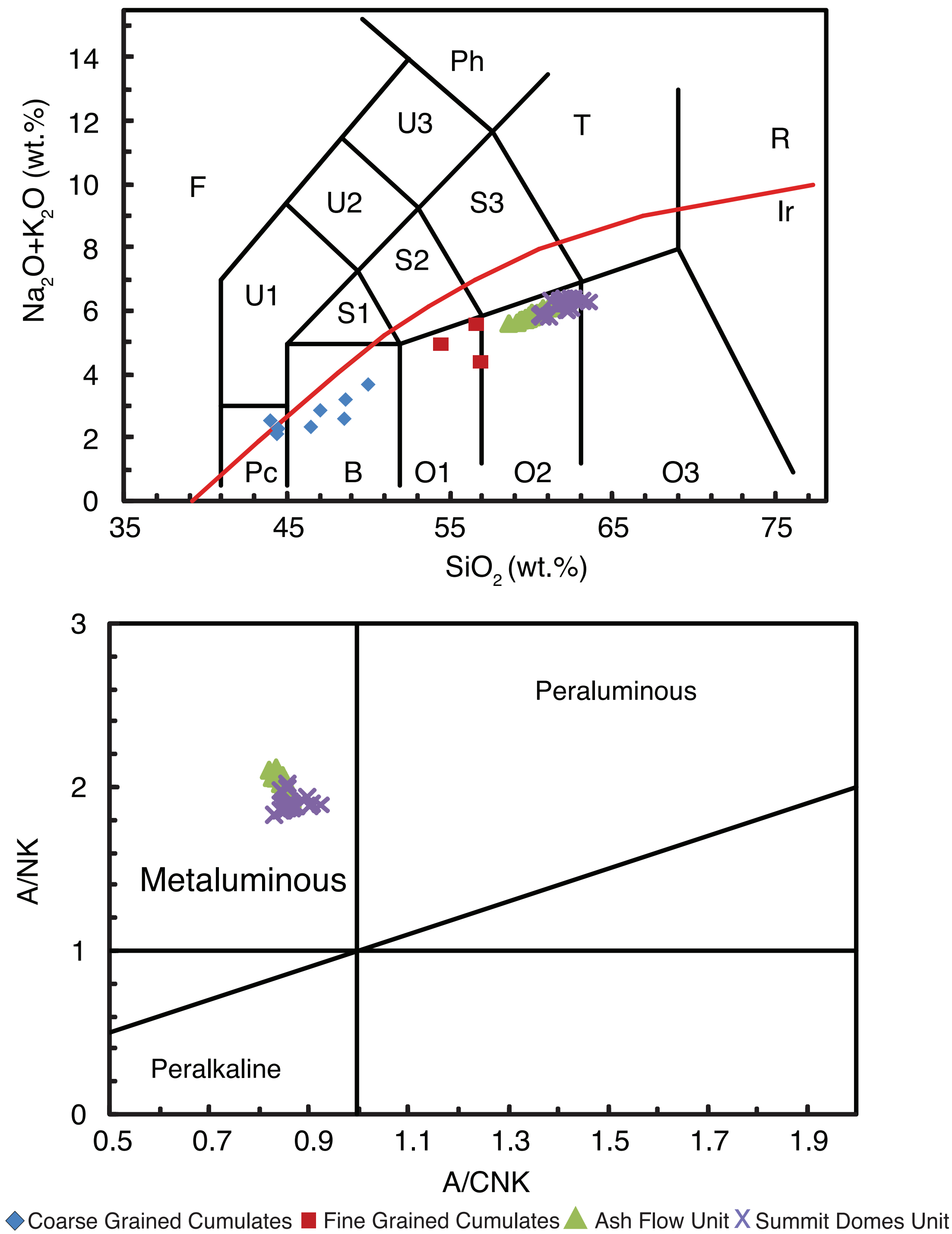

Ph
U3
T
R
F
U2
S3
Ir
S2
U1
S1
Pc
B
O1
O2
O3
Na_2O+K_2O (wt.%)
SiO_2 (wt.%)
0
2
4
6
8
10
12
14
35
45
55
65
75
Peraluminous
Metaluminous
Peralkaline
A/NK
A/CNK
0
1
2
3
0.5
0.7
0.9
1.1
1.3
1.5
1.7
1.9
Coarse Grained Cumulates
Fine Grained Cumulates
Ash Flow Unit
Summit Domes Unit

Figure 2.5.

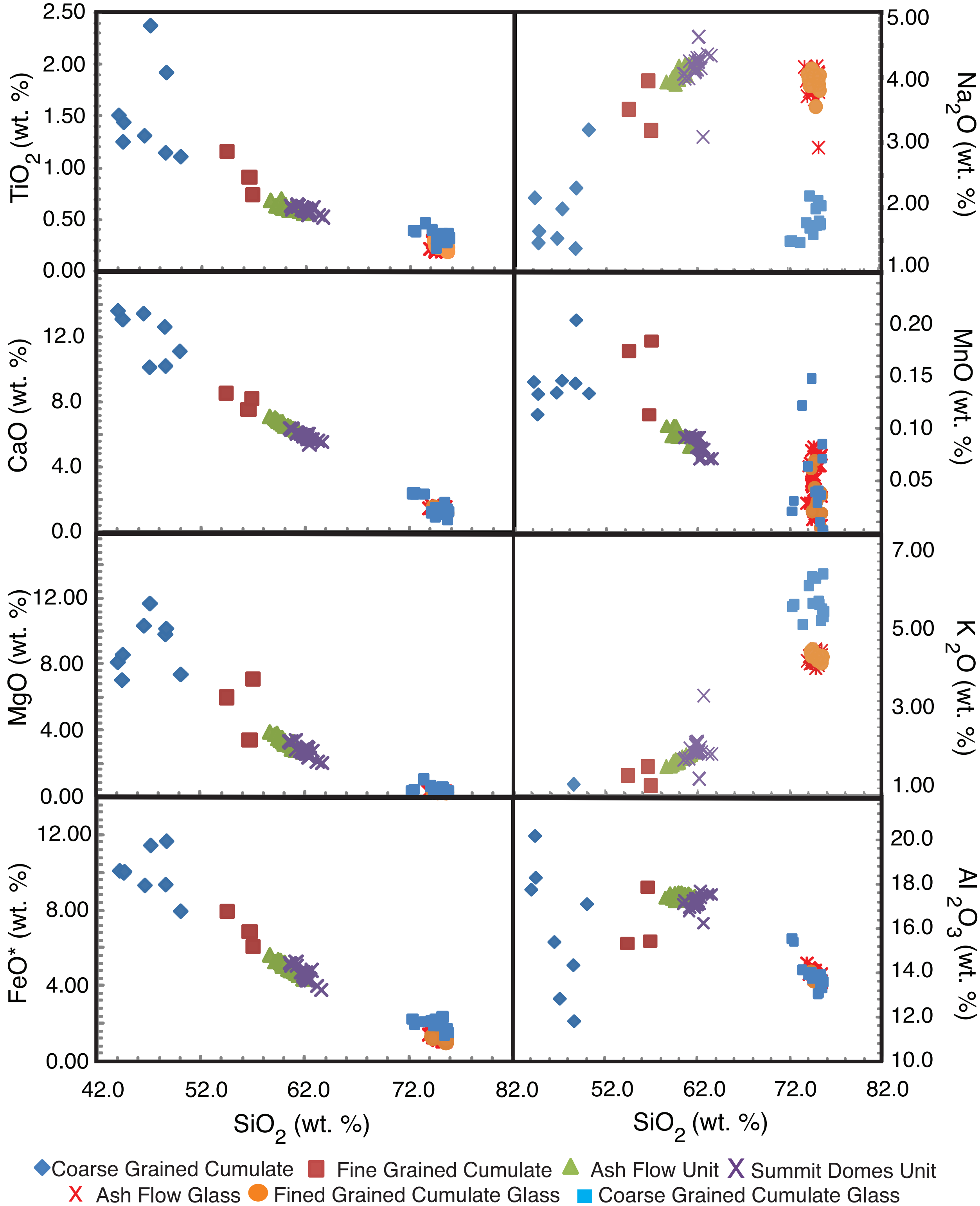
2.50
2.00
1.50
1.00
0.50
0.00
TiO_2 (wt. %)
5.00
4.00
3.00
2.00
1.00
Na_2O (wt. %)
12.0
8.0
4.0
0.0
CaO (wt. %)
0.20
0.15
0.10
0.05
MnO (wt. %)
12.00
8.00
4.00
0.00
MgO (wt. %)
7.00
5.00
3.00
1.00
K_2O (wt. %)
12.00
8.00
4.00
0.00
FeO* (wt. %)
20.0
18.0
16.0
14.0
12.0
10.0
Al_2O_3 (wt. %)
42.0
52.0
62.0
72.0
82.0
SiO_2 (wt. %)
52.0
62.0
72.0
82.0
SiO_2 (wt. %)
Coarse Grained Cumulate
Fine Grained Cumulate
Ash Flow Unit
Summit Domes Unit
Ash Flow Glass
Fined Grained Cumulate Glass
Coarse Grained Cumulate Glass

Figure 2.6.

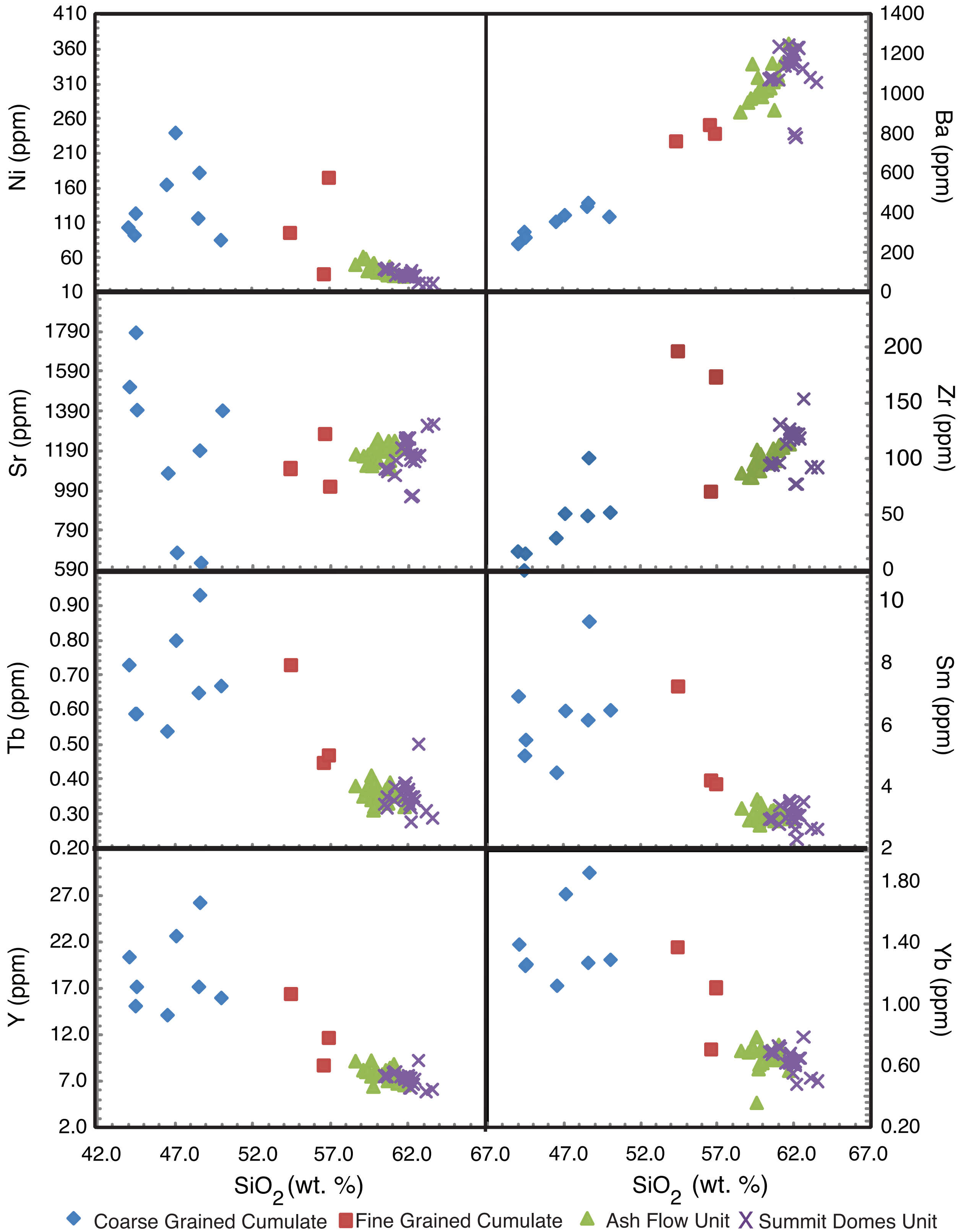

Ni (ppm)
Ba (ppm)
Sr (ppm)
Zr (ppm)
Tb (ppm)
Sm (ppm)
Y (ppm)
Yb (ppm)
SiO2 (wt. %)
SiO2 (wt. %)
Coarse Grained Cumulate
Fine Grained Cumulate
Ash Flow Unit
Summit Domes Unit

Figure 2.7

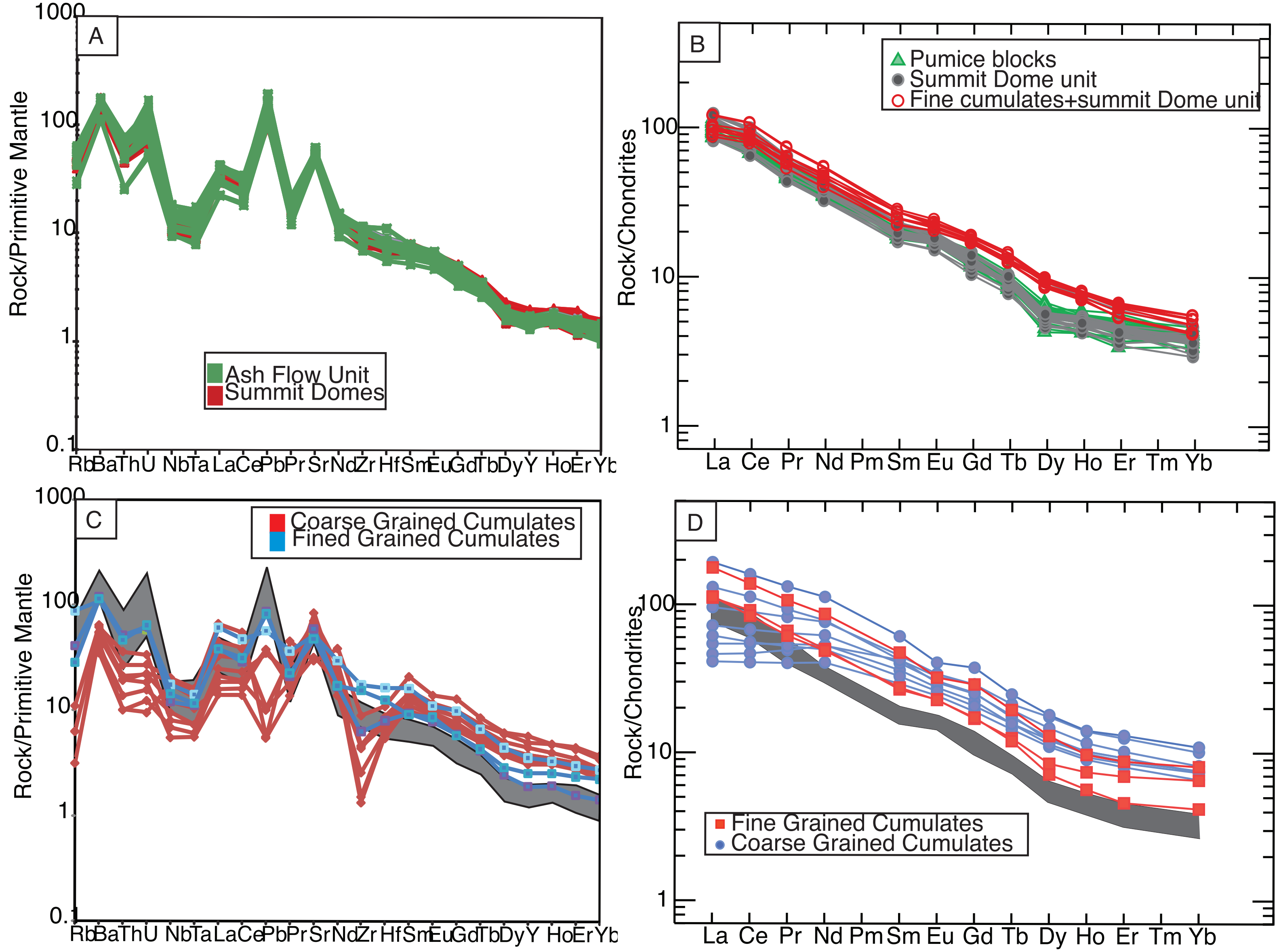
A
1000
100
10
1
0.1
Rock/Primitive Mantle
Ash Flow Unit
Summit Domes
Rb Ba Th U Nb Ta La Ce Pb Pr Sr Nd Zr Hf Sm Eu Gd Tb Dy Y Ho Er Yb
B
Pumice blocks
Summit Dome unit
Fine cumulates+summit Dome unit
Rock/Chondrites
100
10
1
La Ce Pr Nd Pm Sm Eu Gd Tb Dy Ho Er Tm Yb
C
Coarse Grained Cumulates
Fined Grained Cumulates
Rock/Primitive Mantle
D
Fine Grained Cumulates
Coarse Grained Cumulates
Rock/Chondrites

Figure 2.8

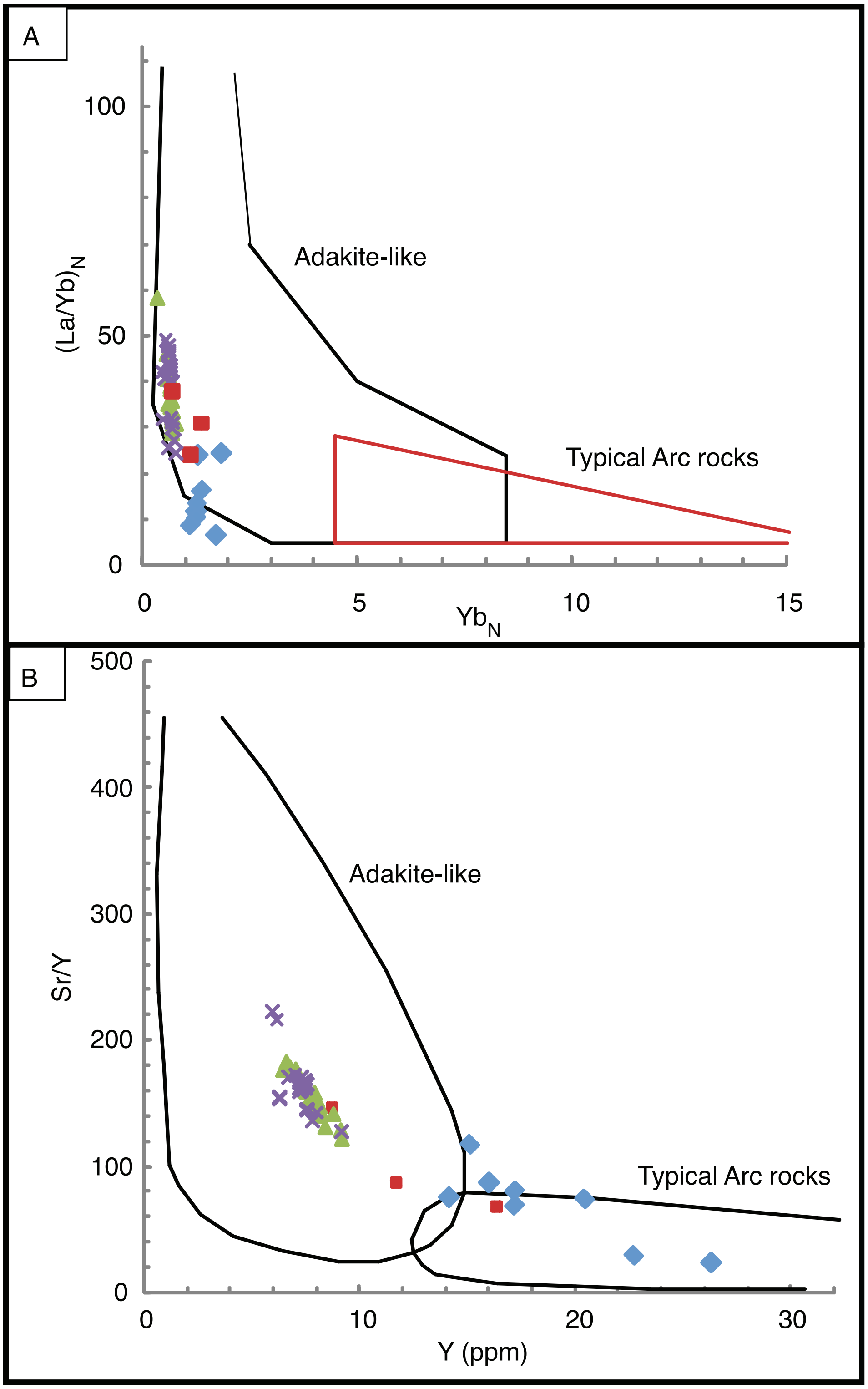

A
100
50
0
(La/Yb)N
Adakite-like
Typical Arc rocks
0
5
10
15
YbN
B
500
400
300
200
100
0
Sr/Y
Adakite-like
Typical Arc rocks
0
10
20
30
Y (ppm)

Figure 2.9.

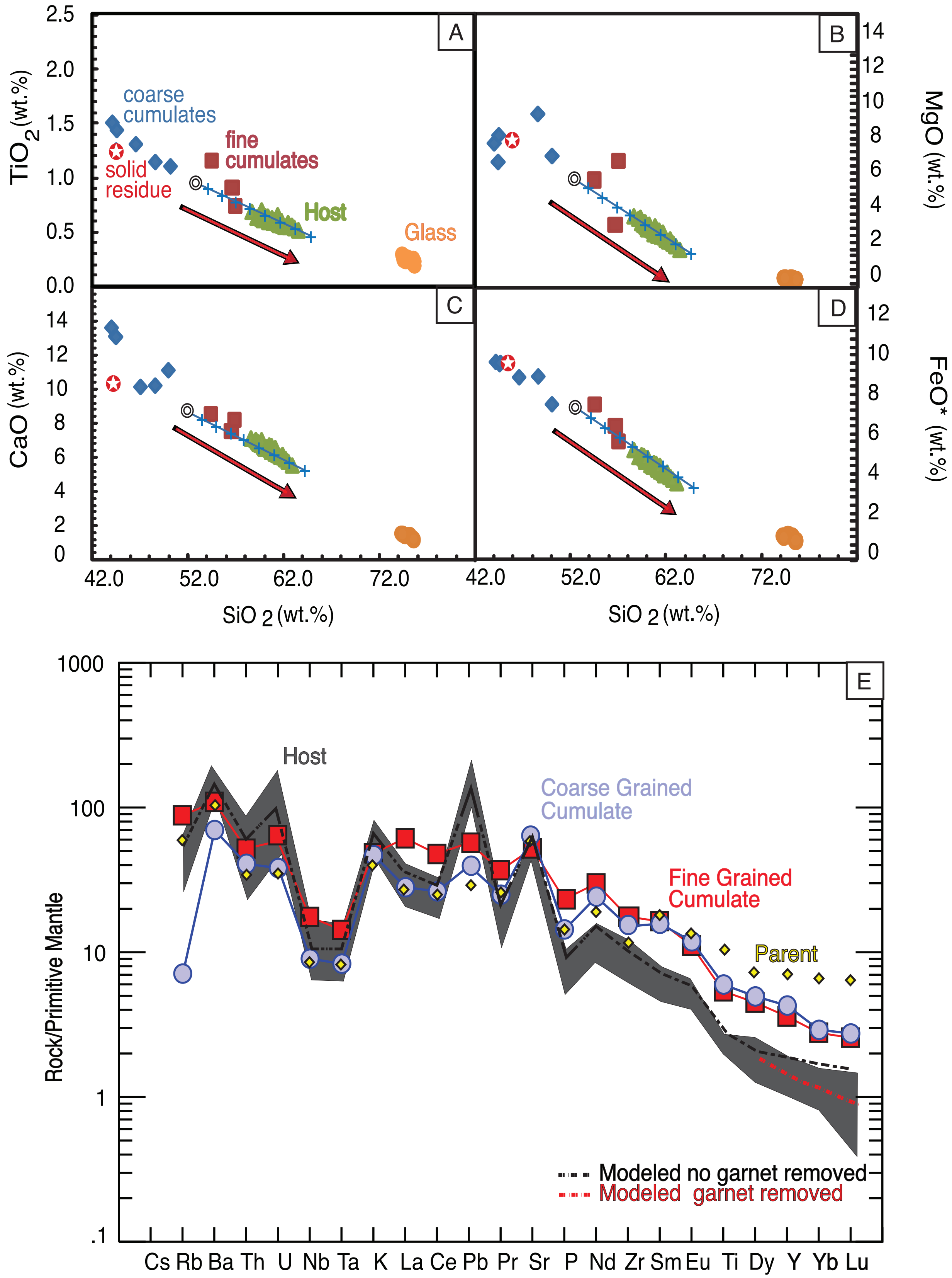

A
B
C
D
E
coarse cumulates
fine cumulates
solid residue
Host
Glass
TiO2 (wt.%)
MgO (wt.%)
CaO (wt.%)
FeO* (wt.%)
SiO 2 (wt.%)
Rock/Primitive Mantle
Coarse Grained Cumulate
Fine Grained Cumulate
Parent
Modeled no garnet removed
Modeled garnet removed
Cs Rb Ba Th U Nb Ta K La Ce Pb Pr Sr P Nd Zr Sm Eu Ti Dy Y Yb Lu

Figure 2.10

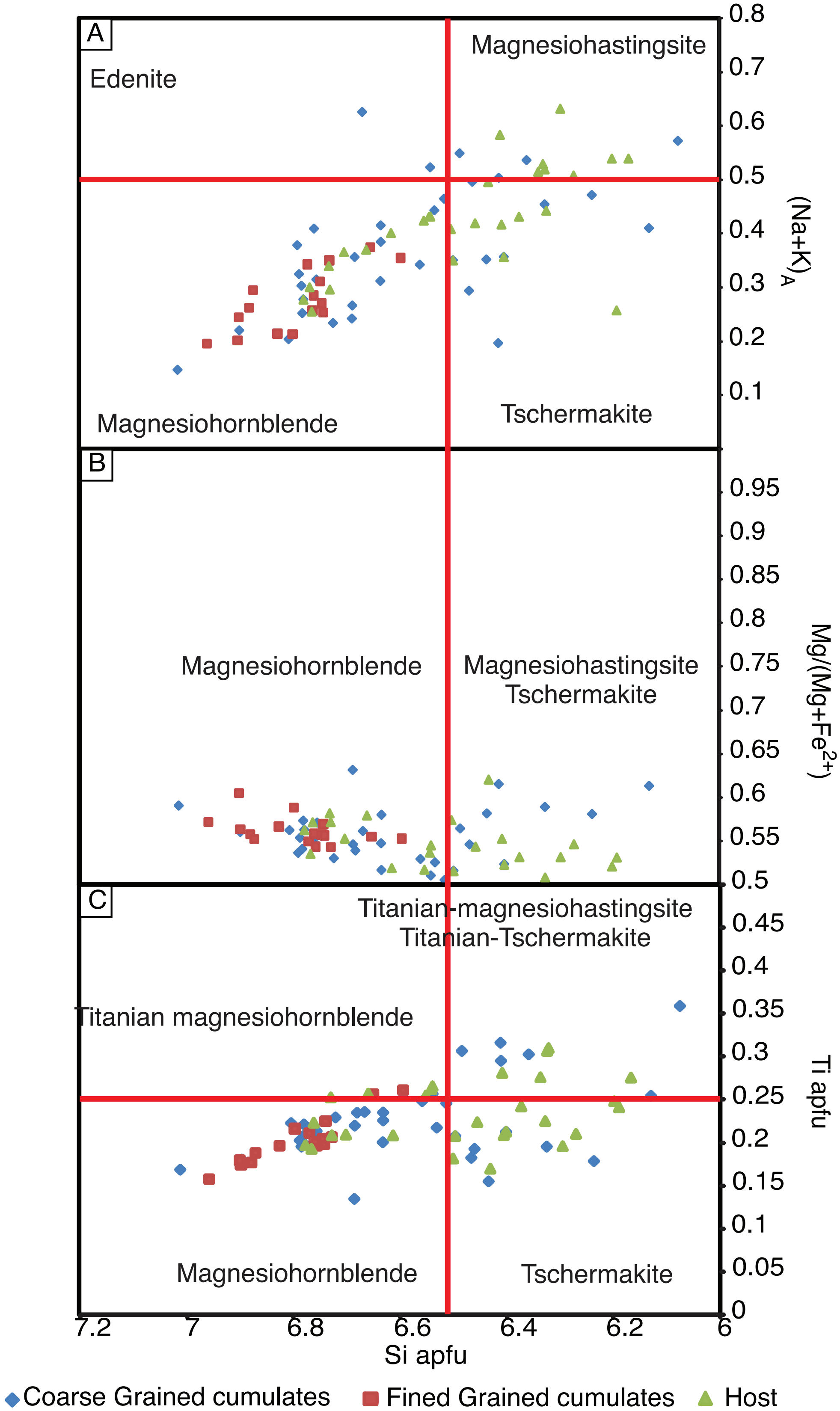
A
Edenite
Magnesiohastingsite
Magnesiohornblende
Tschermakite
0.8
0.7
0.6
0.5
0.4
0.3
0.2
0.1
(Na+K)$_A$
B
Magnesiohornblende
Magnesiohastingsite
Tschermakite
0.95
0.9
0.85
0.8
0.75
0.7
0.65
0.6
0.55
0.5
Mg/(Mg+Fe^{2+})
C
Titanian-magnesiohastingsite
Titanian-Tschermakite
Titanian magnesiohornblende
Magnesiohornblende
Tschermakite
0.45
0.4
0.35
0.3
0.25
0.2
0.15
0.1
0.05
0
Ti apfu
7.2
7
6.8
6.6
6.4
6.2
6
Si apfu
Coarse Grained cumulates
Fined Grained cumulates
Host

Figure 2.11

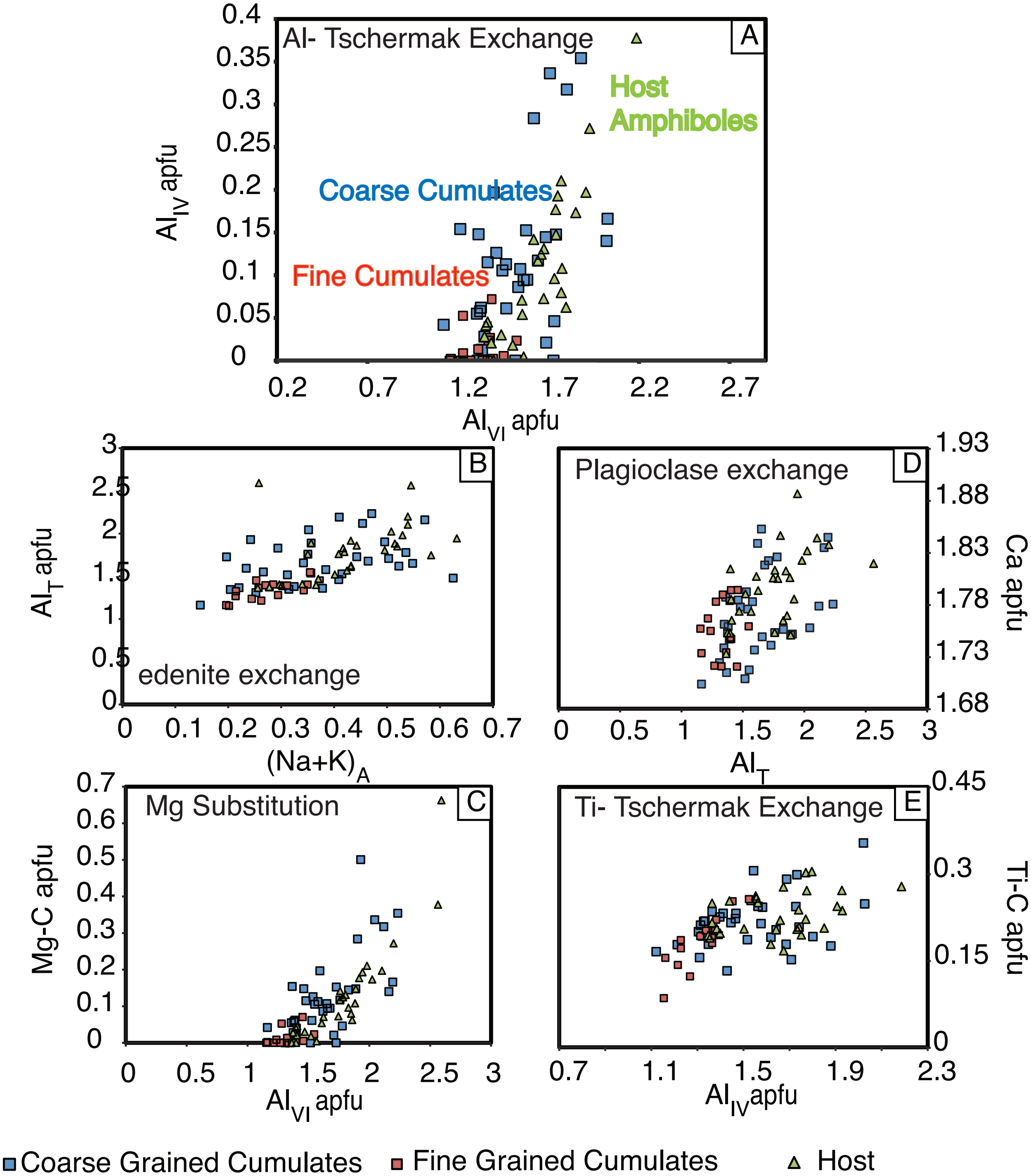

Al- Tschermak Exchange
A
Host Amphiboles
Coarse Cumulates
Fine Cumulates
Al$_{IV}$ apfu
Al$_{VI}$ apfu
0.4
0.35
0.3
0.25
0.2
0.15
0.1
0.05
0
0.2
0.7
1.2
1.7
2.2
2.7
B
edenite exchange
Al$_T$ apfu
(Na+K)$_A$
3
2.5
2
1.5
1
0.5
0
0
0.1
0.2
0.3
0.4
0.5
0.6
0.7
Plagioclase exchange
D
Ca apfu
Al$_T$
1.93
1.88
1.83
1.78
1.73
1.68
0
0.5
1
1.5
2
2.5
3
Mg Substitution
C
Mg-C apfu
Al$_{VI}$ apfu
0.7
0.6
0.5
0.4
0.3
0.2
0.1
0
0
0.5
1
1.5
2
2.5
3
Ti- Tschermak Exchange
E
Ti-C apfu
Al$_{IV}$apfu
0.45
0.3
0.15
0
0.7
1.1
1.5
1.9
2.3
Coarse Grained Cumulates
Fine Grained Cumulates
Host

Figure 2.12

N=78 M=4.75E00 SD=1.43E00 SE=1.62E-01 N=80 M=8.40E02 SD=3.92E01 SE=4.38E00

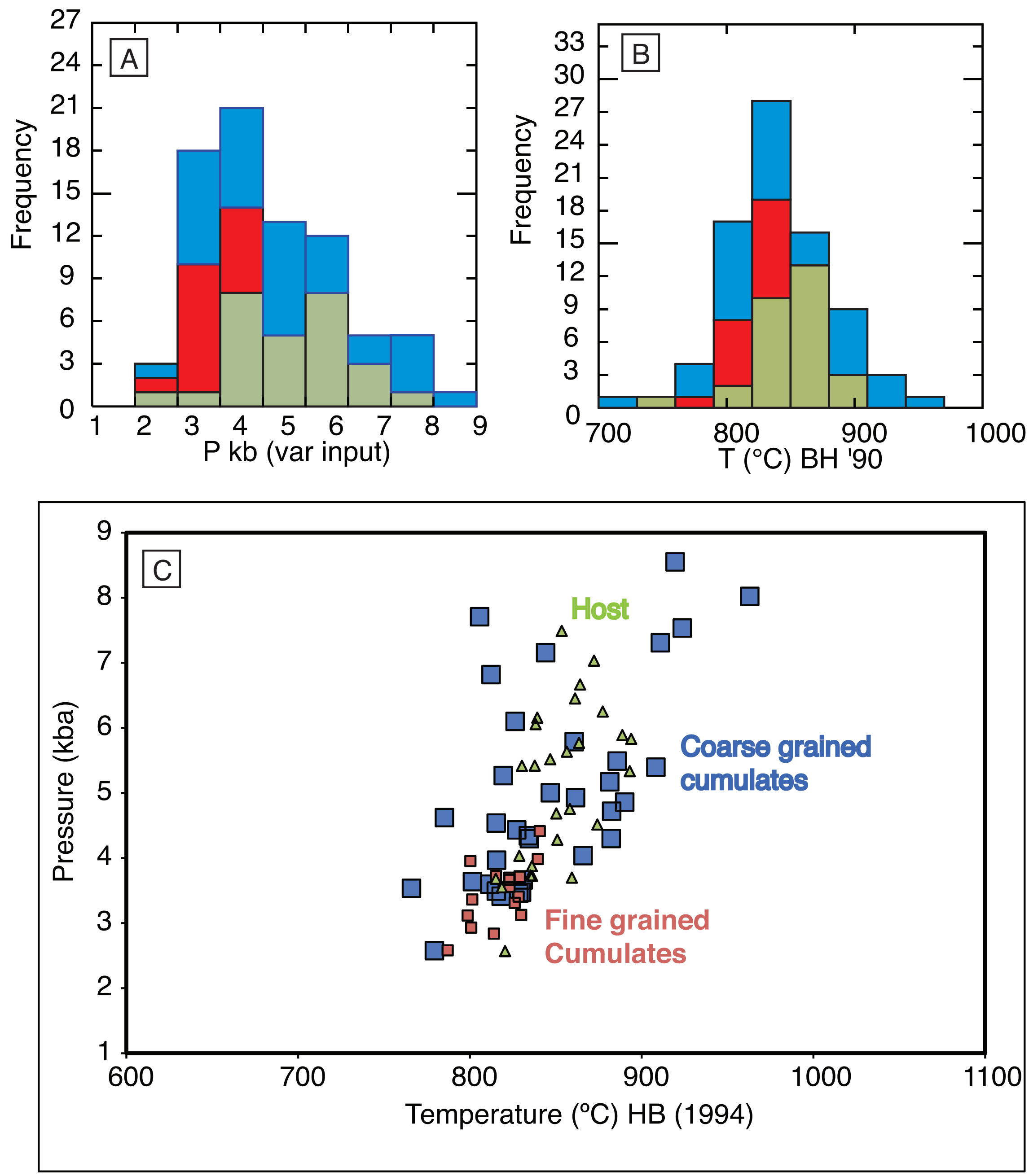

Figure 2.13

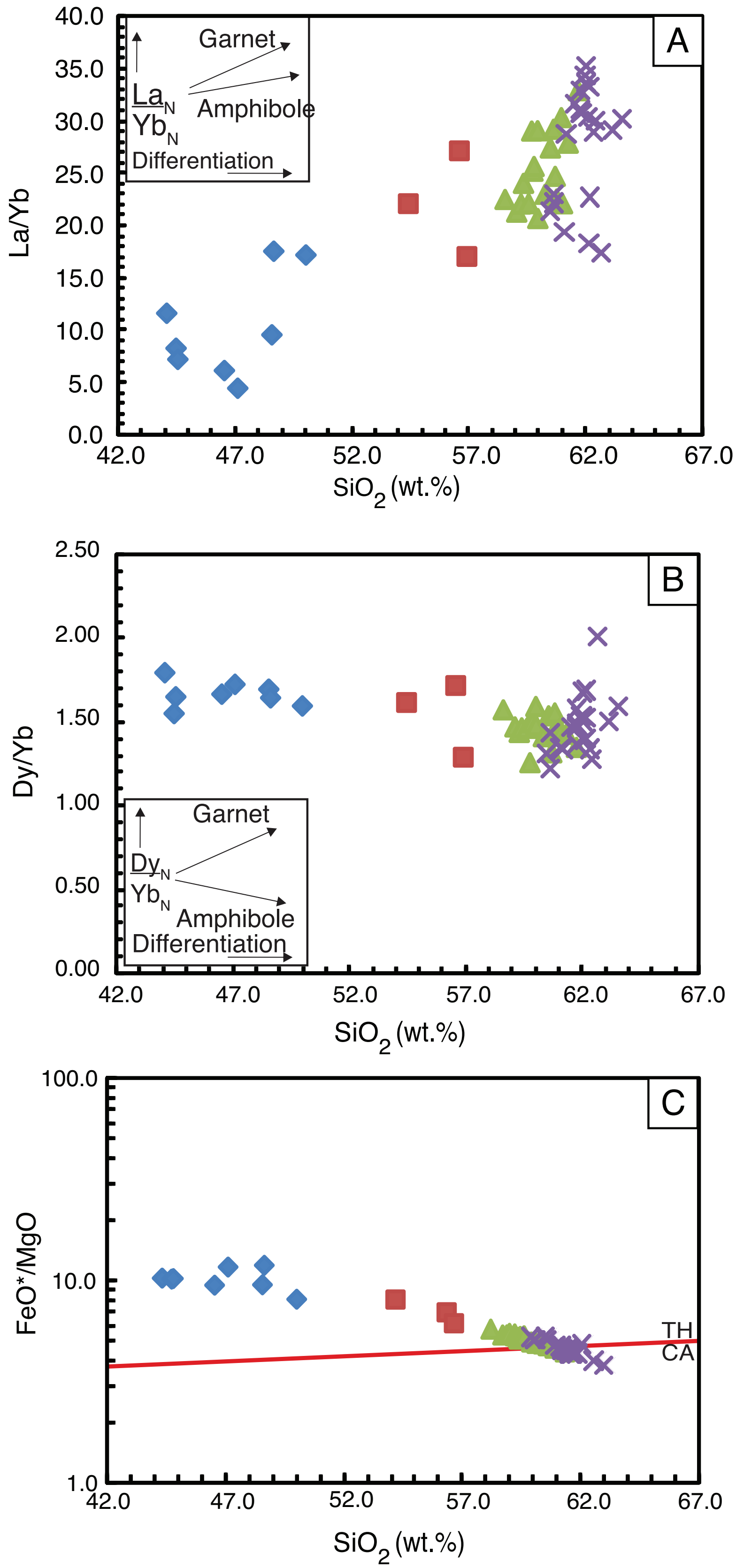
A
Garnet
Amphibole
La_N/Yb_N
Differentiation
La/Yb
SiO2 (wt.%)
B
Garnet
Amphibole
Dy_N/Yb_N
Differentiation
Dy/Yb
SiO2 (wt.%)
C
TH
CA
FeO*/MgO
SiO2 (wt.%)

9.3 Appendix three: Tables

Table 2.1: Average whole-rock chemical composition for the Quaternary units at Baru Volcano.

	Coarse Grained Cumulates		**Fined Grained Cumulates**		**Ash Flow Host**		**Summit Domes Host**	
	Mean	S.D	Mean	S.D	Mean	S.D	Mean	S.D
XRF								
SiO_2	46.76	2.09	56	1.1	60.18	0.79	61.88	0.73
TiO_2	1.51	0.41	0.94	0.17	0.63	0.03	0.59	0.03
Al_2O_3	15.98	2.7	16.24	1.15	17.49	0.12	17.2	0.28
Fe_2O_3T	11.11	1.24	7.75	0.84	5.62	0.35	5.14	0.39
FeO	9.99	1.12	6.98	0.75	5.06	0.31	4.62	0.35
MnO	0.14	0.02	0.16	0.03	0.09	0.01	0.09	0.01
MgO	9.17	1.49	5.52	1.54	3.29	0.35	2.75	0.34
CaO	12.16	1.35	8.07	0.41	6.59	0.28	5.96	0.24
Na_2O	1.95	0.57	3.55	0.31	4.06	0.1	4.17	0.28
K_2O	0.78	0.25	1.44	0.18	1.82	0.09	2.02	0.35
	0.43	0.28	0.32	0.14	0.23	0.01	0.21	0.03
Ni	139	49	102	57	44	8	35	6
Cu	308	175	415	337	129	32	143	37
Zn	77	16	92	8	62	2	61	8
Rb	2	2	33	16	30	3	35	6
Sr	1210	376	1128	109	1178	43	1172	92
Zr	39	29	147	55	99	9	113	18
LA-ICP-MS								
Ba	354.87	68.03	801.57	32.71	1042.22	83.84	1120.01	120.75
La	20.6	11.53	31.73	7.33	23.48	2.02	24.52	4.47
Ce	47.99	23.3	63.98	14.74	47.39	4.17	49.89	8.46
Pr	6.75	2.71	7.44	1.93	4.88	0.38	4.99	0.75
Nd	30.71	10.05	28.86	8.15	17.67	1.23	17.71	2.36
Sm	6.32	1.39	5.2	1.47	3.67	2.41	3.07	0.34
Eu	1.78	0.28	1.55	0.23	1.04	0.04	1.02	0.1
Gd	5.36	1.14	4.34	1.15	2.69	0.17	2.65	0.33
Tb	0.69	0.12	0.55	0.13	0.36	0.03	0.35	0.04
Y	18.67	3.9	12.26	3.15	7.82	0.74	7.28	0.7

Cont. Table 2.1

Dy	3.49	0.65	2.43	0.64	1.47	0.16	1.4	0.23
Ho	0.63	0.11	0.43	0.09	0.29	0.03	0.28	0.04
	1.65	0.29	1.12	0.28	0.76	0.09	0.72	0.08
Yb	1.4	0.24	1.06	0.27	0.66	0.09	0.63	0.07
Lu	0.19	0.04	0.15	0.04	0.09	0.02	0.08	0.02
V	318.08	59.98	190.51	22.52	179.97	14.33	164.69	31.1
Cr	245.67	92.47	174.2	122.09	71.55	11.05	63.58	20.57
Nb	8.82	3.91	10.47	1.57	8.57	1.03	9.45	1.95
Hf	2.28	0.54	3.84	1.08	2.37	0.16	2.6	0.44
Ta	0.42	0.16	0.51	0.05	0.43	0.05	0.49	0.1
Pb	1.27	1.08	5.38	0.95	15.86	25.85	11.25	2.05
Th	1.67	0.7	4.27	0.21	4.52	0.45	5.15	1.27
U	0.42	0.16	1.3	0.05	1.77	0.33	2.2	0.66

Table 2.2: Mineral compositions are averages of natural minerals in the Coarse Grained cumulates. The mineral proportions (wt%) were calculated by least squares optimization schemes.

	Amph	Plag	Ol	Opx	Fe-Ti ox
Fract. proportions	83.72	5.7	1.5	2.98	4.6
wt%					
SiO_2	47.77	53.05	39.57	53.32	0.13
TiO_2	1.27		0	0.31	9.78
Al_2O_3	11.9	29.13	0	2.1	2.68
FeO*	9.33	0.75	14.01	14.4	77.14
MnO	0.01		0.2	0.63	0.4
MgO	16.05	0.18	46.02	27.16	2.5
CaO	11.06	12.3	0.1	2.04	0
Na_2O	1.9	4.34	0	0.03	0
K_2O	0.59	0.25	0.1		
P_2O_5	0.12		0	0.01	0.61
NiO				0	
Mg#	75.04		0.78	0.71	0.05
An (mol%)		60.48			

Table 2.3: Mass Balance Model results

	Parent CR1100747	**Modeled Dacite**	**Evolved Host WVB22100723B**	**Residuals**	**Modeled Cumulate**
wt%					
SiO_2	51.92	64.13	64.05	-0.08	44.25
TiO_2	1.01	0.58	0.58	0	1.26
Al_2O_3	17.36	17.25	17.18	-0.07	20.78
FeO*	7.83	4.31	4.29	-0.02	9.61
MnO	0.13	0.1	0.09	-0.01	0.15
MgO	7.02	2.17	2.27	0.1	7.91
CaO	9.14	5.09	4.97	-0.12	10.44
Na_2O	3.29	4.43	4.48	0.05	2.88
K_2O	1.06	1.3	1.29	-0.01	0.3
P_2O_5	0.35	0.18	0.18	0	0.3

Table 2.4: Partition coefficients for the mafic to intermediate melts used in the Rayleigh fractionation model. For REE preferred value and range of published partition coefficients are given. References used to create this table come from: 1, Fujimaki (1986); 2, Arth (1976); 3, Gill (1981); 4, Pearce and Norry (1979); 5, Philpotts and Schnetzler (1970) and Schnetzler and Philpotts (1970); 6, Fujimaki et al. (1984); 7, Green and Pearson (1983); 8, Drake and Weill (1975); 9, Matsui et al. (1977); 10, Ewart and Griffin (1994); 11, Dostal et al. (1983); 12, Watson and Green (1981); 13 Botazzi et al. (1999); 14 Dalpe and Baker (1994); 15 Sisson (1994); 16 McKenzie and O'Nions (1991); 17 Hauri et al. (1994); 18 Klemme and Blundy (2002); Kelemen and Dunn (1992); 20 Johnson (1998).

Element	$\mathbf{D^{amph}_{melt}}$	$\mathbf{D^{plag}_{melt}}$	$\mathbf{D^{opx}_{melt}}$	$\mathbf{D^{mt}_{melt}}$	$\mathbf{D^{Gnt}_{melt}}$
Rb	0.29[10]	0.053[5]	0.022[5]	0.01[3]	0.0007[16]
Ba	0.436[9]	0.160[5]	0.013[5]	0.01[3]	0.0007[16]
U	0.10[10]				0.00588[17]
Th	0.50[11]	0.01[5]	0.050[3]	0.10[3]	0.0015[18]
K	0.96[2]	0.12[5]	0.014[5]	0.01[3]	0.0007[19]
Sr	0.46[2]	1.600[5]	0.032[5]	0.01[3]	0.0099[17]
Nb	1.30[4]	0.025[4]	0.350[5]	1.00[3]	0.0538[17]
Zr	1.798[10]	0.010[5]	0.100[3]	0.20[3]	0.9[19]
Hf	1.731[6]	0.015[4]	0.100[3]		0.23[16]
La	0.116[13] (0.039-1.92)	0.302[6]	0.031[6]		0.0164[17] (0.0005-0.121)
Ce	0.185[13] (0.67-4.23)	0.221[6]	0.028[6]	0.20[3]	0.065[16] (0.005-0.144)
Nd	0.396[13] (0.142-8.7)	0.149[6]	0.028[6]		0.087[16] (0.026-0.363)
Sm	0.651[13] (0.651-7.76)	0.102[6]	0.028[6]	0.30[3]	0.217[16] (0.074-1.38)
Eu	0.657[13] (0.351-5.14)	0.079[8]	0.028[6]	0.25[3]	0.32[16] (0.19-2.02)
Gd	0.933[13] (0.368-10)	0.056[8]	0.039[6]		0.498[16] (0.27-5.2)
Ti	3.06[15]	0.050[4]	0.250[6]	12.5[2]	0.1[16]
Y	0.873[13] (0.333-11)	0.060[4]	0.450[6]	0.50[4]	3.1[20] (0.19-9.1)
Dy	0.967[13] (0.78-3.7)				1.06[16] (1.06-4.13)
Er	0.851[13] (0.787-8.2)	0.045[6]	0.153[6]		3.95[17] (2-8)
Yb	0.787[13] (0.31-4.3)	0.041[6]	0.254[6]	0.25[3]	6.6[20] (0.7-8.7)
Lu	0.698[13] (0.246-5.5)	0.039[6]	0.323[6]		7.1[20] (0.061-11.22)

Table 2.5: Results for the Rayleigh fractional crystallization model. Samples from enclaves and the andesitic-dacitic host are included for comparison.

Element	Parent CR1100747	Modeled dacite	Enclave NB1510072IE	LL dacite WBV22100723B
ppm				
Rb	8	22	4	27
Ba	432	1020	389	1054
U	0.8	1.59	0.46	1.65
Th	2.14	3.8	1.81	4.21
K	8560	18850	7554	19400
Sr	808	1256	680	1326
Nb	5.27	7.85	8.54	7.91
Zr	58	79	51	93
Hf	1.87	2.31	2.26	2.41
La	19.09	20.1	10.95	21.02
Nd	18.67	14.76	24.64	15.26
Sm	5.23	2.44	6.48	2.63
Eu	1.12	0.86	1.9	0.88
Gd	3.53	2.02	5.96	2.14
Ti	4796	2893	14268	2980
Y	11.53	5.88	22.72	6.16
Er	1.22	0.55	0.79	0.58
Yb	1.03	0.47	1.72	0.5
Lu	0.13	0.05	0.23	0.06

10. REFERENCES

10.REFERENCES

Abers, G., van Keken, P., Kneller, E., Ferris, A., Stachnik, J., 2006. The thermal structure of subduction zones constrained by seismic imaging: Implications for slab dehydration and wedge flow. Earth and Planetary Science Letters 241, 387-397.

Abratis, M., Worner, G., 2001. Ridge collision, slab-window formation, and the flux of Pacific asthenosphere into the Caribbean realm. Geology 29, 127-130.

Allen, J.C., Boettcher, A.L., 1983. The stability of amphibole in andesite and basalt at high pressures. American Mineralogist 68, 307-314.

Alonso-Perez, R., Müntener, O., Ulmer, P., 2009. Igneous garnet and amphibole fractionation in the roots of island arcs: experimental constraints on andesitic liquids. Contributions to Mineralogy and Petrology 157, 541-558.

Anderson, J.L., Smith, D., 1994. The effects of temperature and ƒ02 on the Al-in-hornblende barometer. American Mineralogist 80, 549-559.

Annen, C., Blundy, J.D., Sparks, R.S.J., 2006. The Genesis of Intermediate and Silicic Magmas in Deep Crustal Hot Zones. Journal of Petrology 47, 505-539.

Aoki, K., Kuno, H., 1972. Gabbro-quartz diorite inclusions from Izu-Hakone Region, Japan. Bulletin of Volcanology 36, 164-173.

Arcay, D., Doin, M., Tric, E., Bousquet, R., De Capitani, C., 2006. Overriding plate thinning in subduction zones: Localized convection induced by slab dehydration, Geochemistry Geophysics Geosystems, p. Q02007.

Arculus, R., Wills, K., 1980. The petrology of plutonic blocks and inclusions from the Lesser Antilles island arc. Journal of Petrology 21, 743-799.

Arth, J., 1976. Behavior of trace elements during magmatic processes-a summary of theoretical models and their applications. J. Res. US Geol. Surv 4, 41ñ47.

Bachmann, O., Bergantz, G.W., 2004. On the origin of crystal-poor rhyolites: extracted from batholithic crystal mushes. Journal of Petrology, 1565-1582.

Bachmann, O., Bergantz, G.W., 2008. Rhyolites and their Source Mushes across Tectonic Settings. Journal of Petrology 49, 2277-2285.

Bachmann, O., Dungan, M.A., Lipman, P.W., 2002. The Fish Canyon magma body, San Juan volcanic field, Colorado: Rejuvenation and eruption of an upper-crustal batholith. Journal of Petrology 43, 1469-1503.

Barckhausen, U., Ranero, C.R., von Huene, R., Cande, S.C., Roeser, H.A., 2001. Revised tectonic boundaries in the Cocos Plate off Costa Rica: Implications for the segmentation of the convergent margin and for plate tectonic models. Journal of Geophysical Research 106, 19207-19220.

Barclay, J., Carmichael, I.S.E., 2004. A hornblende basalt from western Mexico: Water-saturated phase relations constrain a pressure-temperature window of eruptibility. Journal of Petrology 45, 485-506.

Beard, J.S., 1986. Characteristic mineralogy of arc-related cumulate gabbros: Implications for the tectonic setting of gabbroic plutons and for andesite genesis. Geology 14, 848-851.

Bird, P., 2003. An updated digital model of plate boundaries. Geochemistry, Geophysics, Geosystems 4, 1027.

Blundy, J., Cashman, K., Humphreys, M., 2006. Magma heating by decompression-driven crystallization beneath andesite volcanoes. Nature 443, 76-80.

Blundy, J.D., Holland, T.J.B., 1990. Calcic amphibole equilibria and a new amphibole-plagioclase geothermometer. Contributions to Mineralogy and Petrology 104, 208-224.

Boettcher, A., 1973. Volcanism and orogenic belts--the origin of andesites. Tectonophysics 17, 223-240.

Boettcher, A., 1977. The role of amphiboles and water in circum-Pacific volcanism. High pressure research: applications in geophysics 664.

Bottazzi, P., Tiepolo, M., Vannucci, R., Zanetti, A., Brumm, R., Foley, S., Oberti, R., 1999. Distinct site preferences for heavy and light REE in amphibole and the prediction of Amph/L D REE. Contributions to Mineralogy and Petrology 137, 36-45.

Briceno-Guarupe, L., 1978. The crustal structure and tectonic framework of the Gulf of Panama, Geological Sciences. Oregon State University, Corvallis, p. 71.

Camacho, E., Hutton, W., Pacheco, J.F., 2010. A New Look at Evidence for a Wadati-Benioff Zone and Active Convergence at the North Panama Deformed Belt. Bulletin of the Seismological Society of America 100, 343-348.

Carmichael, I.S.E., 2002. The andesite aqueduct: perspectives on the evolution of intermediate magmatism in west-central (105-99 degrees W) Mexico. Contributions to Mineralogy and Petrology 143, 641-663.

Carr, M.J., Feigenson, M.D., Patino, L.C., Walker, J.A., 2003. Volcanism and Geochemistry in Central America: Progress and Problems, in: Eiler, J.M. (Ed.), Inside the Subduction Factory. American Geophysical Union, Washington, pp. 153-174.

Chiaradia, M., Müntener, O., Beate, B., Fontignie, D., 2009. Adakite-like volcanism of Ecuador: lower crust magmatic evolution and recycling. Contributions to Mineralogy and Petrology 158, 563-588.

Cigolini, C., Laiolo, M., Bertolino, S., 2008. Probing Stromboli volcano from the mantle to paroxysmal eruptions. Geological Society London Special Publications 304, 33.

Collins, L., Coates, A., Jackson, J., Obando, J., 1995. Timing and rates of emergence of the Limon and Bocas del Toro Basins: Caribbean effects of Cocos Ridge subduction? Special Paper-Geological Society of America 295, 263-263.

Criss, J.W., 1980. Fundamental parameters calculations on a Laboratory microcomputer. Advance X-ray Analisis 23, 93-97.

Dalpe, C., Baker, D., 2000. Experimental investigation of large-ion-lithophile-element-, high-field-strength-element-and rare-earth-element-partitioning between calcic amphibole and basaltic melt: the effects of pressure and oxygen fugacity. Contributions to Mineralogy and Petrology 140, 233-250.

Davidson, J.P., Hora, J.M., Garrison, J.M., Dungan, M.A., 2005. Crustal forensics in arc magmas. Journal of Volcanology and Geothermal Research 140, 157-170.

Davidson, J.P., Turner, S., Handley, H., Macpherson, C., Dosseto, A., 2007. Amphibole "sponge" in arc crust? Geology 35, 787-790.

de Boer, J.Z., Defant, M.J., Stewart, R.H., Bellon, H., 1991. Evidence for active subduction below western Panama. Geology 19, 649-652.

de Boer, J.Z., Drummond, M.S., Bordelon, M.J., Defant, M.J., Bellon, H., Maury, R.C., 1995. Cenozoic magmatic phases of the Costa Rican island arc (Cordillera de Talamanca). Special Paper Geological Society of America, Boulder, CO.

DeBari, S., Coleman, R., 1989. Examination of the deep levels of an island arc: Evidence from the Tonsina ultramafic-mafic assemblage, Tonsina, Alaska, Journal of Geophysical Research, pp. 4373–4391.

Debari, S., Kay, S., Kay, R., 1987. Ultramafic xenoliths from Adagdak volcano, Adak, Aleutian Islands, Alaska: deformed igneous cumulates from the Moho of an island arc. The Journal of Geology, 329-341.

Deering, C., 2009. Cannibalization of an amphibole-rich andesitic progenitor induced by caldera-collapse during the Matahina eruption: Evidence from amphibole compositions. American Mineralogist 94, 1162-1174.

Deering, C.D., Cole, J.W., Vogel, T.A., 2008. A Rhyolite Compositional Continuum Governed by Lower Crustal Source Conditions in the Taupo Volcanic Zone, New Zealand. Journal of Petrology 49, 2245-2276.

Deering, C.D., Gravley, D., Vogel, T., Cole, J., Leonard, G., 2010. Origins of cold-wet-oxidizing to hot-dry-reducing rhyolite magma cycles and distribution in the Taupo Volcanic Zone, New Zealand. Contributions to Mineralogy and Petrology, 1-21.

Defant, M.J., Clark, L.F., Stewart, R.H., Drummond, M.S., de Boer, J.Z., Maury, R.C., Bellon, H., Jackson, T.E., Restrepo, J.F., 1991. Andesite and dacite genesis via contrasting processes: The geology and geochemistry of El Valle volcano, Panama. Contributions to Mineralogy and Petrology 106, 309-324.

Denyer, P., Baumgartner, P.O., Gazel, E., 2006. Characterization and tectonic implications of Mesozoic-Cenozoic oceanic assemblages of Costa Rica and Western Panama. Geologica Acta 4, 219-235.

Devine, J.D., 1995. Petrogenesis of the basalt-andesite-dacite association of Grenada, Lesser Antilles island arc, revisited. Journal of Volcanology and Geothermal Research 69, 1-33.

Dhuime, B., Bosch, D., Bodinier, J., Garrido, C., Bruguier, O., Hussain, S., Dawood, H., 2007. Multistage evolution of the Jijal ultramafic-mafic complex (Kohistan, N Pakistan): implications for building the roots of island arcs. Earth and Planetary Science Letters 261, 179-200.

Dostal, J., Dupuy, C., Carron, J., Le Guen de Kerneizon, M., Maury, R., 1983. Partition coefficients of trace elements: Application to volcanic rocks of St. Vincent, West Indies. Geochimica et Cosmochimica Acta 47, 525-533.

Drake, M., Weill, D., 1975. Partition of Sr, Ba, Ca, Y, Eu2+, Eu3+, and other REE between plagioclase feldspar and magmatic liquid: an experimental study. Geochimica et Cosmochimica Acta 39, 689-712.

Drummond, M.S., Bordelon, M., Deboer, J.Z., Defant, M.J., Bellon, H., Feigenson, M.D., 1995. Igneous Petrogenesis and Tectonic Setting of Plutonic and Volcanic-Rocks of the Cordillera De Talamanca, Costa-Rica Panama, Central-American Arc. American Journal of Science 295, 875-919.

Dufek, J., Bergantz, G., 2005. Lower crustal magma genesis and preservation: A stochastic framework for the evaluation of basalt-crust interaction. Journal of Petrology 46, 2167.

Esawi, E., 2004. AMPH-CLASS: An Excel spreadsheet for the classification and nomenclature of amphiboles based on the 1997 recommendations of the International Mineralogical Association* 1. Computers & geosciences 30, 753-760.

Ewart, A., Griffin, W., 1994. Application of proton-microprobe data to trace-element partitioning in volcanic rocks. Chemical Geology 117, 251-284.

Femenias, O., Mercier, J., Nkono, C., Diot, H., Berza, T., Tatu, M., Demaiffe, D., 2006. Calcic amphibole growth and compositions in calc-alkaline magmas: Evidence from the Motru Dike Swarm (Southern Carpathians, Romania). American Mineralogist 91, 73-81.

Foden, J.D., Green, D.H., 1992. Possible role of amphibole in the origin of andesite: some experimental and natural evidence. Contributions to Mineralogy and Petrology 109, 479-493.

Fujimaki, H., 1986. Partition coefficients of Hf, Zr, and REE between zircon, apatite, and liquid. Contributions to Mineralogy and Petrology 94, 42-45.

Fujimaki, H., Tatsumoto, M., Aoki, K., 1984. Partition coefficients of Hf, Zr and REE between phenocrysts and groundmasses.

Garcia, M., Jacobson, S., 1979. Crystal clots, amphibole fractionation and the evolution of calc-alkaline magmas. Contributions to Mineralogy and Petrology 69, 319-327.

Gardner, T., Verdonck, D., Pinter, N., Slingerland, R., Furlong, K., Bullard, T., Wells, S., 1992. Quaternary uplift astride the aseismic Cocos ridge, Pacific coast, Costa Rica. Bulletin of the Geological Society of America 104, 219-232.

Gazel, E., Carr, M., Hoernle, K., Feigenson, M., Szymanski, D., Hauff, F., van den Bogaard, P., 2009. Galapagos-OIB signature in southern Central America: Mantle refertilization by arc–hot spot interaction, Geochemistry Geophysics Geosystems, p. Q02S11.

Gill, J., 1981. Orogenic andesites and plate tectonics, 390 pp. Springer, New York 1, 76.

Green, T., Pearson, N., 1983. Effect of pressure on rare earth element partition coefficients in common magmas.

Greene, A., Debari, S., Kelemen, P., Blusztajn, J., Clift, P., 2006. A detailed geochemical study of island arc crust: the Talkeetna arc section, south-central Alaska. Journal of Petrology 47, 1051.

Grove, T.L., Baker, M.B., Price, R.C., Parman, S.W., Elkins-Tanton, L.T., Chatterjee, N., Müntener, O., 2005. Magnesian andesite and dacite lavas from Mt. Shasta, northern California: products of fractional crystallization of H_2O -rich mantle melts. Contributions to Mineralogy and Petrology 148, 542-565.

Grove, T.L., Elkins-Tanton, L.T., Parman, S.W., Chatterjee, N., Muntener, O., Gaetani, G.A., 2003. Fractional crystallization and mantle-melting controls on calc-alkaline differentiation trends. Contributions to Mineralogy and Petrology 145, 515-533.

Gust, D., Johnson, R., 1981. Amphibole-bearing inclusions from Boisa Island, Papua New Guinea: Evaluation of the role of fractional crystallization in an andesitic volcano. The Journal of Geology 89, 219-232.

Hammarstrom, J., Zen, E., 1986. Aluminum in hornblende; an empirical igneous geobarometer. American Mineralogist 71, 1297-1313.

Hannah, R., Vogel, T., Patino, L., Alvarado, G., Pérez, W., Smith, D., 2002. Origin of silicic volcanic rocks in Central Costa Rica: a study of a chemically variable ash-flow sheet in the Tiribí Tuff. Bulletin of Volcanology 64, 117-133.

Hattori, K.H., Guillot, S., Saumur, B.-M., Tubrett, M.N., Vidal, O., Morfin, S., 2010. Corundum-bearing garnet peridotite from northern Dominican Republic: A metamorphic product of an arc cumulate in the Caribbean subduction zone. Lithos 114, 437-450.

Hauri, E.H., Wagner, T.P., Grove, T.L., 1994. Experimental and natural partitioning of Th, U, Pb and other trace elements between garnet, clinopyroxene and basaltic melts. Chemical Geology 117, 149-166.

Hey, R., 1977. Tectonic evolution of the Cocos-Nazca spreading center. Bulletin of the Geological Society of America 88, 1404-1420.

Hidalgo, P.J., 2007. Petrology and geochemistry of El Hato silicic ignimbrite, El Valle volcano, Panama, Geological Sciences. Michigan State, East Lansing, p. 218.

Hidalgo, S., Monzier, M., Martin, H., Chazot, G., Eissen, J.-P., Cotten, J., 2007. Adakitic magmas in the Ecuadorian Volcanic Front: Petrogenesis of the Iliniza Volcanic Complex (Ecuador). Journal of Volcanology and Geothermal Research 159, 366-392.

Hoernle, K., Abt, D.L., Fischer, K.M., Nichols, H., Hauff, F., Abers, G.A., van den Bogaard, P., Heydolph, K., Alvarado, G., Protti, M., Strauch, W., 2008. Arc-parallel flow in the mantle wedge beneath Costa Rica and Nicaragua. Nature 451, 1094-1097.

Hoernle, K., van den Bogaard, P., Werner, R., Lissina, B., Hauff, F., Alvarado, G.E., Garbe-Schoenberg, C.D., 2002. Missing history (16-71 Ma) of Galapagos hotspot; implications for the tectonic and biological evolution of the Americas. Geology 30, 795-798.

Holland, T., Blundy, J., 1994. Non-ideal interactions in calcic amphiboles and their bearing on amphibole-plagioclase thermometry. Contributions to Mineralogy and Petrology 116, 433-447.

Jagoutz, O., 2010. Construction of the granitoid crust of an island arc. Part II: a quantitative petrogenetic model. Contributions to Mineralogy and Petrology 160, 359-381.

Jagoutz, O., Muntener, O., Burg, J.P., Ulmer, P., Jagoutz, E., 2006. Lower continental crust formation through focused flow in km-scale melt conduits: The zoned ultramafic bodies of the Chilas Complex in the Kohistan island arc (NW Pakistan). Earth and Planetary Science Letters 242, 320-342.

Jahn, B.M., Glikson, A.Y., Peucat, J.J., Hickman, A.H., 1981. REE geochemistry and isotopic data of Archean silicic volcanics and granitoids from the Pilbara Block, Western Australia: Implications for early crust evolution. Geochimica et Cosmochimica Acta 45, 1633-1652.

Jan, M., Howie, R., 1981. The mineralogy and geochemistry of the metamorphosed basic and ultrabasic rocks of the Jijal complex, Kohistan, NW Pakistan. Journal of Petrology 22, 85.

Jarrard, R.D., 1986. Relations Among Subduction Parameters. Reviews of Geophysics 24, 217-284.

Johnson, K., 1994. Experimental cpx/and garnet/melt partitioning of REE and other trace elements at high pressures; petrogenetic implications. Mineralogical Magazine 58, 454-455.

Johnson, K., 1998. Experimental determination of partition coefficients for rare earth and high-field-strength elements between clinopyroxene, garnet, and basaltic melt at high pressures. Contributions to Mineralogy and Petrology 133, 60-68.

Johnson, M.C., Rutherford, M.J., 1989. Experimental calibration of the aluminum-in-hornblende geobarometer with application to Long Valley Caldera (California) volcanic rocks. Geology 17, 837-841.

Jull, M., Kelemen, P.B., 2001. On the conditions for lower crustal convective instability, Journal of Geophysical Research. AGU, pp. 6423-6446.

Kay, S.M., Kay, R.W., 1985. Role of crystal cumulates and the oceanic crust in the formation of the lower crust of the Aleutian arc. Geology 13, 461-464.

Kelemen, P., Dunn, J., 1992. Depletion of Nb relative to other highly incompatible elements by melt/rock reaction in the upper mantle. Eos 73, 656-657.

Kellogg, J.N., I. J. Ogujiofor, I.J., Kansakar, D.R., 1985. Cenozoic tectonics of the Panama and North Andes blocks, Mem. Congr. Latinoam. Geol, Bogota, Colombia, pp. 40-59.

Kellogg, J.N., Vega, V., Stallings, T.C., Aiken, C.L.V., 1995. Tectonic development of Panama, Costa Rica, and the Columbian Andes: Constraints from Global Positioning System geodetic studies and gravity in: Mann, P. (Ed.), Geologic and Tectonic Development of the Caribbean Plate Boundary in Southern Central America Geological Society of America, pp. 75-86.

Klemme, S., Blundy, J.D., Wood, B.J., 2002. Experimental constraints on major and trace element partitioning during partial melting of eclogite. Geochimica et Cosmochimica Acta 66, 3109-3123.

Kratzmann, D., Carey, S., Scasso, R., Naranjo, J.-A., 2010. Role of cryptic amphibole crystallization in magma differentiation at Hudson volcano, Southern Volcanic Zone, Chile. Contributions to Mineralogy and Petrology 159, 237-264.

LaFemina, P., Dixon, T.H., Govers, R., Norabuena, E., Turner, H., Saballos, A., Mattioli, G., Protti, M., Strauch, W., 2009. Fore-arc motion and Cocos Ridge collision in Central America. Geochem. Geophys. Geosyst. 10.

Larocque, J., Canil, D., 2010. The role of amphibole in the evolution of arc magmas and crust: the case from the Jurassic Bonanza arc section, Vancouver Island, Canada. Contributions to Mineralogy and Petrology 159, 475-492.

Leake, B., Woolley, A., Arps, C., Birch, W., Gilbert, M., Grice, J., Hawthorne, F., Kato, A., Kisch, H., Krivovichev, V., 1997. Nomenclature of amphiboles; report of the subcommittee on amphiboles of the International Mineralogical Association, Commission on New Minerals and Mineral Names. Canadian Mineralogist 35, 219.

LeBas, M.J., LeMaitre, R. W., Streckeisen, A. Zanettin, B., 1986. A chemical classification of volcanic rocks based on the total alkali silica diagram. Journal of Petrology 27, 745-750.

Lee, C., Cheng, X., Horodyskyj, U., 2006. The development and refinement of continental arcs by primary basaltic magmatism, garnet pyroxenite accumulation, basaltic recharge and delamination: insights from the Sierra Nevada, California. Contributions to Mineralogy and Petrology 151, 222-242.

Lonsdale, P., 2005. Creation of the Cocos and Nazca plates by fission of the Farallon plate. Tectonophysics 404, 237-264.

Lonsdale, P., Klitgord, K.D., 1978. Structure and tectonic history of the eastern Panama Basin. Geological Society of America Bulletin 89, 981-999.

Macpherson, C.G., 2008. Lithosphere erosion and crustal growth in subduction zones: Insights from initiation of the nascent East Philippine Arc. Geology 36, 311-314.

Mann, P., Kolarsky, R.A., 1995. East Panama deformed belt: Age, structure, neotectonic significance, in: Mann, P. (Ed.), Geologic and Tectonic development of the Caribbean plate boundary in southern Central America. Geological Society of America Special Paper Geological Society of America, Boulder, pp. 111-129.

Matsui, Y., Onuma, N., Nagasawa, H., Higuchi, H., Banno, S., 1977. Crystal structure control in trace element partition between crystal and magma. Bull. Soc. Fr. Mineral. Cristallogr 100, 315ñ324.

Mckenzie, D., O'nions, R.K., 1991. Partial Melt Distributions from Inversion of Rare Earth Element Concentrations. Journal of Petrology 32, 1021-1091.

Melekhova, E., Blundy, J., 2008. Experimental Constraints on Basalt Differentiation in the Deep Crust, American Geophysical Union, Fall Meeting 2008. AGU, San Francisco, p. 2175.

Meschede, M., Barckhausen, U., Worm, H.U., 1998. Extinct spreading on the Cocos Ridge. Terra Nova 10, 211-216.

Miyashiro, A., 1974. Volcanic rock series in island arcs and active continental margins. American Journal of Science 274, 321.

Moore, G., Carmichael, I., 1998. The hydrous phase equilibria (to 3 kbar) of an andesite and basaltic andesite from western Mexico: constraints on water content and conditions of phenocryst growth. Contributions to Mineralogy and Petrology 130, 304-319.

Morell, K.D., Fisher, D.M., Gardner, T.W., 2008. Inner forearc response to subduction of the Panama Fracture Zone, southern Central America. Earth and Planetary Science Letters 265, 82-95.

Müntener, O., Kelemen, P.B., and Grove, T.L., 2001. The role of H_2O during crystallization of primitive arc magmas under uppermost mantle conditions and genesis of igneous pyroxenites: An experimental study. Contributions to Mineralogy and Petrology 141, 643-658.

Newhall, C.G., 1979. Temporal variation in the lavas of Mayon volcano, Philippines. Journal of Volcanology and Geothermal Research 6, 61-83.

Pearce, J., Norry, M., 1979. Petrogenetic implications of Ti, Zr, Y, and Nb variations in volcanic rocks. Contributions to Mineralogy and Petrology 69, 33-47.

Philpotts, J., Schnetzler, C., 1970. Phenocryst-matrix partition coefficients for K, Rb, Sr and Ba, with applications to anorthosite and basalt genesis. Geochimica et Cosmochimica Acta 34, 307-322.

Rausch, S., 2008. Geochemical signatures in subduction zone magmatism at Volcan Baru Geological Sciences. Georg- August-Universität Göttingen Göttingen p. 110.

Restrepo, J., 1987. A geochemical investigation of Pleistocene to Recent calc-alkaline volcanism in western Panama, Geologial Sciences. University of South Florida, Tampa, p. 103.

Rodriguez, C., Selles, D., Dungan, M., Langmuir, C., Leeman, W., 2007. Adakitic Dacites Formed by Intracrustal Crystal Fractionation of Water-rich Parent Magmas at Nevado de Longavi Volcano (36º 2´ S); Andean Southern Volcanic Zone, Central Chile. Journal of Petrology 48, 2033-2061.

Rooney, T.O., Franceschi, P., Hall, C., 2010a. Water Saturated Magmas in the Panama Canal Region – A Precursor to Adakite-Like Magma Generation? Contrib. Mineral. Petrol.

Rooney, T.O., Franceschi, P., Hall, C., 2010b. Water Saturated Magmas in the Panama Canal Region – A Precursor to Adakite-Like Magma Generation? Contributions to Mineralogy and Petrology.

Roy, A., 1988. Evolution of the Igneous Activity in Southeastern Costa Rica and Southwestern Panama from the Middle Tertiary to the Recent, Geological Sciences. Lousianna State University, Baton Rouge, p. 301.

Rudnick, R., Fountain, D., 1995. Nature and composition of the continental crust: A lower crustal perspective. Reviews of Geophysics 33, 267-310.

Rudnick, R.L., Gao, S., 2005. Composition of the Continental Crust, in: Rudnick, R.L. (Ed.), The Crust. Elsevier, Kidlington, UK, pp. 1-64.

Rutherford, M., Hill, P., 1993. Magma ascent rates from amphibole breakdown: an experimental study applied to the 1980–1986 Mount St. Helens eruptions. Journal of Geophysical Research-Solid Earth 98.

Scaillet, B., Evans, B., 1999. The 15 June 1991 eruption of Mount Pinatubo. I. Phase equilibria and pre-eruption PT-fO2-f H_2O conditions of the dacite magma. Journal of Petrology 40, 381.

Schmidt, M.W., 1992. Amphibole composition in tonalite as a function of pressure: an experimental calibration of the Al-in-hornblende barometer. Contributions to Mineralogy and Petrology 110, 304-310.

Schnetzler, C., Philpotts, J., 1970. Partition coefficients of rare-earth elements between igneous matrix material and rock-forming mineral phenocrysts--II. Geochimica et Cosmochimica Acta 34, 331-340.

Sherrod, D.R., Vallance, J.W., Tapia-Espinoza, A., McGeehin, J.P., 2007. Volcan Baru, Eruptive History and Volcano Hazards Assessment, Open-File Report 2007-1401. U.S. Geological Survey p. 33.

Sisson, T., 1994. Hornblende-melt trace-element partitioning measured by ion microprobe. Chemical Geology 117, 331-344.

Sisson, T.W., Bacon, C.R., 1999. Gas-driven filter pressing in magmas. Geology 27, 613-616.

Sisson, T.W., Grove, T.L., 1993. Experimental investigation of the role of H_2O in calc-alkaline differentiation and subduction zone magmatism. Contributions to Mineralogy and Petrology 113, 143-166.

Spear, F., 1981. An experimental study of hornblende stability and compositional variability in amphibolite. American Journal of Science 281, 697.

Sun, S., McDonough, W.F., 1989. Chemical and isotopic systematics of oceanic basalts: implications for mantle compositions and processes., in: Saunders, A.D., Norry, M.J. (Eds.), Magmatism in the Ocean Basins. Geological Society Special Publications, pp. 313-345.

Tamura, Y., Tatsumi, Y., 2002. Remelting of an andesitic crust as a possible origin for rhyolitic magma in oceanic arcs: An example from the Izu-Bonin arc. Journal of Petrology 43, 1029-1047.

Tatsumi, Y., Takahashi, T., Hirahara, Y., Chang, Q., Miyazaki, T., Kimura, J.I., Ban, M., Sakayori, A., 2008. New Insights into Andesite Genesis: the Role of Mantle-derived Calc-alkalic and Crust-derived Tholeiitic Melts in Magma Differentiation beneath Zao Volcano, NE Japan. Journal of Petrology 49, 1971-2008.

Thomas, W., Ernst, W., 1990. The aluminium content of hornblende in calc-alkaline granitic rocks: A mineralogic barometer calibrated experimentally to 12 kbars. Geochemical Society Special Publication 2, 59-63.

Trenkamp, R., Kellogg, J.N., Freymueller, J.T., Mora, H.P., 2002. Wide plate margin deformation, southern Central America and northwestern South America, CASA GPS observations. Journal of South American Earth Sciences 15, 157-171.

Vogel, T.A., Flood, T.P., Patino, L.C., Wilmont, M.S., Maximo, R.P.R., Arpa, C.B., Arcilla, C.A., Stimac, J.A., 2006. Geochemistry of silicic magmas in the Macolod Corridor, SW Luzon Philippines: evidence of distinct, mantle-derived, crustal sources for silicic magmas. Contributions to Mineralogy and Petrology 151, 267-281.

Walker, J.A., 1984. Volcanic rocks from the Nejapa and Granada cinder cone alignments, Nicaragua, Central America. Journal of Petrology 25, 299-342.

Walther, C.H.E., 2003. The crustal structure of the Cocos ridge off Costa Rica. Journal of Geophysical Research-Solid Earth 108, DOI: 10.1029/2001JB000888.

Watson, E., Green, T., 1981. Apatite/liquid partition coefficients for the rare earth elements and strontium. Earth and Planetary Science Letters 56, 405-421.

Werner, R., Hoernle, K., Barckhausen, U., Hauff, F., 2003. Geodynamic evolution of the Galápagos hot spot system (Central East Pacific) over the past 20 my: Constraints from morphology, geochemistry, and magnetic anomalies. Geochemistry, Geophysics, Geosystems 4, 1108.

Westbrook, G.K., Hardy, N.C., Heath, R.P., 1995. Structure and tectonics of the Panama-Nazca plate boundary, in Geologic. Geological Society of America Special Paper 295, 91-110.

Yamamoto, M., 1988. Picritic primary magma and its source mantle for Oshima- shima and back-arc side volcanoes, Northeast Japan arc. Contributions to Mineralogy and Petrology 99, 352-359.

CHAPTER THREE PETROGENESIS OF A VOLUMINOUS QUATERNARY ADAKITIC VOLCANO: THE CASE OF BARU VOLCANO.

1. INTRODUCTION

Rates of magma formation, transfer, storage and eruption beneath arc volcanoes provide important insights into the physical processes active in subduction zones (Hawkesworth et al., 2004; Zellmer et al., 2005; Zellmer et al., 2003). These physical processes are directly related to thermal structure of the arc and may aid in the identification of magma sources and contributions from the different components involved during magma generation. For example, regional short-lived isotope studies of destructive plate magmatism have indicated that partial melting is induced by fluid release from the subducting oceanic crust and that this typically occurs 20-50 ky prior to eruption (Elliott, 1997; Hawkesworth et al., 1993; Hawkesworth et al., 1997; Sigmarsson et al., 1991; Turner et al., 2003; Turner et al., 1997; Turner et al., 2006). Rates of magma formation within a given arc and in particular the concept of volcanic output rates (Qe) (Crisp, 1984; Wadge, 1984), may be of particular utility in placing constraints on models discussing the origin of atypical arc rocks such as adakites that require conditions different to that which occur in most arcs (Aguillon-Robles et al., 2001; Castillo et al., 1999; Defant et al., 2002; Kay and Kay, 2002; Macpherson et al., 2006).

The origin of adakite-like magmas remains controversial as its initial usage had petrogenetic significance. Adakites were initially hypothesized to have been derived from direct melting of the eclogitized subducting oceanic crust (not sediments, as is typical) and are observed only infrequently in subduction settings (Defant, 1990; Defant et al., 1991a; Kay, 1978; Kay and Kay, 2002; Kay et al., 1993). However, many other models have been proposed for their origin: lower crust fractionation of mantle derived magmas (e.g., Macpherson et al., 2006), and partial melting of underplated basaltic lower crust (e.g., Rapp and Watson, 1995). The intense study of adakite magmas since their recent rediscovery (Defant, 1990) has yielded important thermal constraints on the generation of melts from the subducting oceanic crust. Partial melting models of the subducting slab predict low melt productivity (Liang, 2003; Peacock et al., 1994; Prouteau and Scaillet, 2003), consistent with inferences that adakites derived from the subducting slab, are volumetrically insignificant when compared to the volume of typical arc magmas (Castillo, 2006; Gazel et al., 2009; Hoernle et al., 2008). Detailed chronological and geochemical studies of individual adakitic edifices allows for the deduction of the Qe parameter, which has been correlated directly to the rates of magma generation deep within subduction zones (White et al., 2006). By providing temporal and mass balance estimates, we provide constraints on the possible petrogenetic processes involved in the generation of adakites.

We have collected more than 100 samples from an exceptionally well-controlled stratigraphic sequence at Baru volcano in Panama where adakite-like magmas have been previously reported (Defant, 1990; Hidalgo and Rooney, 2010; Restrepo, 1987; Sherrod et al., 2007). We explore the hypothesis that adakite-like magmas erupted at Baru volcano, are derived from typical arc magmas by high-pressure fractionation processes (e.g. Hidalgo & Rooney 2010). By combining detailed stratigraphy, $^{40}Ar/^{39}Ar$ dating , and geochemical characterization we show that (1) the entire volcanic edifice at Baru volcano is constructed from magmas with of adakite-like composition, (2) the volume of volcanism at Baru is substantial (~450 km^3) and comparative to other arc volcanoes such as Mt. Shasta or Irazu (3) that most of the volcanic edifice of Baru volcano was constructed extremely rapidly (less than ~213 k.a.) in comparison to other typical adakitic volcanoes (Adagdak and Cook), but in time frames that have been observed in typical arc volcanoes, (4) the Qe values are much higher in Baru volcano in comparison to any of the archetypical adakite volcanoes, and (5) there are is no significant difference between the calculated values of Qe for Baru with other arc volcanoes. These observations support regional models that explain the adakite signatures from Baru as derived from flux-induced mantle melting that later fractionated in the lower crust rather than melting of the subducting slab (Hidalgo and Rooney, 2010).

2. TECTONIC SETTING AND MAGMATIC HISTORY

The region where Baru volcano is located is tectonically very complex, with a convergent margin on the southern side and a largely passive margin on the northern side (Figure 3.1). The present day plate configuration was produced by the split of the Farallon plate in to the Nazca and Cocos plates during the early Miocene (~23) (Lonsdale, 2005). The byproducts of this event included: (1) change of spreading direction at the East Pacific Rise (Goff and Cochran, 1996; Wilson, 1996) and (2) faster and less oblique subduction at subduction margins of the Americas (Sempere et al., 1990; Sigurdsson et al., 2000). The subduction of the Cocos plate is normal to the middle America trench (76-91 mm/yr, DeMets, 2001; Trenkamp et al., 2002) while the Nazca plate subduction is oblique (50 mm/yr: Jarrard, 1986; Trenkamp et al., 2002) (Figure 3.1). The boundary between the Cocos and the Nazca Plates are the seismically active right-lateral Panama Fracture-Balboa Fracture-Coiba Fracture zones. The triple junction generated by the intersection of the Panama fracture zone with the trench is migrating southeast at ~55 mm/yr (Morell et al., 2008). Throughout Panama and in southern Costa Rica the Caribbean plate is underthrusting Central America along the North Panama Deformed Belt (Kellogg and Vega, 1995; Mann and Kolarsky, 1995).

Subduction zone magmatism has been active in Panama since early the early Tertiary (Lissinna et al., 2006; Maury et al., 1995). In that time period, three volcanic arcs have been identified: (1) The Oligocene arc, which is characterized by tholeiitic to (low-K) calc-alkaline volcanism (Abratis and Worner, 2001; Alvarado et al., 1992; de Boer et al., 1995) (2) The Miocene arc, which is characterized by a continuum of low-K calc-alkaline through high-K calc-alkaline lava compositions (Wegner et al., 2011). (3) The currently active arc commenced with spatially widespread volcanism displaying an adakite-like signature in western Panama and southern Costa Rica at ~2 Ma (Abratis and Worner, 2001; Defant et al., 1991a; Defant et al., 1991b; Johnston and Thorkelson, 1997). Baru volcano is located in Western Panama, 35 km east of the Costa Rica – Panama border at the eastern terminus of the Talamanca Cordillera and is one of the most significant edifices in the modern arc. The summit of the volcano at 3,374 m, overlooks populated valleys 2,000 m below. In this massive composite stratovolcano (350 km^3-450 km^3) a large sector collapse that has exposed lower stratigraphic levels (Sherrod et al., 2007). Sampling within the sector collapse scar, has allowed for a complete record of the stratigraphic sequence of Baru volcano. In this study we have subdivided the quaternary volcanic sequence in 4 main units on the basis of: (1) field stratigraphy, that has allowed for the identification of some of the contacts between units, (2) $^{40}Ar/^{39}Ar$ geochronology, and (3) the petrography and (4) geochemistry of Baru volcano, which vary consistently across the stratigraphic column. The units are La Cuesta, Aguacate, Nuevo Bambito and Volcan (Figure 3.2).

3. ANALYTICAL TECHNIQUES

3.1 Geochronology

8 representative samples that exhibited minimal alteration were selected for $^{39}Ar/^{40}Ar$ step heating analysis at the Argon Geochronology Laboratory at the University of Michigan. Fresh matrix chips (0.2g) were carefully handpicked under a binocular microscope and Ar analysis was undertaken using standard procedures outlined in Frey et al., (2007). Samples were wrapped in pure Al foil packets and irradiated in location 5C of the McMaster Nuclear Reactor. Samples were step-heated using a continuous 5W Ar-ion laser and Ar isotopes were analyzed using a VG- 1200S mass spectrometer operating with a total electron emission setting of 150 micro-amps. The mass spectrometer is equipped with a Faraday detector and a Daly detector operated in analog mode. All samples were analyzed with the Daly detector. Mass discrimination

(source + detector) was monitored daily with ~4x10^{-9} ccSTP of atmospheric Ar. Typically, the measured atmospheric $^{40}Ar/^{36}Ar$ ratio has been about 290 for the past several years. All measured isotope measurements were corrected for a standard $^{40}Ar/^{36}Ar$ value of 295.5. Isotope measurements were fitted to a signal decay plus memory effect function and extrapolated back to inlet time. Error estimates for each isotope were based upon the fit of individual measurements to the signal decay function and these 5 isotope error estimates were propagated through all isotope ratios, J values and age estimates. Isotope concentration values for ^{37}Ar and ^{39}Ar were corrected for decay since the samples were irradiated. Corrections were made for interference reactions from Ca and K and for the build-up of ^{36}Ar from the decay of ^{36}Cl. Within the irradiation packages, samples were interspersed with standards packets and J was calculated for samples by interpolating a fitted cosine function for J as a function of vertical position within the can. J error estimates include the uncertainties in the isotope measurements for the standards plus any scatter of measured J about the fitted interpolating function. J error does not include uncertainty in the assumed K-Ar age, nor does it include decay constant uncertainties.

3.2 Major and Trace elements.

Samples (1-2 kg) were taken from the least-altered outcrops. They were subsequently trimmed to exclude visible alteration/weathering. Sample billets were polished to remove saw marks and cleaned in an ultra sonic bath with deionized water. After drying, the billets were crushed in a steel jaw-crusher and then powdered in a ceramic Bico flat plate grinder. The sample powders were fused into lithium tetraborate glass disks using the procedures outlined in Deering et al. (2008). Major elements, Zr, Sr, Rb and Ni were analyzed by Brucker XRF, the balance of the trace elements were obtained by laser-ablation using a Cetac LSX-200 coupled to a Micromass Platform ICP-MS at Michigan State University. Trace element reproducibility based on standard analyses is typically better than 5% (Vogel et al., 2006). Results of these analyses are presented in the supplementary material of this study.

4. RESULTS

4.1 ^{40}Ar/^{39}Ar Results

A summary of the calculated ages is provided in Table 3.1 and Figure 3.2; and a complete data table is provided in the Appendix. All ages are quoted to the ± 1-σ level. All units were processed using whole rock samples. Geologically meaningful plateau and plateau ages were obtained from whole rock samples (Appendix B). High Ca/K fractions were excluded from plateau calculations, as these were likely due to the degassing of feldspar phenocrysts. The calculated ages are described with detail in the next subsection.

4.2 Stratigraphy and geochemistry

(21-71 Ma) Local Basement, Caribbean Large Igneous Province.

The regional basement in western Panama is commonly referred to as an over thickened section of the lithosphere composed of oceanic assemblages (21 Ma to 71 Ma, Hoernle et al., 2002). This local basement is part of the Caribbean Large Igneous Province (CLIP), which is related to Galapagos hot spot; these assemblages are referred to as the Azuero-Soná Complex. The CLIP outcrops in the Azuero and Soná peninsulas, and various islands of the Chiriquí and Montijo gulfs (Denyer et al., 2006). The thickness of crust is has been estimated at ~50 km north of Baru volcano in the Talamanca cordillera (Dzierma et al., 2010).

(~5- ~15 Ma) Late Miocene arc in the Baru volcano area

The Northern elevations that surround Baru volcano (Figure 3.2) are composed of an undetermined number of pyroclastic flows, lava flows and lahar deposits (Sherrod et al., 2007). These deposits are not part of the modern volcanic edifice and have been attributed to effusive activity during the Late Miocene (de Boer et al., 1995). This volcanic sequence has not been dated, and is the subject of ongoing research. More importantly, these deposits have not been found in the lower stratigraphic sequence at Baru volcano. This observation may indicate that the volcanic arc has migrated slightly southward from its original location during the Late Miocene.

(~0.213-~0.122 Ma) La Cuesta unit (Px+Ol dominated)

The La Cuesta unit is the oldest in the Quaternary sequence (0.213 ± 0.048 Ma – 0.122 ± 0.055 Ma, table 3.1, Figure 3.2) and is composed of voluminous lava flows. It has been further subdivided in two subunits based on age and chemical characteristics. The lower subunit outcrops in river canyons in the vicinity of La Cuesta (Figure 3.1) and lays uncomformably over volcanic lahar deposits related to the Late Miocene Panamanian arc (Figure 3.2). This lower unit records the oldest $^{40}Ar/^{39}Ar$ age in the Quaternary (0.213 ± 0.048 Ma, table 3.1). The upper subunit outcrops on the eastern flank of the edifice (in Bajo Mono, Figure 3.1), where the base of the headwall of an ancient debris avalanche scarp has exposed lower stratigraphic levels. In this location, $^{40}Ar/^{39}Ar$ calculated dates for this unit are slightly younger and range from 0.185 ± 0.058 Ma to 0.122 ± 0.055 Ma (Table 3.1).

Petrographically, the La Cuesta unit is characterized by abundant olivine (5-12%), plagioclase (12-15%) and pyroxene (~5-9%) in a hypocrystalline groundmass (Table 3.2). The lower section of this unit contains amphibole ghosts, probably xenocrysts from lower crustal levels, while in the upper section these ghosts are absent. In addition, the upper subunit is more olivine rich (up to ~15%), while the lower subunit is pyroxene rich (up to 9%). Chemically, the lower subunit ranges from 52-56 % SiO_2 1-

1.1 % TiO_2 and 4-8% MgO (basaltic andesite), while the upper subunit ranges from 47-49% SiO_2, ~0.8 % TiO_2 and 10-15% MgO (Figs. 3.3, 3.4). The differences between these subunits might be associated to their evolutionary trend. The lower subunit magmas have experience fractionation from primary basalts, while samples from the upper subunit have either experience pyroxene and/or olivine accumulation (high Ni and Cr) or represent melts that were in equilibrium with mantle peridiotites (Hidalgo et al. 2012).

Compared to other units at Baru volcano, La Cuesta Unit has higher TiO_2, CaO, Fe_2O_3 and P_2O_5 (Figure 3.4). In addition, this unit is characterized by high Mg# (within the HMA field, 55-70, Figure 3.3), high Ni and Cr, lower large ion lithophile elements (LILE) and higher high field strength elements (HFSE) than other Quaternary units at Baru volcano The rare Earth elements (REE) are more enriched than other Quaternary units, however when compared to typical Central American volcanic arc magmas the heavy REE are distinctly depleted (Figure 3.5, 3.6). Low heavy REE and Y concentrations (Figure 3.6), high La/Yb and high Sr/Y ratios (Figure 3.3) in La Cuesta unit, are clear indicators for the adakitic signature in this unit. However, this signature is considerably weaker than that found in the other Quaternary units of Baru.

(~0.122 - 0 Ma) Bambito Unit (px dominated)

This unit outcrops on the northwest flank of Baru volcano outside the depression left by the sector collapse and it has been dated at -0.018 ± 0.051Ma (Table 3.1). These lavas are observed to rest uncomformably over the La Cuesta group at Bajo Mono, and are overlain by the Aguacate unit at Nuevo Bambito (Figs. 3.1 and 3.2), which clarifies the uncertainties derived from the $^{40}Ar/^{39}Ar$ derived ages (Table 3.1 Figure 3.2).

Samples from this unit are crystal rich and are composed of pyroxene (15%), amphibole (8%), plagioclase (20%) and olivine (2%) (Table 3.2). In addition, lavas contain abundant olivine+enstatite cumulate enclave material where amphibole and plagioclase have crystallized interstitially and clinopyroxene has crystallized as a reaction rim around the cumulate enclave nodules. Olivine and orthopyroxene in the cumulate nodules display incipient triple junction contacts with abundant glass. In some samples pyroxene surrounded by amphibole is widespread; clinopyroxene surrounding olivine crystals is also frequent. This type of cumulate material is also observed in La Cuesta unit, although more infrequently.

Samples from this unit are medium- to high-K and high-magnesium basaltic andesites to andesites (Mg# 60-70) (Figure 3.3). Typically, this unit has higher concentrations of K_2O, Na_2O, LILE, middle REE and light REE, Ni, Cr and lower concentrations of, FeO, CaO, Al_2O_3 and TiO_2 when compared to other Central American arc lavas (Figure 3. 3. 3.4, 3.5, 3.6). The heavy REE are more depleted than in La Cuesta unit and are comparable to the ones observed in the overlying Aguacate unit. In addition, the Bambito unit is characterized by elevated Sr/Y and La/Yb, a signature typical in adakite-like rocks (Figure 3.3).

(0 Ma) Cerro Aguacate unit (Amph+Px)

This unit outcrops at the summit and in the flanks of Baru volcano. The most recent dates for this unit are recorded in the summit of Baru volcano (-0.030±0.044 Ma**)**; while in the East flank of the volcano these lavas have been dated at -0.001±0.043 Ma in Bajo Boquete and in the west flank at Cerro Aguacate at 0.011±0.020 Ma (Table 3.1, Figure 3.1, 3.2). On the east flank, these lavas are exposed in a series of faults that have uncovered lower stratigraphic levels, while in the west flank they outcrop on a collapse scar that has exposed this unit. These lavas are observed to rest uncomformably over the Bambito unit at Bajo Mono. This observation clarifies the uncertainties derived from the $^{40}Ar/^{39}Ar$ derived ages (Table 3.1 Figure 3.2).

Petrographically, this unit has abundant amphibole (10-15%) and clinopyroxene (~10) with plagioclase (20-30%) and olivine (3-5%). Amphibole occurs mostly as a phenocryst phase, but occasionally it can be observed within plagioclase reaction rims that surround enclave cumulate nodule material. These enclave nodules are mainly composed of olivine and orthopyroxene.

All samples from this unit are medium to high K-andesites (SiO_2 57-62%) (Figure 3.3), with high Mg# (50-60). The Aguacate unit has similar major element composition to the overlying Volcan unit, except for an alkali content that is typically higher in the former. Trace elements abundances are also similar to the Volcan unit, except for the LILE and heavy REE elements, which are consistently higher in the Aguacate unit (Figure 3.6). The variation between these units is treated during the discussion of the Volcan unit.

Compared to Central American volcanic front lavas, the Aguacate unit has higher concentrations of K_2O, Na_2O, LILE, middle REE and light REE, Ni, Cr and lower concentrations of, FeO, CaO, Al_2O_3 and TiO_2 (Figure 3.4, 3.5, 3.6).

Volcan Unit (upper ~500 YBP), Domes unit (-0.008Ma ± 0.036), Amphibole rich

The Volcan unit rests at the top of the volcanic sequence and could be subdivided according to age in two subunits: Lower subunit and upper subunit (Figure 3.2). The lower subunit is composed of andesitic to dacitic lavas (-0.008 ± 0.036 Ma) that have constructed the dome sequence at the summit of the volcanic edifice. The upper unit corresponds with recent (~500 YBP) andesitic pyroclastic flows that have been extensively described and dated by Sherrod et al (2007).

These subunits have only one mafic phase (amphibole) and have similar chemistry. Chemical analyses from this subunits show that they are metaluminous calc-alkaline andesites, with a few samples extending into the dacite field. They generally present little variation in most of the major and trace elements (Figs. 3.4, 3.5 and 3.6). Compared to other units they have distinctively low K_2O, high, Na_2O, TiO_2, Y and high

Sr at a given SiO_2 content. Both of the subunits in this unit have depleted heavy REE, low Y, high Sr, high Sr/Y, and low K_2O / Na_2O) that is typical of adakite-like volcanism.

The low K_2O, high, Na_2O, TiO_2, depleted HREE (and Y) and high Sr and SiO_2, of this unit when compared to the Aguacate unit are associated with the dissimilar fractionating assemblage in between these units. Aguacate lavas present pyroxene +amphibole +olivine +plagioclase while the fractionating assemblage at the Volcan unit is controlled by amphibole (Hidalgo and Rooney, 2010). An important consequence of early removal of large quantities of amphibole from water-saturated magmas (e.g. Volcan unit; Hidalgo and Rooney, 2010) is that this process would rapidly increase the SiO_2 (and K_2O) content of the residual magmas (*Carmichael*, 2002). In comparison with gabbroic assemblages (e.g. Aguacate unit), amphibole fractionation will rapidly elevate differentiation indices with relatively less mass removal. A geochemical consequence of these contrasting fractionation paths is that trace elements concentrations within a hydrous-magma increase far less than in a dry magma at similar SiO_2 due to the lower volume of mass removed from the hydrous magmas (*Rooney et al.*, 2010). Increased amphibole fractionation may explain why samples from Volcan unit exhibit more depleted REE than the Aguacate unit and other dissimilarities between these units.

5. DISCUSSION

In the previous section, our $^{40}Ar/^{39}Ar$ results showed that volcanism at Baru volcano is juvenile. Our geochemical results confirmed that at all stratigraphic levels, Baru volcano is an adakitic volcano. It has been suggested that melting of the subducting slab is responsible for the recent adakitic signature along the Panamanian volcanic front, and specifically at Baru volcano (Clark, 1989; de Boer et al., 1991; de

Boer et al., 1995; Defant et al., 2002; Defant, 1990; Defant et al., 1991a; Defant et al., 1992; Drummond et al., 1995; Drummond and Defant, 1990). However, the origin of the adakitic signature is equivocal and may be produced through a number of processes that do not require the partial melting of the oceanic crust (Atherton and Petford, 1993; Castillo et al., 1999; Eiler et al., 2007; Kay and Kay, 2002; Kessel et al., 2005). Morphometric indicators and magmatic output rates from Baru volcano can be used to investigate the possible modes of origin of Baru magmas. To aid in with our approach, we have included in our analyses data from key localities (Cook Island and Adagdak volcano) where the involvement of subducting slab melts is well constrained.

5.1 Morphometry of Baru volcano

Volcano edifice shape and size is a consequence of the interplay between constructive and destructive (erosional and deformational) processes (Grosse et al., 2009). During a volcano's life, its shape evolves depending on the prevailing processes. Thus, volcano morphology potentially contains information on the balance of such factors as age, growth stage, composition, eruption rate, vent position and migration, degree of erosion lava/tephra ratio, deformation, and ultimately and more importantly for the context of this study, it may contain information of underlying factors such as magma flux and petrotectonic setting (Grosse et al., accepted). As detailed in the previous section, Baru volcano has grown extremely fast (~213 ka) and has reached volcanic edifice instability just as fast

Using morphometric parameters such as: volcanoes height/ width, summit width/ base width, ellipticity index (contour elongation) and irregularity indexes (contour complexity) Grosse at al (2009) have grouped volcanic edifices from Central American volcanic front (CAVA) and the South America Central volcanic zone (SACVZ) in discrete morphometric classes that suggest distinct evolutionary trends. Despite different tectonic settings used in their study (CAVA oceanic arc and South American continental arc), the two studied arcs have volcanoes that are in similar morphometric classes (Figure 3.7). This suggests that volcano morphometry depends on general processes and tectonic setting is a secondary factor (Grosse et al., 2009). In figure 3.7, we have plotted morphometric aspects of Baru volcano (volume, height, width and elipticity index) alongside with other volcanic centers that fall in the sub-cones, cones and massif categories described extensively in Grosse et al. (2009) from South America and the CAVA. The morphometric characteristics found at Baru volcano are those typically found in massif type volcanoes that develop by volume increase with limited high increase (Grosse et al., 2009), while other adakitic volcanoes (Cook and Adagdak) that have been interpreted as type localities for slab melts (Kay, 1978; Peacock et al., 1994) are morphometrically similar to sub-cones and/or cones. Sub-cones and cones have been described to evolve by progressive vent migration (Grosse et al., 2009)

5.2 Volcanic rates

From the data we have presented, it is apparent that volcanic edifices in subduction environments where melting of the subducting slab is considered the controlling magma generation process, tend to be considerably smaller than volcanic edifices that have been derived by typical arc volcanism (Figure 3.7). These contrasting properties could be attributed to local tectonics and magma fluxes: for example, in Nicaragua, sub-cones and massifs (large volcanic centers) are located on fault zones, while cones (small volcanic centers) are on undisturbed crust where eruptive rates tend to be lower (van Wyk de Vries, 1993; van Wyk de Vries et al., 2007). However, such larger fault zones have not been identified at Baru volcano and there is no active seismicity in the region. In addition, the balance of constructive and destructive processes at Baru volcano can be obviated; even without counting the volume removed by a large debris avalanche collapse (50 km^3) Baru volcano volume is still comparable to large massifs such as Shasta and Irazu. These constrains indicate that the expedite construction of large volcanic edifice must be controlled by magmatic fluxes.

Rates of magma generation and eruption are key factors that affect the petrological and geochemical evolution of magma bodies as well as eruptive styles due to the intrinsic coupling between magma recharge, fractional crystallization, wall rock assimilation and melt volatile saturation (Shaw, 1985; Spera et al., 1982). In figure 3.8, we have compared the volcanic output rates at Baru volcano with rates at other adakitic volcanoes considered to be type localities for slab melts. Volcanic output rates at Baru volcano have the high rates observed in typical oceanic arc environments (Figure 3.8). These output rates are dissimilar to the ones observed for Cook Island and Adagdak volcano, which are much smaller. Output rates at these volcanic centers are remarkably low and are comparable to lowest values observed in oceanic or continental arc environments. White et al. (2006) determined that oceanic hot spots, oceanic arcs, and ridges have an average volcanic output rate of 10^{-2} km^3/yr while continental arcs and continental hot spots have an average output rate of 10^{-3} km^3/yr, implying that thinner crust/lithosphere facilitates higher volcanic output rates on average. Despite being built over thin crust, Adagdak and Cook Islands have Qes that might be controlled by magma generation processes rather than crustal features.

Hardee (1982) showed that there is a critical volcanic output rate of ~10^{-3} km^3/yr that represents a "thermal threshold" where magmatic heat from the intruding magma tends to keep a conduit open and begin formation of a magma chamber. Baru volcano's volcanic output rate is at that "thermal threshold" while the adakites from Cook Island and Adagdak volcano are well under it (Figure 3.8). Long term volcanism such as the one at Baru volcano that have lasted for ~0.2 Ma, is likely to occur if there is an open magma conduit that supplies and focuses melt delivery. The existence of an established magma conduit that delivers high volcanic output rates and/or high intrusive rates, is dependent on several aspects of a subduction zone setting and influences the morphometry of any given volcanic edifice.

A series of factors could be invoked to explain the contrasting output rates at Baru volcano when compared to other adakite localities that are a product of slab melting (e.g., Cook Island and Adagdak). Some of these are: local crustal thickness, tectonic setting (magnitude and orientation of principal stresses), magma composition, and melt generation rate in the source region. Continental crust thickness has been described to reduce the average volcanic output rate (White et al., 2006). Nonetheless, this is not the case with our chosen localities (Baru volcano, Cook Islands and Adagdak) where the crustal thickness is approximately the same (Dzierma et al., 2010; Leahy and Park, 2005; Shillington et al., 2004). In addition, the tectonic setting and age of the subducting plate are comparable among these localities and the chemical variation overlaps. Given these similarities, the only parameter that might be responsible for the contrast in volcanic output rates, might be associated with the melt generation rate at the source region.

5.3 Melting rates

Geochronological evidence presented in this study has showed that the totality of the lava flows and pyroclasts that compose the Baru volcano edifice appears to have been erupted in the last ~200 k.a., indicating magma eruption rates in the order of other normal oceanic arc volcanoes despite having a much thicker crust (~50 km) (Figure 3.8). The rate at which magmas migrate to upper crustal levels and are ultimately erupted depends on the rate of magma generation within the mantle wedge, the geometry of the plumbing system and the dynamics of the magma ascent through the crust (Zellmer, 2008). Our Qe calculations for Baru volcano indicate that the plumbing system at Baru is extremely efficient, given that it is at an ideal thermal threshold were magmas conduits can readily transport magmas from the source region to the crust in relatively short periods of time. Fast transport in the plumbing system of Baru volcano is further confirmed by the presence of un-equilibrated subarc mantle cumulates in the Quaternary magmas (Roy, 1988). These type of cumulate nodules must be transported in timescales of km/days in order to avoid re-equilibration (Blatter and Carmichael, 1998).

These constrains on the plumbing system of Baru volcano, allow us to postulate that the volcanic output rate at Baru volcano is controlled primarily by the rate of magma generation within the mantle wedge. Mantle melting occurs in the mantle wedge in response to fluid release from the subducted slab (e.g. Gill 1981; Arculus, 1984), and therefore the rate of magma generation is largely a function of the rate of fluid release into the wedge, which in turn is controlled by the degree of hydration of the subducting slab and the rate at which it descends into the mantle (i.e. the plate convergence rate) (Cagnioncle et al., 2007).

Cagnioncle et al. (2007) have described that the plate convergence rate controls the area of the potential melting region. Potential melting region directly influences melt production rates but reduces the flux of water to that melting region by advecting a greater fraction of released water to a greater depth (Cagnioncle et al., 2007). These authors have calculated that a convergence rate of 70 km/Myr (similar to the convergence rate in the Baru region) should yield at least 30 km^3/Myr-arc km in typical arc settings with typical magmatic eruptive rates (e.g. Baru volcano). Considering that the volcanic activity at Baru volcano is concentrated in a portion of the arc that has about ~50 km of diameter, such melting rate could potentially generate roughly 1500 km^3/My that could mobilized to the arc region. The indicated potential melting rate is calculated using a conservative flux of water off the slab of 20 km^3/Myr-arc km (~ 100 km^3/My for the Baru arc segment). However, melting rates at the Baru volcano region could reach the upper limit threshold of 45 km^3/Myr-arc km if greater water contents are considered (40 km^3/Myr-arc km). This could potentially produce nearly 2225 km^3/Myr of arc magmas on this portion of the arc. Greater water contents might be achievable in the Baru volcano region due to the heavily faulted downgoing lithosphere outboard Baru volcano. The faulting is a result of the interaction of 3 fault systems: Panama fracture zone, the Balboa fracture zone and the Coiba fracture zone (Figure 3.1). In other regions of the Central American arc (i.e. Nicaragua) heavily faulted and highly serpentinized subducting lithosphere has been described as the source of the large flux of hydrous fluids that has been reported for this section of the arc (Rupke et al., 2002; Von Huene et al., 2000). Similar models have been proposed at Lassen and Shasta regions to explain their unusually high magma production and transport rates (Borg et al., 2002).

The typical arc volcanism magmatic production rates in the Baru region are difficult to achieve by via dehydration melting of an amphibolitic source (typical protolith used to model adakite signatures in the melting of the subducting slab model), which can be as high as 10 km^3/Myr-arc km for extreme optimistic conditions of at least a 0.3 melt fraction (Drummond et al., 1995; Liang, 2003). However, Prouteau et al (1999), determined that in order to produce a the typical dacitic bulk composition of subducting slab melts via dehydration and flux induced melting, a melt fraction of 0.028 at 15 wt% H_2O content in the melt is needed. These estimates of melt fractions are significantly lower than the 0.3 melt fraction that was calculated in dehydration melting geochemical modeling by Drummond et al. (1995) and Liang (2003) and will result in lower estimates of melt productivity in the mantle wedge. Even whit the extremely optimistic melting rate of 10 km^3/Myr-arc km, this process will only be able to produce about 500 km^3/My of arc magmas, which is close to the volume of erupted magmas in the ~0.213 My period at Baru volcano.

The controlling factors on mantle melting can explain why adakitic volcanism derived from melting of the subducting slab are be volumetrically smaller. Higher temperatures in the subducting slab (widely reported for this kind of adakites) not only will cause the slab to loose fluids at shallower levels in the subduction zone (Mibe et al., 2011), but also will enhance subducting plate buoyancy increasing plate coupling and reduce the convergence rate. The effect of reducing the convergence rate and the fluid flux is a reduced melt production rate in the mantle wedge (Zellmer et al., 2008 and Cagnioncle et al., 2007) .

6. CONCLUDING REMARKS

In this study we have presented a complete magmatic record of Baru volcano and have provided insight into magma generation processes in this region of the Central American and Panamanian arc which has been previously been understudied. Adakitic volcanism in this region has previously been described as insignificant, however, our study has modified this notion by highlighting the importance of adakitic volcanism in the construction of a major volcanic edifice. Combining detailed stratigraphy, $^{40}Ar/^{39}Ar$ dating, and geochemical characterization we have shown that (1) Baru is an adakitic volcano, (2) the adakitic volcanism is substantial at Baru (~450 km^3) and comparable to other arc massif arc volcanoes (3) the volcanic edifice of Baru volcano was build rapidly (less than ~213 k.a.) in comparison to other typical adakitic volcanoes (Adagdak and Cook), but in time scales observed in typical arc volcanoes, (5) that the Qe values are higher in Baru volcano in comparison to thee archetypical adakite volcanoes, and (5) there are is no significant difference between the calculated values of Qe for Baru with other arc volcanoes. The observed chemical and mineralogical variation coupled with the high magma production rates, indicate that Baru volcano is typical arc volcano that has an adakitic signature. These observations support regional models that explain the adakite signatures from Baru as derived from flux-induced mantle melting that later fractionated in the lower crust rather than melting of the subducting slab (Hidalgo and Rooney, 2010).

7. APPENDICES

7.1 Appendix one: figure captions.

Figure 3.1: A. Location map. This figure displays the dissected geomorphology of Baru volcano, which is a product of the overlapping recent (Quaternary) and older (Miocene) volcanic products. In this inset the locations of the samples used on this study are indicated by black triangles. B. Tectonic map for this study. Dashed lines with teeth marks represent zones of convergence; zippered line is the Panama - Colombia suture zone as described by Bird (2003). Dashed lines in the continental areas represent the approximate location of the Central American Volcanic Arc (CAVA). Oceanic ridges and plateaus are in dark grey. Ages indicated for the Coiba Plateau, Malpelo ridge, and the Cocos and Nazca Plates are derived from Lonsdale (2005). West of the Panama Fracture Zone the ages of the seafloor are from Barckhausen et al. (2001). Age for the Cocos ridge is from Werner et al. (2003), Hey (1977) and Lonsdale and Klitgord (1978). Subducting rates are from Trenkamp et al. (2002). Close to the trench in the Panama Basin between the Panama Fracture Zone and the Coiba Fracture zone the subducting crust is interpreted to be 10-20 Ma according to Barckhausen et al. (2001).

Figure 3.2. Stratigraphy of Baru Volcano and surrounding areas correlated to the geographic position of some of the outcrops of each of the units. Digital Elevation model of the Baru volcano region has no scale and is supposed to serve only as a schematic visual aid. Elevation data is derived from the NASA/JPL SRTM dataset. Sample locations and a dotted area that represents the Miocene volcanism are indicated in the SRTM DEM.

Figure 3.3. A. Alkalis versus silica *LeBas* (1986) for samples from Baru volcano. Samples from the Ash Flow unit come from pumice blocks within the ash flow while samples from other units come from lava samples (Pc= Alkali Basalt, S1=Trachybasalt, S2=Basaltic-Trachyandesite, S3=Trachyandesite, T=Trachyte, Trachydacite, R=Rhyolite, Ph=Phonolite, U1=Tephri-basanite, U2=Phono-tephrite, U3=Tephri-phonolite). B. K_2O vs SiO_2. C. Plot of chondrite normalized La/Yb vs chondrite normalized Yb. D. TiO_2 vs. Mg. The Central American arc lavas in this figures are derived from data presented in Bolge et al. (2009) and Carr et al., 2007 (a, b).

Figure 3.4. Bulk rock geochemistry – major element variation versus MgO diagrams shown. Complete composition and standard deviations for major- and trace elements for analysis of glassy pumice fragments and lava samples are provided in the supplementary material. Samples with totals lower than 96% are excluded because it was assumed that these samples were secondarily hydrated or altered. All major elements have been normalized on an anhydrous basis to 100%.

Figure 3.5. Bulk rock geochemistry – trace element variation versus MgO diagrams shown. Complete composition and standard deviations for major- and trace elements for

analysis of glassy pumice fragments and lava samples are provided in the supplementary material.

Figure 3.6. Chondrite and Primitive Mantle normalized diagrams (Sun and McDonough 1989) for Baru Volcano Quaternary deposits. Black shaded area represents compositional range for CAVA volcanics A. Primitive Mantle normalized spider diagram. Extreme depletion is evident on the Baru volcano suite except in Sr, Zr, and Eu. B. Chondrite-normalized spider diagrams for Baru volcano deposits. Samples from Baru volcano are extremely depleted in all the REE when compared to other CAVA ignimbrites.

Figure 3.7. A. Height versus volume diagram showing different types of studied volcanic edifices from CAVA and southern Central Andes Volcanic Zone (SCAVZ). The data for these volcanic edifices are from Grosse et al. (2009) with the exception of Adagdak, Cook Island, Baru and Shasta. B. Other morphometrical parameters, Volume vs. Height/width and C. Volume vs. Elipticity Index.

Figure 3.8. A. Volumes and volcanism durations for locations from White et al. (2006), with the exception of Adagdak, Cook Island, and Baru. B. Volcanic rates grouped by petrotectonic setting for all locations in White et al (2006). Shaded boxes represent the range of one standard deviation from the mean rate. The lines show the minimum and maximum rates for each setting. For all settings, mean magmatic output rate (Q(e)) is skewed toward high values, which may imply a natural upper limit set by magma generation but no lower limit.

7.2 Appendix 2: Figures

Figure 3.1

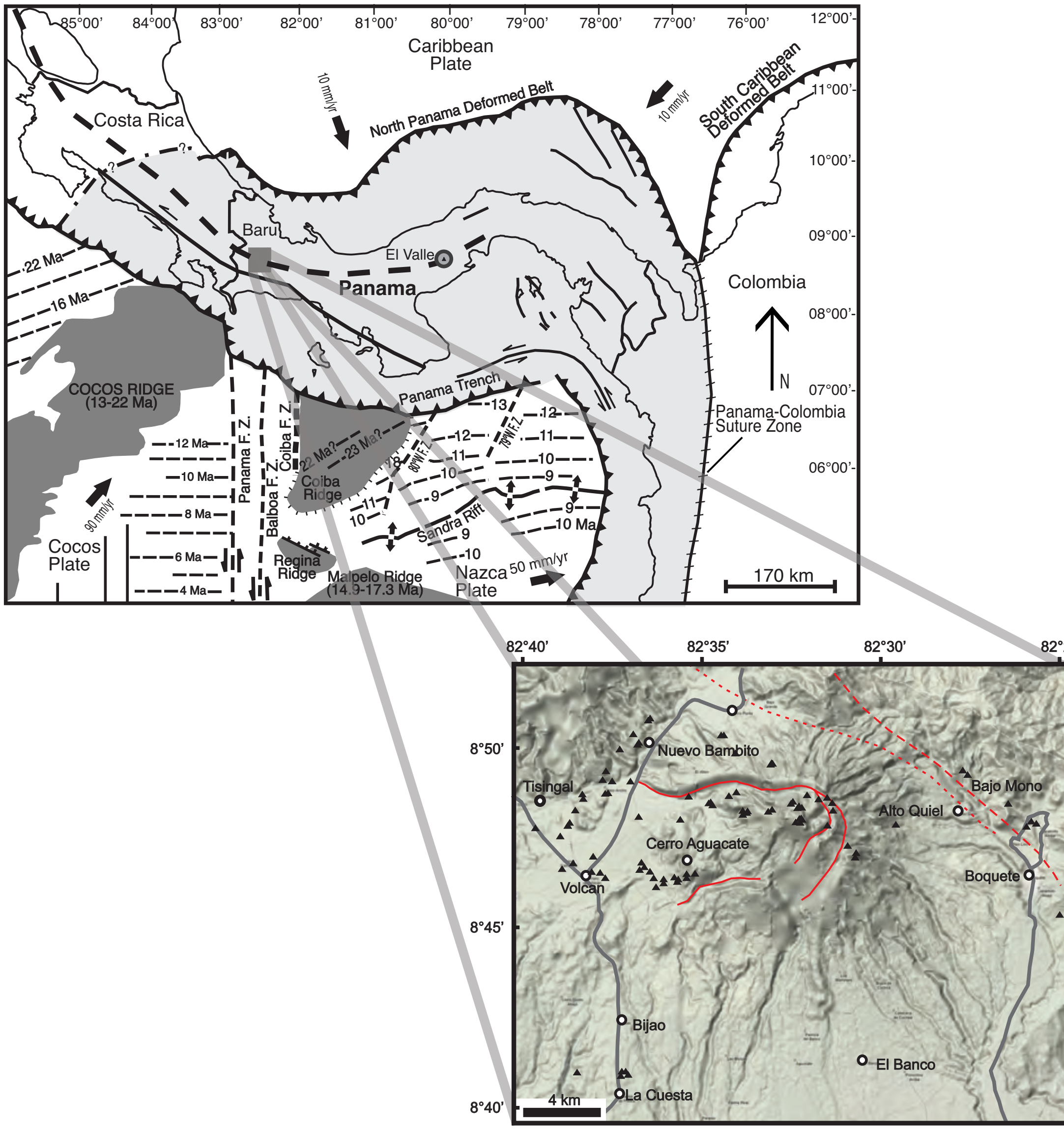

Figure 3.2

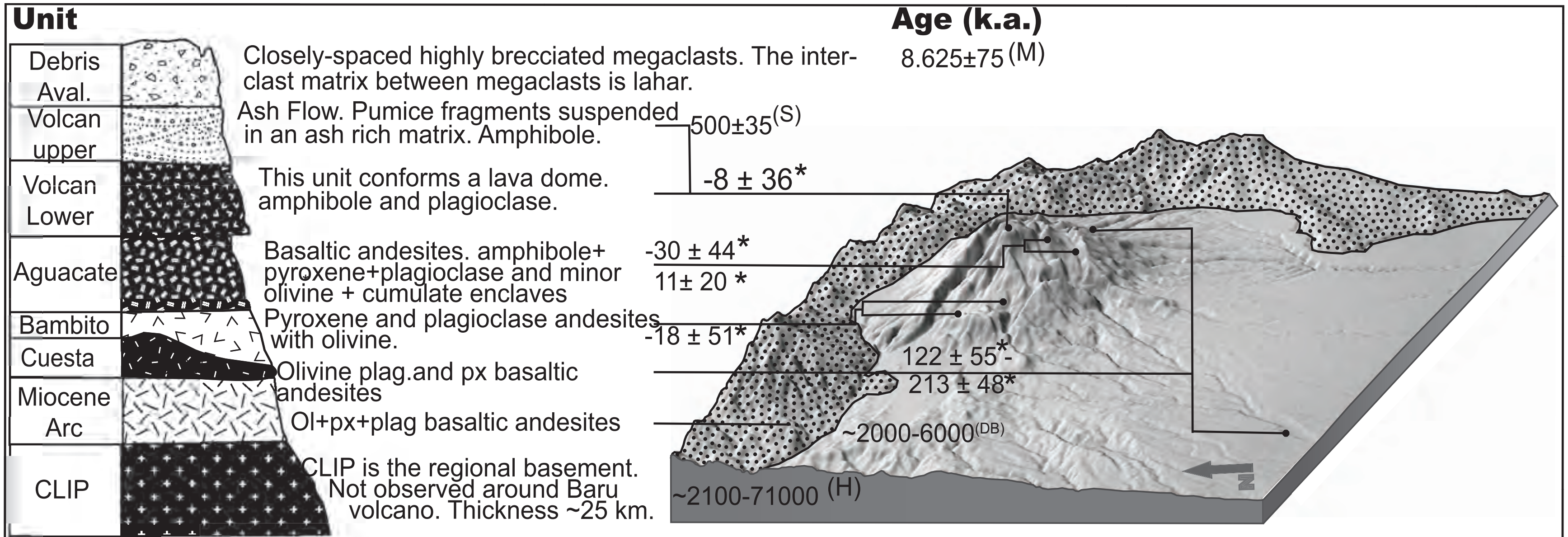

(*) Data presented in this study, (H) Hoernle et al. (2002), (DB) Deboer and Drummond et al (1991), (M) Morell et al. (2010, (S) Sherrod et al, 2007

Figure 3.3

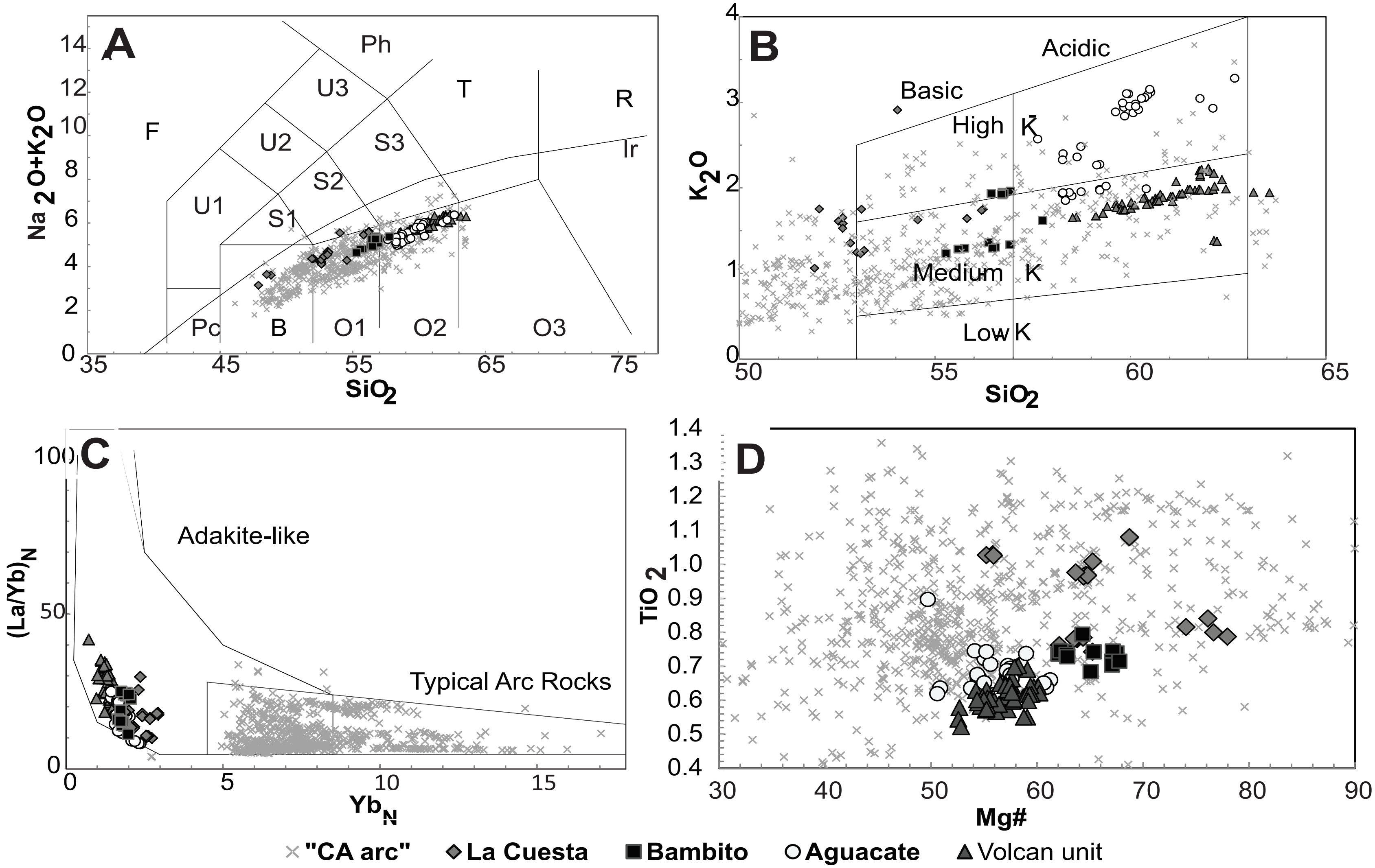
A
Ph
U3
T
R
F
U2
S3
Ir
U1
S2
S1
Pc
B
O1
O2
O3
Na_2O+K_2O
SiO_2
B
Acidic
Basic
High K
Medium K
Low K
K_2O
SiO_2
C
Adakite-like
Typical Arc Rocks
$(La/Yb)_N$
Yb_N
D
TiO_2
Mg#
"CA arc"
La Cuesta
Bambito
Aguacate
Volcan unit

Figure 3.4

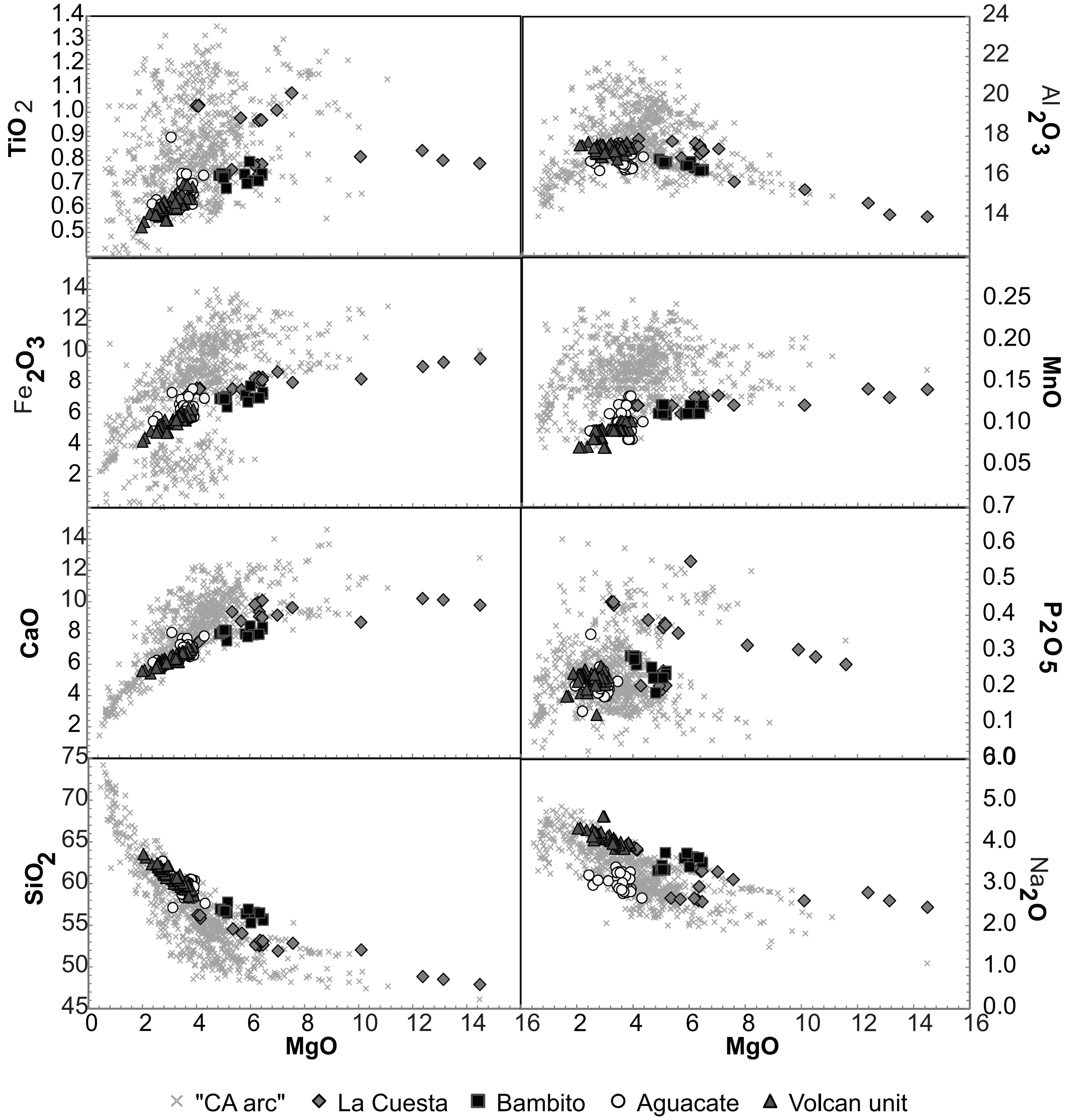
TiO2
Al2O3
Fe2O3
MnO
CaO
P2O5
SiO2
Na2O
MgO
MgO
"CA arc"
La Cuesta
Bambito
Aguacate
Volcan unit

Figure 3.5

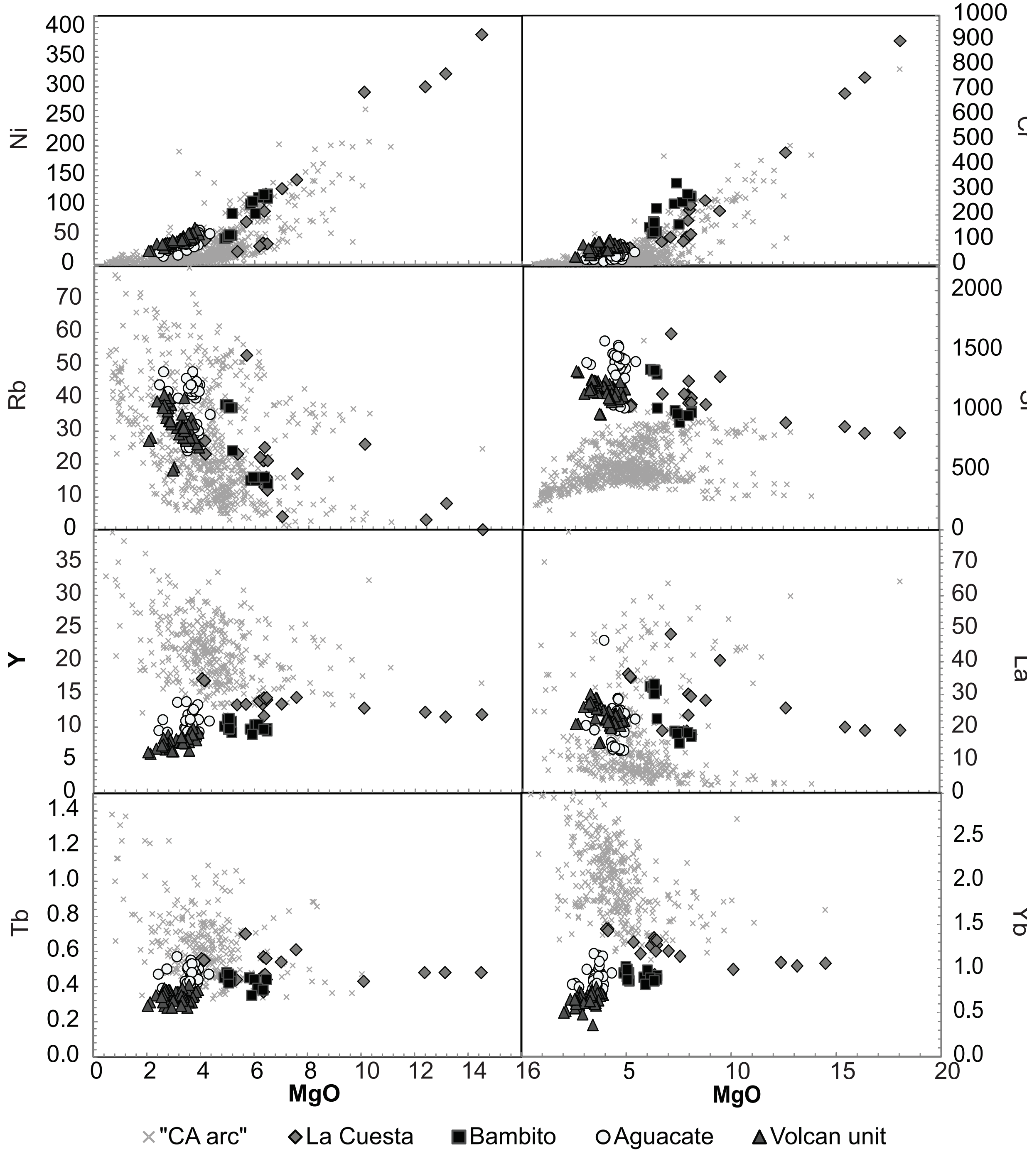

Ni
Cr
Rb
Sr
Y
La
Tb
Yb
MgO
MgO
"CA arc"
La Cuesta
Bambito
Aguacate
Volcan unit

Figure 3.6

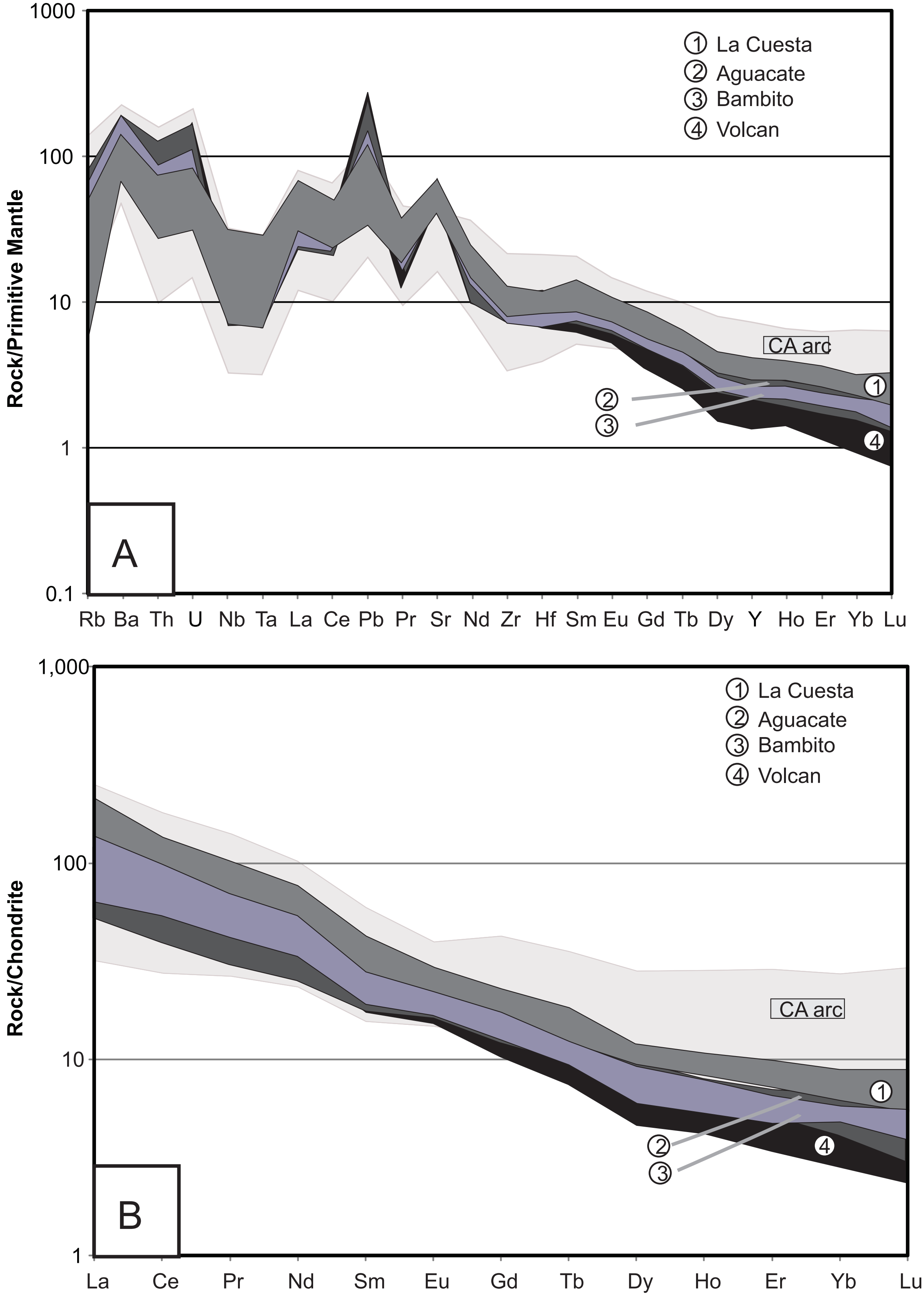
1000
100
10
1
0.1
Rock/Primitive Mantle
① La Cuesta
② Aguacate
③ Bambito
④ Volcan
CA arc
A
Rb Ba Th U Nb Ta La Ce Pb Pr Sr Nd Zr Hf Sm Eu Gd Tb Dy Y Ho Er Yb Lu
1,000
100
10
1
Rock/Chondrite
① La Cuesta
② Aguacate
③ Bambito
④ Volcan
CA arc
B
La Ce Pr Nd Sm Eu Gd Tb Dy Ho Er Yb Lu

Figure 3.7

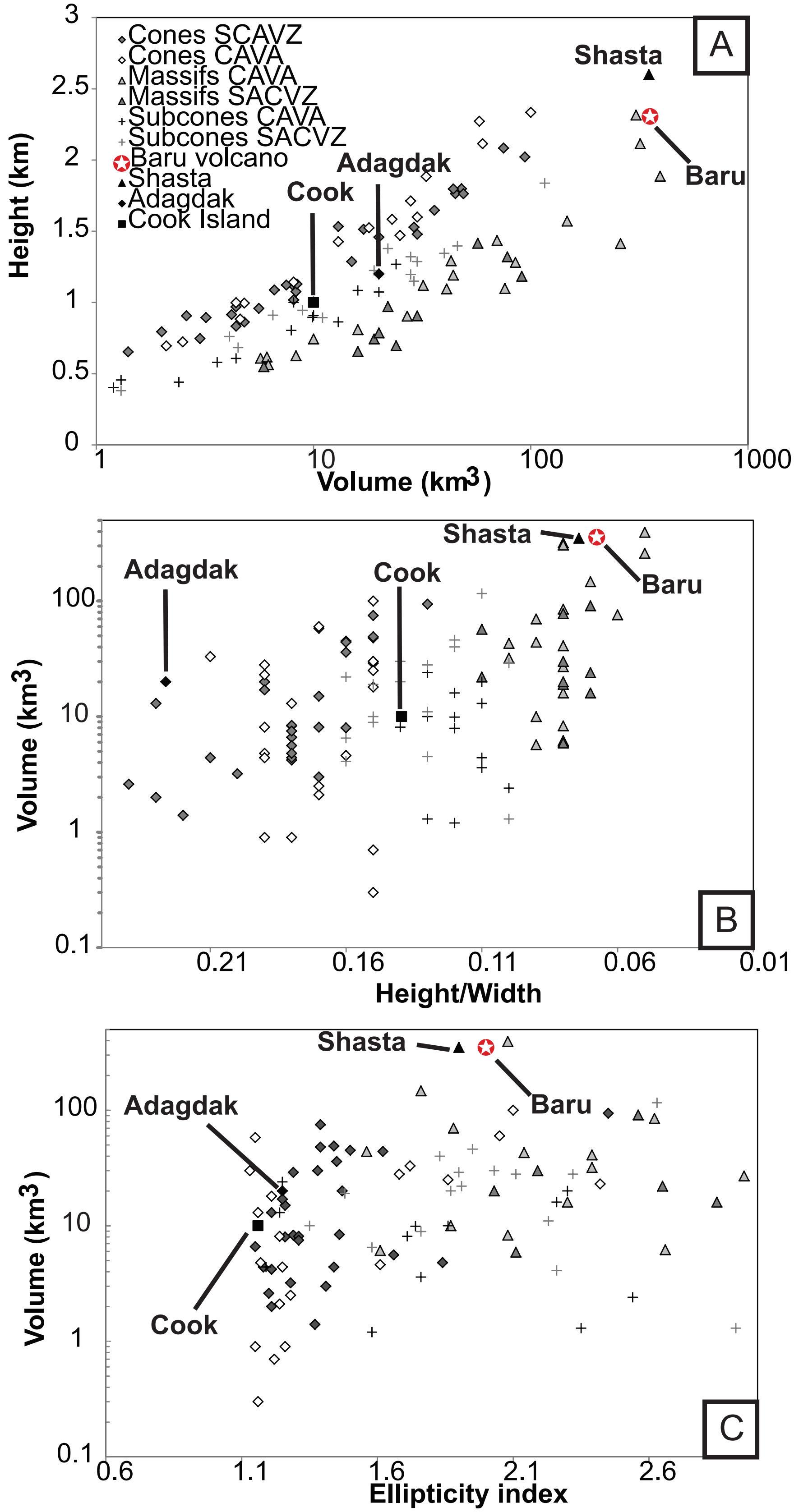

A
Height (km)
Volume (km3)
Cones SCAVZ
Cones CAVA
Massifs CAVA
Massifs SACVZ
Subcones CAVA
Subcones SACVZ
Baru volcano
Shasta
Adagdak
Cook Island
Shasta
Adagdak
Cook
Baru
B
Volume (km3)
Height/Width
Adagdak
Cook
Shasta
Baru
C
Volume (km3)
Ellipticity index
Shasta
Baru
Adagdak
Cook

Figure 3.8

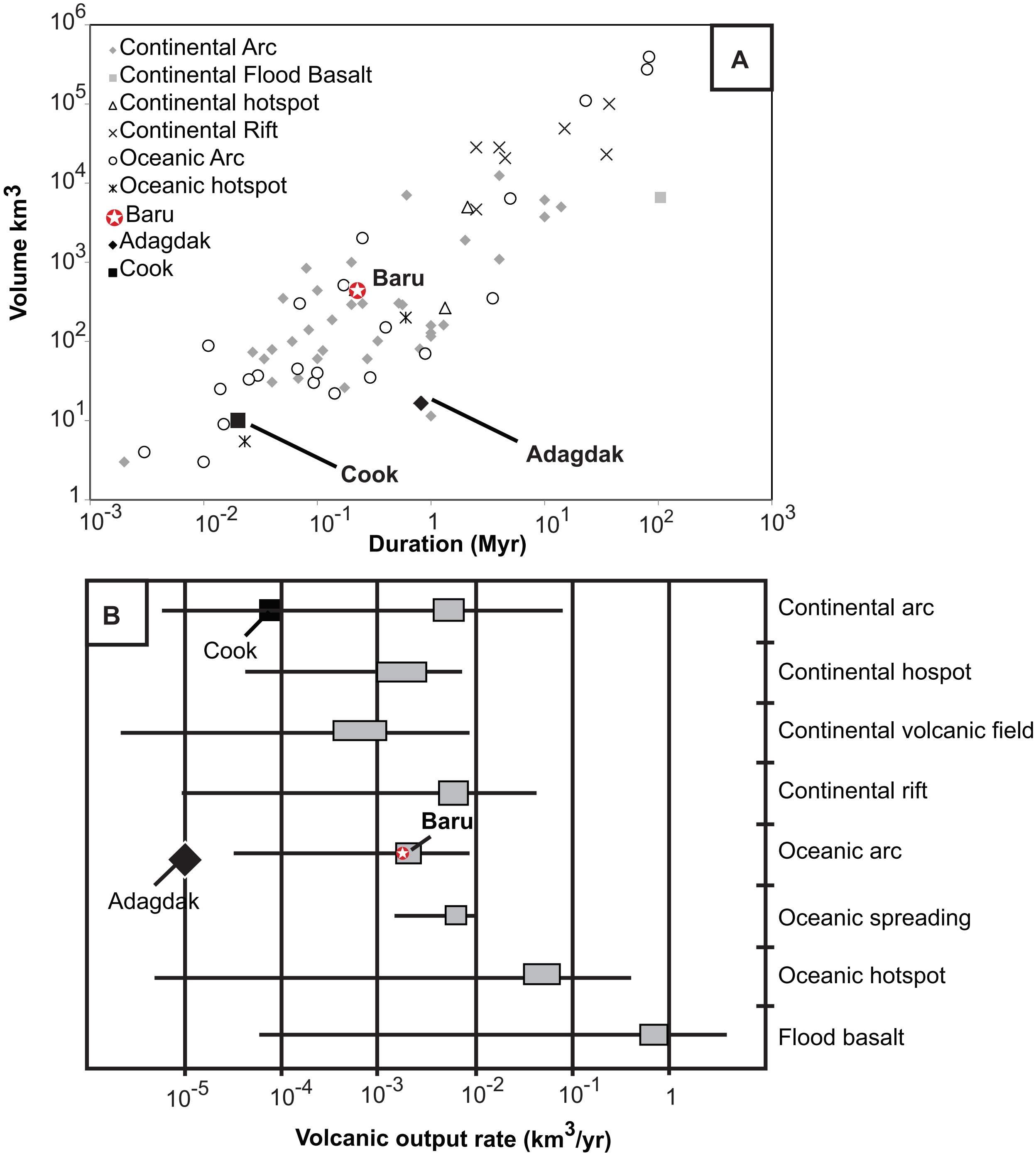
A
Continental Arc
Continental Flood Basalt
Continental hotspot
Continental Rift
Oceanic Arc
Oceanic hotspot
Baru
Adagdak
Cook
Volume km3
Duration (Myr)
B
Continental arc
Continental hospot
Continental volcanic field
Continental rift
Oceanic arc
Oceanic spreading
Oceanic hotspot
Flood basalt
Volcanic output rate (km3/yr)

8.REFERENCES

8.REFERENCES

Abratis, M., Worner, G., 2001. Ridge collision, slab-window formation, and the flux of Pacific asthenosphere into the Caribbean realm. Geology 29, 127-130.

Aguillon-Robles, A., Calmus, T., Benoit, M., Bellon, H., Maury, R.O., Cotten, J., Bourgois, J., Michaud, F., 2001. Late miocene adakites and Nb-enriched basalts from Vizcaino Peninsula, Mexico: Indicators of East Pacific Rise subduction below Southern Baja California? Geology 29, 531-534.

Alvarado, G.E., Kussmaul, S., Chiesa, S., Guillot, P.Y., Appel, H., Wörner, G., Rundle, C., 1992. Cuadro cronoestrátigrafico de las rocas ígneas de Costa Rica basado en dataciones radiométricas K-Ar y U-Th. Journal of South American Earth Sciences 6, 151-168.

Atherton, M.P., Petford, N., 1993. Generation of sodium-rich magmas from newly underplated basaltic crust. . Nature 362, 144-146.

Blatter, D., Carmichael, I., 1998. Hornblende peridotite xenoliths from central Mexico reveal the highly oxidized nature of subarc upper mantle. Geology 26, 1035-1038.

Borg, L.E., Blichert-Toft, J., Clynne, M.A., 2002. Ancient and modern subduction zone contributions to the mantle sources of lavas from the Lassen region of California inferred from Lu-Hf isotopic systematics. Journal of Petrology 43, 705-723.

Cagnioncle, A.-M., Parmentier, E.M., Elkins-Tanton, L.T., 2007. Effect of solid flow above a subducting slab on water distribution and melting at convergent plate boundaries. J. Geophys. Res. 112, B09402.

Castillo, P.R., 2006. An Overview of adakite petrogenesis. Chinese Science Bulletin 51, 257-376.

Castillo, P.R., Janney, P.E., Solidum, R.U., 1999. Petrology and geochemistry of Camiguin Island, southern Philippines: insights to the source of adakites and other lavas in a complex arc setting. Contributions to Mineralogy and Petrology 134, 33-51.

Clark, L.F., 1989. The Geology, Geochemistry, and Petrogenesis of El Valle volcano, Panama., Geological Sciences. University of South Florida, Tampa, Florida, p. 150.

Crisp, J.A., 1984. Rates of magma emplacement and volcanic output. Journal of Volcanology and Geothermal Research 20, 177-211.

de Boer, J.Z., Defant, M.J., Stewart, R.H., Bellon, H., 1991. Evidence for active subduction below western Panama. Geology 19, 649-652.

de Boer, J.Z., Drummond, M.S., Bordelon, M.J., Defant, M.J., Bellon, H., Maury, R.C., 1995. Cenozoic magmatic phases of the Costa Rican island arc (Cordillera de Talamanca). Special Paper Geological Society of America, Boulder, CO.

Deering, C.D., Cole, J.W., Vogel, T.A., 2008. A Rhyolite Compositional Continuum Governed by Lower Crustal Source Conditions in the Taupo Volcanic Zone, New Zealand. Journal of Petrology 49, 2245-2276.

Defant, M., Kepezhinskas, P., Xu, J., Wang, Q., Zhang, Q., Xiao, L., 2002. Adakites: some variations on a theme. Acta Petrologica Sinica 18, 129-142.

Defant, M.J., 1990. Derivation of some modern arc magmas by melting of young subducted lithosphere. Nature 347, 662-665.

Defant, M.J., Clark, L.F., Stewart, R.H., Drummond, M.S., de Boer, J.Z., Maury, R.C., Bellon, H., Jackson, T.E., Restrepo, J.F., 1991a. Andesite and dacite genesis via contrasting processes: The geology and geochemistry of El Valle volcano, Panama. Contributions to Mineralogy and Petrology 106, 309-324.

Defant, M.J., Jackson, T.E., Drummond, M.S., Deboer, J.Z., Bellon, H., Feigenson, M.D., Maury, R.C., Stewart, R.H., 1992. The Geochemistry of Young Volcanism Throughout Western Panama and Southeastern Costa-Rica - an Overview. Journal of the Geological Society 149, 569-579.

Defant, M.J., Richerson, P.M., Deboer, J.Z., Stewart, R.H., Maury, R.C., Bellon, H., Drummond, M.S., Feigenson, M.D., Jackson, T.E., 1991b. Dacite Genesis Via Both Slab Melting and Differentiation - Petrogenesis of La-Yeguada Volcanic Complex, Panama. Journal of Petrology 32, 1101-1142.

DeMets, C., 2001. A New Estimate for Present-Day Cocos-Caribbean Plate Motion: Implications for Slip Along the Central American Volcanic Arc. Geophysical Research Letters 28, 4043-4046.

Denyer, P., Baumgartner, P.O., Gazel, E., 2006. Characterization and tectonic implications of Mesozoic-Cenozoic oceanic assemblages of Costa Rica and Western Panama. Geologica Acta 4, 219-235.

Drummond, M.S., Bordelon, M., Deboer, J.Z., Defant, M.J., Bellon, H., Feigenson, M.D., 1995. Igneous Petrogenesis and Tectonic Setting of Plutonic and Volcanic-Rocks of the Cordillera De Talamanca, Costa-Rica Panama, Central-American Arc. American Journal of Science 295, 875-919.

Drummond, M.S., Defant, M.J., 1990. A model for trondhjemite-tonalite-dacite genesis and crustal growth via slab melting; Archean to modern comparisons Journal of Geophysical Research 95, 21503-21521.

Dzierma, Y., Thorwart, M.M., Rabbel, W., Flueh, E.R., Alvarado, G.E., Mora, M.M., 2010. Imaging crustal structure in south central Costa Rica with receiver functions. Geochem. Geophys. Geosyst. 11, Q08S26.

Eiler, J.M., Schiano, P., Valley, J., Kita, N.T., Stolper, E.M., 2007. Oxygen-isotope and trace element constraints on the origins of silica-rich melts in the subarc mantle. Geochemistry, Geophysics, Geosystems 8.

Elliott, T., 1997. Fractionation of U and Th during mantle melting: A reprise. Chemical Geology 139, 165-183.

Frey, H.M., Lange, R.A., Hall, C.M., Delgado-Granados, H., Carmichael, I.S.E., 2007. A Pliocene ignimbrite flare-up along the Tepic-Zacoalco rift: Evidence for the initial stages of rifting between the Jalisco block (Mexico) and North America. Bulletin of the Geological Society of America 119, 49.

Gazel, E., Carr, M., Hoernle, K., Feigenson, M., Szymanski, D., Hauff, F., van den Bogaard, P., 2009. Galapagos-OIB signature in southern Central America: Mantle refertilization by arc–hot spot interaction, Geochemistry Geophysics Geosystems, p. Q02S11.

Goff, J., Cochran, J., 1996. The Bauer scarp ridge jump: A complex tectonic sequence revealed in satellite altimetry. Earth and Planetary Science Letters 141, 21-33.

Grosse, P., van Wyk de Vries, B., Euillades, P.A., Kervyn, M., Petrinovic, I.n.A., accepted. Systematic morphometric characterization of volcanic edifices using digital elevation models. Geomorphology In Press, Accepted Manuscript.

Grosse, P., van Wyk de Vries, B., Petrinovic, I.A., Euillades, P.A., Alvarado, G.E., 2009. Morphometry and evolution of arc volcanoes. Geology 37, 651.

Hardee, H., 1982. Incipient magma chamber formation as a result of repetitive intrusions. Bulletin of Volcanology 45, 41-49.

Hawkesworth, C., George, R., Turner, S., Zellmer, G., 2004. Time scales of magmatic processes. Earth and Planetary Science Letters 218, 1-16.

Hawkesworth, C.J., Gallagher, K., Hergt, J.M., McDermott, F., 1993. Mantle and Slab Contributions in Arc Magmas. Annual Review of Earth and Planetary Sciences 21, 175-204.

Hawkesworth, C.J., Turner, S.P., McDermott, F., Peate, D.W., vanCalsteren, P., 1997. U-Th isotopes in arc magmas: Implications for element transfer from the subducted crust. Science 276, 551-555.

Hidalgo, P.J., Rooney, T.O., 2010. Crystal fractionation processes at Baru volcano from the deep to shallow crust. Geochemistry Geophysics Geosystems 11, Q12S30.

Hoernle, K., Abt, D.L., Fischer, K.M., Nichols, H., Hauff, F., Abers, G.A., van den Bogaard, P., Heydolph, K., Alvarado, G., Protti, M., Strauch, W., 2008. Arc-parallel flow in the mantle wedge beneath Costa Rica and Nicaragua. Nature 451, 1094-1097.

Hoernle, K., van den Bogaard, P., Werner, R., Lissina, B., Hauff, F., Alvarado, G.E., Garbe-Schoenberg, C.D., 2002. Missing history (16-71 Ma) of Galapagos hotspot; implications for the tectonic and biological evolution of the Americas. Geology 30, 795-798.

Jarrard, R.D., 1986. Relations Among Subduction Parameters. Reviews of Geophysics 24, 217-284.

Johnston, S.T., Thorkelson, D.J., 1997. Cocos-Nazca slab window beneath Central America. Earth and Planetary Science Letters 146, 465-474.

Kay, R.W., 1978. Aleutian magnesian andesites: melts from subducted Pacific ocean crust. Journal of Volcanology and Geothermal Research 4, 117-132.

Kay, R.W., Kay, S.M., 2002. Andean adakites: Three ways to make them. Acta Petrologica Sinica 18, 303-311.

Kay, R.W., Ramos, V.A., Marquez, M., 1993. Evidence in Cerro Pampa volcanic rocks for slab-melting prior to ridge-trench collision in southern South America. . Journal of Geology 101, 103-114.

Kellogg, J., Vega, V., 1995. Tectonic development of Panama, Costa Rica, and the Colombian Andes: constraints from global positioning system geodetic studies and gravity, in: Mann, P. (Ed.), Geologic and Tectonic Deelopment of he Caribbean PLate Boundary in Southern Central America. Geological Society of America, Boulder, Colorado, pp. 75-75.

Kessel, R., Schmidt, M., Ulmer, P., Pettke, T., 2005. Trace element signature of subduction-zone fluids, melts and supercritical liquids at 120-180 km depth. Nature(London) 437, 724-727.

Leahy, G.M., Park, J., 2005. Hunting for oceanic island Moho. Geophysical Journal International 160, 1020-1026.

Liang, Y., 2003. On the thermo-kinetic consequences of slab melting, Geophysical research letters, p. 2270.

Lissinna, B., Hoernle, K., Hauff, F., van den Bogaard, P., Sadofsky, S., 2006. The Panamanian island arc and Gal·pagos hotspot: A case study for the long-term evolution of arc/hotspot interaction. Geophysical Research Abstracts.

Lonsdale, P., 2005. Creation of the Cocos and Nazca plates by fission of the Farallon plate. Tectonophysics 404, 237-264.

Macpherson, C.G., Dreher, S.T., Thirlwall, M.F., 2006. Adakites without slab melting: High pressure differentiation of island arc magma, Mindanao, the Philippines. Earth and Planetary Science Letters 243, 581-593.

Mann, P., Kolarsky, R.A., 1995. East Panama deformed belt: Age, structure, neotectonic significance, in: Mann, P. (Ed.), Geologic and Tectonic development of the Caribbean plate boundary in southern Central America. Geological Society of America Special Paper Geological Society of America, Boulder, pp. 111-129.

Maury, R., Defant, M., Bellon, H., De Boer, J., 1995. Early Tertiary arc volcanics from eastern Panama. SPECIAL PAPERS-GEOLOGICAL SOCIETY OF AMERICA, 29-29.

Morell, K.D., Fisher, D.M., Gardner, T.W., 2008. Inner forearc response to subduction of the Panama Fracture Zone, southern Central America. Earth and Planetary Science Letters 265, 82-95.

Peacock, S.M., Rushmer, T., Thompson, A.B., 1994. Partial melting of subducting oceanic crust. Earth and Planetary Science Letters 121, 227-244.

Prouteau, G., Scaillet, B., 2003. Experimental constraints on the origin of the 1991 Pinatubo dacite. Journal of Petrology 44, 2203-2241.

Restrepo, J., 1987. A geochemical investigation of Pleistocene to Recent calc-alkaline volcanism in western Panama, Geologial Sciences. University of South Florida, Tampa, p. 103.

Roy, A., 1988. Evolution of the Igneous Activity in Southeastern Costa Rica and Southwestern Panama from the Middle Tertiary to the Recent, Geological Sciences. Lousianna State University, Baton Rouge, p. 301.

Rupke, L.H., Morgan, J.P., Hort, M., Connolly, J.A.D., 2002. Are the regional variations in Central American arc lavas due to differing basaltic versus peridotitic slab sources of fluids? Geology 30, 1035-1038.

Sempere, T., Hérail, G., Oller, J., Bonhomme, M., 1990. Late Oligocene-early Miocene major tectonic crisis and related basins in Bolivia. Geology 18, 946-949.

Shaw, H.R., 1985. Links between magma-tectonic rate balances, plutonism, and volcanism. Journal of Geophysical Research 90, 11275-11211,11288.

Sherrod, D.R., Vallance, J.W., Tapia-Espinoza, A., McGeehin, J.P., 2007. Volcan Baru, Eruptive History and Volcano Hazards Assessment, Open-File Report 2007-1401. U.S. Geological Survey p. 33.

Shillington, D.J., Van Avendonk, H.J.A., Holbrook, W.S., Kelemen, P.B., Hornbach, M.J., 2004. Composition and structure of the central Aleutian island arc from arc-parallel wide-angle seismic data. Geochemistry Geophysics Geosystems 5, Q10006.

Sigmarsson, O., Hemond, C., Condomines, M., Fourcade, S., Oskarsson, N., 1991. Origin of silicic magma in Iceland revealed by Th isotopes. Geology 19, 621-624.

Sigurdsson, H., Kelley, S., Leckie, R.M., Carey, S.N., Browing, J.M., Rogers, R.D., 2000. History of Circum-Caribbean explosive volcanism: Ar/Ar dating of tephra layers, in: Leckie, R.M., Sigurdsson, H., Acton, G.D., Draper, G. (Eds.), Proceeding of the Ocean Drilling Program, pp. 299-314.

Spera, F.J., Yuen, D.A., Kirschvink, S.J., 1982. Thermal boundary layer convection in silicic magma chambers: effects of temperature-dependent rheology and implications for thermogravitational chemical fractionation. Journal of Geophysical Research 87, 8755-8767.

Trenkamp, R., Kellogg, J.N., Freymueller, J.T., Mora, H.P., 2002. Wide plate margin deformation, southern Central America and northwestern South America, CASA GPS observations. Journal of South American Earth Sciences 15, 157-171.

Turner, S., Bourdon, B., Gill, J., 2003. Insights into magma genesis at convergent margins from U-series isotopes, Uranium-Series Geochemistry, pp. 255-315.

Turner, S., Hawkesworth, C., Rogers, N., King, P., 1997. U-Th isotope disequilibria and ocean island basalt generation in the Azores. Chemical Geology 139, 145-164.

Turner, S., Regelous, M., Hawkesworth, C., Rostami, K., 2006. Partial melting processes above subducting plates: Constraints from 231Pa-235U disequilibria. Geochimica et Cosmochimica Acta 70, 480-503.

van Wyk de Vries, B., 1993. Tectonics and magma evolution of Nicaraguan volcanic systems. Open University, p. 328.

van Wyk de Vries, B., Grosse, P., Alvarado, G.E., 2007. Volcanism and volcanic landforms, in: Bundschuh, J., Alvarado, G.E. (Eds.), Central America: Geology, resources and hazards, , pp. 123-158.

Vogel, T.A., Flood, T.P., Patino, L.C., Wilmont, M.S., Maximo, R.P.R., Arpa, C.B., Arcilla, C.A., Stimac, J.A., 2006. Geochemistry of silicic magmas in the Macolod Corridor, SW Luzon Philippines: evidence of distinct, mantle-derived, crustal sources for silicic magmas. Contributions to Mineralogy and Petrology 151, 267-281.

Von Huene, R., Ranero, C., Weinrebe, W., 2000. Quaternary convergent margin tectonics of Costa Rica segmentation of the Cocos Plate and Central American volcanism. Tectonics 19, 314-334.

Wadge, G., 1984. Comparison of volcanic production rates and subduction rates in the Lesser Antilles and Central America. Geology 12, 555-558.

Wegner, W., Worner, G., Harmon, R.S., Jicha, B.R., 2011. Magmatic history and evolution of the Central American Land Bridge in Panama since Cretaceous times. Geological Society of America Bulletin 123, 703-724.

White, S.M., Crisp, J.A., Spera, F., 2006. Long-term volumetric eruption rates and magma budgets, Geochemistry, Geophysics, Geosystems.

Wilson, D.S., 1996. Fastest known spreading on the Miocene Cocos-Pacific plate boundary. Geophysical Research Letters 23.

Zellmer, G.F., 2008. Some first-order observations on magma transfer from mantle wedge to upper crust at volcanic arcs. Geological Society, London, Special Publications 304, 15.

Zellmer, G.F., Annen, C., Charlier, B.L.A., George, R.M.M., Turner, S.P., Hawkesworth, C.J., 2005. Magma evolution and ascent at volcanic arcs: constraining petrogenetic processes through rates and chronologies. Journal of Volcanology and Geothermal Research 140, 171-191.

Zellmer, G.F., Sparks, R.S.J., Hawkesworth, C.J., Wiedenbeck, M., 2003. Magma emplacement and remobilization timescales beneath Montserrat: Insights from Sr and Ba zonation in plagioclase phenocrysts. Journal of Petrology 44, 1413-1431.

CHAPTER FOUR GEOCHEMICAL EVOLUTION OF BARU VOLCANO AND THE ORIGIN OF THE ADAKITE SIGNATURE

1. INTRODUCTION

Subduction zones constitute environments where the exchange of mantle and crustal material is possible. This exchange plays a central role in the evolution of the continental crust and the Earth's mantle. The mantle and crustal components of this exchange are the subducting oceanic crust (including overlying sediment) along with the peridiotites within the mantle wedge. This process initiates when fluids from the dewatering subducted sediments and hydrothermally metamorphosed crustal materials are fluxed in to mantle rocks triggering melting (Davies and Stevenson, 1992; Forneris and Holloway, 2003; Grove et al., 2002; Schmidt and Poli, 1998; Tatsumi and Eggins, 1995; Ulmer, 2001). This process may be aided by mantle decompression from subduction induced corner flow in the mantle wedge (Elkins-Tanton et al., 2001; Hasegawa and Nakajima, 2004; Sisson and Bronto, 1998). The resulting primary magmas are subsequently transferred in to the overlying crust where AFC (Assimilation, Fractional Crystallization) (DePaolo, 1981) and mixing processes are responsible for the chemical variety observed on island arcs.

While the mantle melting model is broadly successful in accounting for most of the observed variety in island arcs, it has been suggested that melting of a subducting slab might be an important magma source (Clark, 1989; de Boer et al., 1991; Defant et al., 2002; Defant, 1990; Defant et al., 1991a; Defant et al., 1991b; Drummond and Defant, 1989, 1990). Melting of the subducted slab in subduction zones will imprint the resulting magma, termed adakites, with high SiO_2 (>56 wt.%), high Al_2O_3 (>15%), low MgO (<3%), high Sr (>300 ppm), no Eu anomaly, Low Y(<15 ppm), high Sr/Y (>20), low Yb (<1.9 ppm), high La/Yb (>20), low HFSEs (Nb, Ta), and isotopic signatures similar to MORBS (Castillo, 2006; Defant, 1990). The term adakite has been controversial as this geochemically defined rock type was also synonymous with a particular petrogenetic process – namely melting of the subducting slab. Subsequent studies have shown that adakitic signature may be derived from numerous processes: (1) Partial melting of the underplated basaltic lower crust (Rapp et al., 2002) or delaminated lower crust (Macpherson, 2008; Xu et al., 2002); (2) Melting of underplated basalt at the base of a tectonically thickened crust (Atherton and Petford, 1993; Kay and Kay, 2002); (3) Assimilation and crystallization processes of basaltic magma under high pressure (Castillo et al., 1999) and (4) Transport of elements not typically thought of as fluid-mobile by super-critical fluids may yield adakite-like trace-element patterns (Kessel et al., 2005).

In some island arcs (e.g. East Phillipines Arc, Southern Central American arc, Izu-Bonin, Aleutian, etc), periods of “typical” calc-alkaline arc magmatism swiftly transition to periods of adakitic volcanism (Defant et al., 1991a; Defant et al., 1991b; Drummond et al., 1995; Hidalgo et al., 2012.; Macpherson, 2008; Macpherson et al., 2006; Pearce et al., 1992; Yogodzinski and Kelemen, 1998). The transition between periods of typical island arc and adakitic volcanism is an important observation that has significant consequences for the thermal state of subduction zones.

Most models for the origin of adakites in southern Central America have invoked slab-melting processes (Abratis and Worner, 2001; Defant et al., 1992). These processes have been used by Hoernle et al. (2008) and Gazel et al. (2009) to explain the transport of the Galapagos plume signature from Southern Costa Rica to Southern Nicaragua by suggesting a 'melt-like slab component' from the Galapagos track. This 'melt-like slab component' has reacted with overlying peridiotite forming pyroxenites that are later transported northwards beneath the arc by mantle flow.

To account for the depleted heavy rare earth element (HREE) concentrations in some lavas in Central America, Drummond and Defant (1989), in one of the seminal papers for adakite generation, propose that the adakite signature is derived from residual garnet in the subducting slab. This model was supported by the concept that the Panamanian crust was too thin for garnet to have been a stable fractionating phase, thereby requiring garnet as restite in the subducting eclogitized oceanic crust. Recent experimental work has substantially revised the estimates for garnet stability; water saturated melts may now produce and fractionate igneous garnet at pressure and temperature ranges expected in the Panama arc (e.g. Alonso-Perez et al., 2009), removing the requirement that the garnet signature must have been derived from the eclogitized subducting slab. In addition, new geophysical studies in the Talamanca cordillera (which underlies Western Panama) have concluded that the crust in this region is high standing and unusually thick (up to ~50 km, Dzierma et al., 2010). These recent findings support inferences regarding garnet stability at lower crustal levels in the western Panamanian subarc lithosphere (e.g. Hidalgo and Rooney, 2010).

In this study, we address the chemical and petrological variations in rocks from the western Panamanian Arc, observed during transition from normal arc volcanism in the Miocene to adakitic volcanism in the Quaternary. We present new geochemical and geochronological analyses of the Miocene sequence at Baru volcano (and surroundings areas), which fill a critical gap in the geochemical record in the region. Here we show that (1) the typical arc basalts and andesites from the Miocene period (~15 Ma) at Baru volcano were derived from arc basalts with typical water contents (3.5%-6.0%), (2) during the Miocene, melts may have stalled in the Panamanian lower crust to form abundant amphibole rich cumulates, and (3) the transition from typical arc volcanism (10-9 Ma) to adakitic volcanism (Quaternary) coincides with reduced water contents in the primitive melts, smaller degrees of melting, and crustal thickening processes that allowed for garnet to be a stable phase in the Panamanian sub arc lithosphere.

Our focus on western Panama allows us to evaluate the existing robust geochronological and geochemical dataset (Hidalgo and Rooney, 2010; Hidalgo et al., in preparation) in order to examine processes that are responsible for generation of the adakite signature in arc magmas. If mantle fluxing is responsible for adakite generation, then the link between young subducted lithosphere and those adakites identified by Drummond and Defant (1990) could reflect the thermal and dynamic effect of young slabs on the shallow mantle wedge and overriding lithosphere, rather than melting of the slab itself. Furthermore, variation from “normal” arc volcanism to adakitic volcanism (without melting of the slab) may signal fluctuations in the subduction zone architecture (crust thickness, plate subduction angle and configuration, etc.), variations in the contributions from the subducting slab (mantle fluxing), mantle rheology, and/or thermal structure of a subduction zone.

2. GEOTECTONIC SETTING

2.1 Tectonic background

Western Panama is a narrow landmass with a convergent margin on the southern side and a largely passive margin on the northern side (Figure 4.1) (Camacho et al., 2010). The present arrangement of the plates is the product of the ~23 Ma (Lonsdale, 2005) split of the Farallon plate into the Nazca and Cocos plates. This event had important tectonic and volcanic consequences in the region including change in direction and acceleration of spreading at the East Pacific Rise (Goff and Cochran, 1996; Wilson, 1996), and faster, less oblique subduction at the western margins of the American trenches (Sempere et al., 1990; Sigurdsson et al., 2000). In Panama, subduction of the Cocos plate occurs beneath the westernmost parts of the country, with the Nazca plate outboard of the trench further to the east. Baru Volcano, near the border with Costa Rica is the most prominent of several volcanoes that extend to El Valle, near Panama City. Elevations increase progressively to the northwest, where the Talamanca Mountains overlap the modern volcanic front (Drummond et al., 1995), and form a high elevation (nearly 4 km), isostatically supported range (Dzierma et al., 2010) that extends into southern Costa Rica.

The Cocos Ridge, an area of topographically elevated seafloor, extends from the Galapagos islands to the Middle America Trench (Figure 4.1), where it may be underthrusting the Talamanca range (Kolarsky and Mann, 1995). There are no present-day manifestations of subduction (active volcanoes, deep earthquakes) east of the location where the Cocos Ridge impacts the coast. Since the Cordillera de Talamanca (the area of topographic uplift and exhumation) is placed directly opposite to the area of indentation of the Cocos Ridge subduction, a potential causal relationship has been suggested.

The subduction zone with which the Cocos oceanic ridge is interacting is produced by the subduction of the Cocos plate (76-91 mm/yr, normal to the Middle America Trench: DeMets, 2001; Trenkamp et al., 2002) and Nazca plate (oblique subduction at 50 mm/yr: Jarrard, 1986; Trenkamp et al., 2002) (Figure 4.1). The seismically active right-lateral Panama Fracture-Balboa Fracture-Coiba fracture zones define the limit between the Cocos and Nazca Plates (Lonsdale, 2005). The triple junction generated by the intersection of the Panama fracture zone with the trench has been described as migrating southeast at ~55 mm/yr (Morell et al., 2008). Throughout Panama and in southern Costa Rica the Caribbean plate is underthrusting Central America along the North Panama Deformed Belt (Kellogg and Vega, 1995; Mann and Kolarsky, 1995). The presence of this underthrusting belt may enhance the compressional effects of ridge subduction (e.g. Fisher et al., 2004).

Receiver function studies by Dzierma et al. (2011) in the neighboring region of the Talamanca cordillera has identified a steeply (80°) dipping slab that extends to at least 70-100 km depth and may extend underneath Baru volcano. This may indicate that only a short length of the Cocos Ridge has entered the subduction zone and that shallow angle underthrusting is still being developed. The imaged slab by Dzierma et al. (2011) agrees with previous results from local seismicity (Dinc et al., 2010; Protti et al., 1994 and Quintero and Kissling, 2001) and tomography studies (Dinc et al., 2010). On the basis of this evidence for steep slab subduction, it is possible that the slab outboard Panama may dehydrate in the forearc.

2.2 Volcanic history

Subduction zone magmatism has been active in Panama since the early Tertiary (64 - 61 Ma, Lissinna et al., 2006; and Maury et al., 1995,). In the region, three volcanic arcs have been identified, with the first arc being developed at the beginning of the Oligocene epoch (Maury et al., 1995). The volcanic products of this arc have been described by Alvarado et al. (1992), de Boer et al. (1995), and Abratis (1998) as a primarily tholeiitic to calc-alkaline (low K). The second arc developed during the middle to late Miocene, and is characterized by effusive activity that ranges from low-K calc-alkaline toward high-K calcalkaline compositions (Wegner et al., 2011).

Coincident with this middle-late Miocene period of arc magmatism, accretion of Galapagos-derived ocean island basalt (OIB)–type basalt complexes continued along the southern Panamanian margin (Alvarado et al., 1992; Hauff et al., 1997; Hauff et al., 2000; Hoernle et al., 2002). The late Neogene period saw the progressive closure of the oceanic connection between the Caribbean Sea and Pacific Ocean during the interval between 6.2 and 3.5 Ma (Coates et al., 2003; Coates et al., 1992; Collins et al., 1996; Duque-Caro, 1990) as a consequence of terrane collision, magmatism, and tectonic uplift along transverse fault systems in present-day central Panama (de Boer et al., 1995; Hoernle et al., 2002).

The most recent arc commenced with extensive volcanism displaying an adakitic signature in central-western Panama (Hidalgo et al., 2010; Hidalgo et al., 2011; Hidalgo et al., in preparation;) and southern Costa Rica at ~2 Ma (Abratis, 1998; Defant et al., 1991a; Defant et al., 1992; Defant et al., 1991b; Johnston and Thorkelson, 1997). In contrast to other sections of the Central American Arc (e.g. Northern Costa Rica) where the Oligocene and Miocene arc sequences lie behind the currently active arc front (Carr et al., 2003; Gazel et al., 2009), the most recent period of volcanism at the Panamanian arc has developed directly over the Miocene volcanic sequence (Figure 4.1).

3. ANALYTICAL TECHNIQUES

3.1 Geochronology

Three representative least-altered samples from the Miocene sequence in Panama were selected for $^{39}Ar/^{40}Ar$ step heating analysis at the Argon Geochronology Laboratory at the University of Michigan. After crushing, fresh matrix chips (0.2g) were carefully handpicked under a binocular microscope and Ar analysis was undertaken using standard procedures outlined in Frey et al. (2007). Samples were wrapped in pure Al foil packets and irradiated in location 5C of the McMaster Nuclear Reactor. Samples were step-heated using a continuous 5W Ar-ion laser and Ar isotopes were analyzed using a VG- 1200S mass spectrometer operating with a total electron emission setting of 150 micro-amps. The mass spectrometer is equipped with a Faraday detector and a Daly detector operated in analog mode. All samples were analyzed with the Daly detector. Mass discrimination (source + detector) was monitored daily with ~$4x10^{-9}$ ccSTP of atmospheric Ar. Typically, the measured atmospheric $^{40}Ar/^{36}Ar$ ratio has been about 290 for the past several years. All measured isotope measurements were corrected for a standard $^{40}Ar/^{36}Ar$ value of 295.5. Isotope measurements were fitted to a signal decay plus memory effect function and extrapolated back to inlet time. Error estimates for each isotope were based upon the fit of individual measurements to the signal decay function and these 5 isotope error estimates were propagated through all isotope ratios, J values and age estimates. Isotope concentration values for ^{37}Ar and ^{39}Ar were corrected for decay since the samples were irradiated. Corrections were made for interference reactions from Ca and K and for the build-up of ^{36}Ar from the decay of ^{36}Cl. Within the irradiation packages, samples were interspersed with standards packets and J was calculated for samples by interpolating a fitted cosine function for J as a function of vertical position within the can. J error estimates include the uncertainties in the isotope measurements for the standards plus any scatter of measured J about the fitted interpolating function. J error does not include uncertainty in the assumed K-Ar age, nor does it include decay constant uncertainties (isochrons are included in the supplementary material). Table 3.1 summarizes the results presented in this section.

3.2 Major and Trace elements.

About 35 Samples (1-2 kg) were taken from the least-altered outcrops. They were subsequently trimmed to exclude visible alteration/weathering. Sample billets were polished to remove saw marks and cleaned in an ultra sonic bath with deionized water. After drying, the billets were crushed in a steel jaw-crusher and then powdered in a ceramic Bico flat plate grinder. The sample powders were fused into lithium tetraborate glass disks using the procedures outlined in Deering et al. (2008). Major elements, Zr, Sr, Rb and Ni were analyzed by Brucker XRF, the balance of the trace elements were obtained by laser-ablation using a Cetac LSX-200 coupled to a Micromass Platform ICP-MS at Michigan State University. Trace element reproducibility based on standard analyses is typically better than 5% (Vogel et al., 2006). Results of these analyses are presented in the supplementary material of this study.

4. RESULTS

4.1 $^{40}Ar/^{39}Ar$ Geochronology

A summary of the calculated ages is provided in Table 4.1 and Figure 4.2. Error estimates from all ages are reported at the 1-σ level. All ages were processed using whole rock samples. Geologically meaningful plateau ages were obtained from whole rock samples (Figures. 2a, 2b, 2c and 2d; Table 4.1). High Ca/K fractions were excluded from plateau calculations, as these were likely due to the degassing of feldspar phenocrysts.

The temporal and stratigraphic controls at Baru volcano have been made possible by sampling the stratigraphic sequence in the sector collapse depression. This has proven to be vital for unraveling the eruptive history of Western Panama. The stratigraphic sequence during the Quaternary at Baru volcano has been recently revised by high precision $^{39}Ar/^{40}Ar$ techniques (Hidalgo et al., in prep). In this study, we have collected samples from the Miocene sequence at Baru volcano and have produced new high precision $^{39}Ar/^{40}Ar$ dates for lava sequences in Respingo (15.73± 0.26 Ma) and Cerro Punta (10.13± 0.15 Ma; 9.377±0.041 Ma) on the north flank of Baru volcano (Figure 4.1). These locations are part of the limited exposures of the Miocene sequence in the region; given the overlap of the Quaternary arc and the Miocene arc. Miocene samples recovered from along the Pacific coast (Isla Muertos), outboard of Baru volcano are within the same age range (10.46±0.21 Ma) as the Cerro Punta unit and exhibit similar geochemical characteristics, and have therefore been grouped with these samples.

Based on these results we have organized the Miocene and Pliocene volcanism at Baru volcano and surrounding areas in 3 groups using several criteria: (1) Field mapping that has allowed us to identify stratigraphic units, (2) $^{40}Ar/^{39}Ar$ geochronology, and (3) geochemistry. The combined units are: Respingo (15.73± 0.26 Ma), Cerro Punta (11.24± 0.36 to 9.377±0.041 Ma). In addition, we have included Boquete unit (0.77 ma, Gazel et al., 2010) because it is the first recorded occurrence of the Quaternary arc sequence at the Baru volcano region, and is important for constraining the transition from the Miocene arc to the present arc magmatism.

4.2 Major elements

Our bulk rock major and trace element analyses include new data that we have collected from the Miocene sequence and the nascent Quaternary arc at Baru volcano in Panama and surrounding areas. These data fill a critical spatial and temporal gap in the geochemical record of the Panamanian Arc. Complete chemical analyses for the new samples presented in this study are presented in table 4.2.

Our major element XRF analytical results are similar to those reported previously in the region (Hidalgo and Rooney, 2010). At Baru volcano, Hidalgo and Rooney (2010) explained that the chemical variation observed in the volcanic sequence of the region was controlled by the fractionation of amphibole with minor but important contributions from garnet, plagioclase and pyroxene. Fractionation processes are evident in the set of samples that we present in this study. This is supported by the covariation in key elements (SiO_2 and MgO vs TiO_2 or Na_2O + K_2O; Figure 4.3). Almost all the Baru volcano Miocene lavas plot as subalkaline basalts to dacites on the total alkalis versus silica diagram (Figure 4.3), although a few samples from the Cerro Punta unit and from the Respingo unit are on the alkaline field (Figure 4.3). In addition, the Cerro Punta and the Respingo units have extremely variable total alkalis (~1%-~9%), and samples from the Cerro Punta unit and the Boquete unit tend to extend to higher concentrations of these elements than lavas from the Respingo unit (Figure 4.3). Overall, major element concentrations (K_2O, MgO, TiO_2 and SiO_2) tend to increase from the Respingo unit (~14 Ma) to the Cerro Punta unit period (~10-9 Ma) to the Boquete unit (~0.77 Ma)

(Figure 4.3). Perhaps the clearest distinction between the Respingo unit and the more recent units Cerro Punta and Boquete, is the K_2O content (Figure 4.3). The Respingo unit is distinctly lower in K_2O (low K to medium K); while a greater number of the Cerro Punta and Boquete lavas plot within the high K or the shoshonite series field.

The MgO content of the lavas the ranges from 0.85 to ~11 wt % with relatively high MgO in Boquete lavas at given silica content (Figure 4.3). The FeO*/MgO diagram reveals that most lavas from the Respingo and Cerro Punta have tholeiitic affinities, whereas the Boquete lavas are calc-alkaline. Although some of the Cerro Punta lavas are rich in FeO*, the FeO*/MgO ratio is constant suggesting an atypical tholeiitic trend. The TiO_2 contents of the lavas from the Respingo, Cerro Punta and Boquete units, tend to decrease with increasing silica. Lavas from these units do not behave like typical tholeiites, which show TiO_2-silica covariation but instead, have their highest TiO_2 content in lavas with the lowest silica content. The TiO_2 contents of the most mafic lavas increase from the Respingo unit period (~14 Ma) through the Boquete unit period (~0.77 Ma), similar to the variations in total alkali contents. This may indicate that lavas in the region are derived from primitive magmas that are a result of progressively lower degrees of melting (F), or from lavas that are derived from a progressively more enriched mantle source.

4.3 Trace elements

Trace element abundances and variation are shown in normalized multi-element plots (Figure 4.4 and trace element X- SiO_2 are included in the Appendix). The data presented in these diagrams is from selected samples with excellent stratigraphic control.

Across units there is no consistent temporal variation of incompatible elements. The Respingo basalts and basaltic andesites have lower K_2O and the Cerro Punta lavas have lower P_2O_5 (Figure 4.3 and 4.4). There is some rare Earth element (REE) variation across units with pronounced heterogeneity in the heavy rare Earth elements (HREE) and middle rare Earth elements (MREE). These elements are most enriched in the Cerro Punta unit and most depleted in the Boquete unit. Respingo unit stands out in having the smallest Na-Ta anomalies. The light rare Earth elements (LREE) are more depleted in the Respingo unit, while high field strength elements (HFSE) are more depleted in the Boquete unit.

An interesting feature of samples of the Cerro Punta unit is the concave upwards patterns on the middle to heavy rare earth elements. This is similar to those described by Rooney et al. (2011) in older sections of the Panamanian arc (~25 Ma). In the Boquete unit, the negative slope in the HREE that tend to decrease from Tb to Lu has been described for the recent Quaternary volcanism by Hidalgo et al. (in prep.) and Hidalgo and Rooney (2010).

5. Discussion

5.1 Geochronology and temporal chemical variation

The temporal and chemical stratigraphic controls established at Baru volcano are unique in the region and serve as an important guide for unraveling the eruptive history and magmatic evolution of the region. Our new high precision $^{39}Ar/^{40}Ar$ dates, add to the previous work in this volcanic center on plutonic and lava flows from the Oligocene sequence (Drummond et al., 1995), lava flows from the Miocene (Wegner et al., 2011) and Quaternary (Gazel et al., 2009; Hidalgo et al., in preparation). Of great importance is the new stratigraphic control and dates combined with chemical analyses (Hidalgo et al. in prep). These data, along with previous contributions allows us to examine the temporal geochemical evolution of the Panamanian Arc from the Mid-Miocene through to the Quaternary.

Mid-Miocene Lavas – Respingo unit (~15 Ma)

Lavas from this unit have abundant olivine and pyroxene phenocrysts and are less enriched in SiO_2 and K_2O than samples from late Miocene (10-9 Ma) (Figures. 4.4 and 4.6). Similarly, these lavas are more depleted in the HFSE and LILE elements (Figure 4.4), exemplified by the slightly lower LREE and lower Cs, Rb, and Ba when compared to the Cerro Punta and the Boquete Quaternary unit. Heavy rare Earth elements (HREE) concentrations fall between those of the Cerro Punta and Boquete units (Figure 4.4).

Late Miocene Lavas – Cerro Punta unit (~10-9 Ma)

These are predominantly amphibole+pyroxene bearing tholeiitic lavas that are progressively more enriched in K_2O (medium K calc-alkaline series to rocks from the-shoshonite series), and more depleted in TiO_2, Fe_2O_3, and CaO. SiO_2 content is more variable than the observed in other units (Figures 4.3, 4.6). The Cerro Punta Lavas and the Quaternary lavas have similar large-ion lithophile elements (LILE, Sr, Ba, Rb, etc) systematics (Figure 4.4). MREE and HREE are typically more enriched in the Cerro Punta unit. A limited number of samples from the Miocene (Cerro Punta) show the initial stages of Sr enrichment observed in the Quaternary arc (Boquete unit, Figure 4.4 and ESM 2). Lavas from the Cerro Punta unit have concave upwards MREE-HREE patterns that have been observed in other parts of the Panamanian arc (Cerro Patacon; Rooney et al., 2010).

Quaternary Lavas

In these lavas, amphibole is the only mafic phase present (Hidalgo and Rooney, 2010). Lava samples from the Boquete unit range from medium to high K cal-alkaline lavas that have higher TiO_2 and MgO for any given SiO_2 than lavas from the Miocene. The recent sequence of Quaternary rocks (excluding Boquete unit) has been described extensively in Hidalgo and Rooney (2010) and Hidalgo et al. (in prep). These authors have described the most recent Quaternary lavas at Baru volcano having restricted chemical major element composition and displaying similar K_2O (medium to high K calc-alkaline series). This is similar to what has been the late mid-Miocene lavas (Quaternary field in Figure 4.6). However, TiO_2 is lower while MgO and Na_2O (not shown in Figure 4.6) are more enriched. Compared to the Boquete lavas, the samples presented by Hidalgo and Rooney (2010) from Quaternary lavas are more restricted in SiO_2, while other major element variations are similar. Quaternary lavas have extremely depleted HREE concentrations (high La/Yb ratios, Figure 4.6) typical of adakite-like signatures.

5.2 Arc crust processes

The trace element variations that we have observed at Baru volcano during the Miocene (MREE-HREE concave upwards patterns) have been observed previously in Panamanian arc region. The concave upward HREE pattern has been described from late Oligocene magmas in Cerro Patacon (Canal Zone), and has been explained by the fractionation of considerable amounts of amphibole from water-rich magmas, supported by the presence of abundant monomineralic lower-mid crustal amphibole cumulate nodules (Rooney et al., 2010).

Abundant amphibole-rich cumulate nodules recovered at Cerro Patacon (Rooney et al., 2010) and Baru volcano (Hidalgo & Rooney 2010) have been interpreted as part of a lower-mid crustal crystal mush region that produces the ‘wet’ end member observed in volcanic arcs (e.g. Bachmann and Bergantz, 2008; Deering et al., 2008). Crystal mush and recharge models have been suggested for magma evolution (e.g.

Eichelberger et al., 2000; Bachmann and Bergantz, 2004; Eichelberger et al., 2006; Bachmann and Bergantz, 2008), and these authors have emphasized the role of lower-crustal 'hot zones' in the generation and evolution of arc magmas (Dufek and Bergantz, 2005; Annen et al., 2006). Central to many models of arc magma evolution is the concept of 'cryptic fractionation' where the geochemical signature of a particular crystal may be evident in the erupted products but the crystal itself is not an observed phase. Cryptic fractionation of garnet is necessary for some models of adakite-like magma genesis (Rodriguez et al., 2007; Chiaradia, 2009; Chiaradia et al., 2009) and has been invoked for the Baru Quaternary volcanism by Hidalgo and Rooney (2010). In lavas from the Boquete unit and some lavas of the Miocene (from the ~10-9 Ma period), the involvement of garnet is supported by the trace element variations (Figures 4.4, 4.5 and 4.6).

The contribution of residual garnet in the basalt source mantle or garnet fractionating in the crust could be assess by using the trace element ratios (La/Yb)n, (Nb/Yb)n and Sr/Y (Pearce et al., 2005; Peate et al., 1997). The Boquete lavas have very high (La/Yb)n and (Nb/Yb)n ratios (Figure 4.5), while a limited amount of lavas from the Cerro Punta unit have (La/Yb)n ratios that are higher compared to other lavas in the region. The variation observed in (La/Yb)n and (Nb/Yb)n in the Boquete unit and some lavas from the Cerro Punta unit, occurs at near constant HFS element ratios (e.g. Nb/Zr), which is consistent with different degrees of garnet fractionation. This observation is also consistent with the high Sr/Y and low Y of some Cerro Punta and Boquete lavas and negative slopes on the HREE (Figure 4.4). However, the Sr/Y ratio could also be influenced by amphibole fractionation, which is more evident in the Cerro Punta unit (Figure 4.4).

In comparison to the typical gabbroic assemblages evident in western Panama Oligocene magmatic sequences, the transition to amphibole-rich magmas during the Miocene may signify a shift towards water-enriched magmas that may have stalled at lower crustal levels. Magma stalling impedes the crystallization of anhydrous phases (olivine+pyroxene), which are favored during decompression and degassing (*Annen et al.*, 2006), and isobaric cooling promotes the widespread precipitation of amphibole in hydrous magmas (Carmichael, 2002). Exhumed arc terranes (e.g., Alaska, Kohistan arc, Bonanza arc) commonly contain amphibole-bearing cumulates, illustrating the important role of amphibole in the sub-arc crust (Jagoutz, et al, 2010).

5.3. Modeling magma generation conditions

In this section, we explore the temporal evolution of magma sources at Baru volcano from Miocene to present and examine the relative contributions from the mantle source and slab fluids (sediments+altered oceanic crust). This approach allows for the determination of the composition of primitive basalts, degree of melting of the mantle source (or slab) necessary to generate them, water content of primitive basalts, and PT conditions of magma generation.

5.3.1 Primary basalt compositions

To probe the conditions of melt generation beneath the Western Panamanian arc, we have first estimated the primary magma composition, that is, the composition of the magma when it was last in equilibrium with the mantle. Because all erupted magmas have gone through some degree of crustal-level crystal fractionation, the primary magma must be inferred by reversing the fractionation process. We have calculated the primary basalts (Table 4.3) for the different periods of activity at Baru volcano using the olivine maximum fractionation model, whereby equilibrium olivine is added until the basalt composition is in equilibrium with mantle peridotite (Takahashi, 1986). This is achieved by monitoring Ni and Mg# in olivine in the basalt until this approach yielded a melt in equilibrium with the mantle olivine (Fo=90). In addition, the effect of garnet fractionation was corrected for primitive basalts by adding garnet (0.5%) and monitoring the Tb/Yb (primitive mantle normalized) until the Tb/Yb approached 1 (Hidalgo and Rooney, 2010).

5.3.2 Arc Basalt simulator 3

After we established the primitive basalt compositions, we have applied the quantitative forward mass balance model Arc Basalt Simulator (ABS 3; Kimura et al., 2009) to our primary magma compositions. This model incorporates slab dehydration during prograde metamorphism in the subducting plate, the reaction between fluid and mantle at the base of the mantle wedge, and the P-T-X H_2O conditions during fluid-fluxed mantle melting.

Model Inputs

Source material compositions

Subducting sediment, altered subducting oceanic crust, and mantle compositions are required inputs for the ABS3 forward modeling. We have selected a sediment composition from Patino et al. (2000) (DSDP site 495), which we infer is suitable for the Baru region given the similarities in the sediment description provided in Van Andel (1971) for cores recovered around the Coiba Ridge area outboard Baru volcano and Sadofsky et al (2009) around the Cocos Ridge area. The composition of the altered subducting oceanic crust was taken from Harpp et al. (2005). A series of mantle compositions were evaluated: the embedded in ABS3 depleted MORB mantle (DMM) composition by Workman and Hart (2005) and the DMM composition proposed for the Central American region (Feigenson et al., 2004). Using these compositions, the model did not converge. More successful results were achieved by using a more enriched mantle source. Feigenson et al. (2004) proposed that one of the mantle reservoirs for Central America has a more enriched composition than the DMM mantle reservoir described for most of the region. Feigenson et al. (2004), explained this enriched mantle reservoir as being derived from remelting of Galapagos hot spot-influenced mantle by modern subduction. Other models have been presented to explain this signature in the region and are summarized in Carr et al. (2007). Gazel et al. (2009), using Pb isotopes, has demonstrated that the contribution from the Galapagos hot spot has been variable over time. These authors suggest that the contribution from Galapagos enriched mantle was minimal during the Oligocene-mid-Miocene, while during mid-Miocene it could have been as high as 0.5%. During the Late-Miocene to Pliocene this contribution was extremely variable (0.1-2%) (Gazel et al., 2009).

A progressively more enriched mantle source through time is additionally supported by trace element ratios of our samples. A ratio of a highly incompatible element (Nb) to a less incompatible element (Yb, Ta or Zr) gives a proxy for mantle enrichment (Pearce et al., 2005). In Figure 4.5, samples from the Respingo and Cerro Punta units have $(Nb/Zr)_n$, $(Nb/Ta)_n$ and $(Nb/Yb)_n$ that approach unity, while for the Boquete unit this ratios is greater than the unity in all samples. The variation of these ratios and the increased concentration of HFSE through time observed for the different units, are consistent with a progressively more enriched mantle source (e.g. Feigenson et al., 2004).

The mantle composition proposed by Gazel et al. (2009) was utilized as a starting point in order to produce our primitive basalts. We have refined the contribution from the Galapagos plume using isotopic information presented in Wegner et al. (2010). The contributions from the Galapagos hot spot were determined by using the mixing lines in Gazel et al. (2009). For the Mid-Miocene lavas ($^{206}Pb/^{204}Pb$=18.771 and $^{208}Pb/^{204}Pb$= 38.417; Wegner et al., 2010), the hot spot contribution was fixed at 0.4%; for the Late Miocene $^{206}Pb/^{204}Pb$=18.960 and $^{208}Pb/^{204}Pb$ = 38.728) a contribution of 1% was used. Finally, early Quaternary lavas found in Baru volcano ($^{206}Pb/^{204}Pb$ =19.289 and $^{208}Pb/^{204}Pb$ = 39.235) record a contribution of 3.5%. These mantle compositional varieties are presented in Table 4.3 and in Figure 4.7.

Other parameters.

A slab P-T path is necessary for the slab flux calculations and ABS 3 contains estimates of slab P-T path for a number of subduction zones worldwide. We have chosen the Costa Rican subduction zone given the constraints that Syracuse et al. (2010) have provided for the Costa Rica region and the similarities between the Central-Southern Costa Rica subduction zone and the northern Panamanian subduction zone outlined by Dzierma et al. (2011).

The slab sediment (SED) and altered oceanic crust (AOC) contributions to the slab flux (either a fluid or melt) were deduced by monitoring mass balance calculations based on trace element abundances and their fit with our primitive basalts (this is done in the macro screen in ABS). Within the ABS module, we adjusted the Fliq(SED) parameter (slab-sediment liquid fraction in the slab flux), together with Slab P(GPa, a variable corresponding to slab depth). In our study, we have found good fit with our selected Fliq (SED) and Slab P(GPa) and have summarized this parameters in Table 4.4 and have shown this good fit graphically in Figure 4.7.

Other required parameters are related to mantle melting, these are: melting pressure (P(GPa)), melting temperature (T(C)), and slab liquid fraction added to the mantle (Fslb liq %). ABS 3 adjusts these parameters iteratively. When a reasonable fit is achieved in terms of trace element compositions of primary basalts this first order adjustment allows approximation of the entire mass balance. We have found a good initial fit using the initial values for these parameters as indicated in table 4.4 and shown in Figure 4.7.

Results from the ABS simulation

An advantage of using the ABS 3 simulator, is that once a good fit for the different parameters (Fliq(SED), Slab P(GPs), P (GPa), T (C) and Fslb liq%) is found, plausible ranges of these parameters could be explored using the macro function of the ABS 3 Excel spreadsheet.

In Figure 4.7, we present graphically our best-fit results for the ABS 3 modeling and in Figure 4.8 we present the intensive parameter ranges by which the modeling was constraint and produced possible scenarios for the generation of the Baru volcano primitive basalts. Overall, our results indicate that slab fluids derived from the dehydrating slab are necessary for all of our primitive basalts to form but more importantly our modeling provides insights into the origins of the adakite signature.

Our model predicts that slab flux parameters for the Mid-Miocene Lavas (Respingo unit) differ significantly from the adakite signature-bearing Late-Miocene to Pliocene Lavas (Cerro Punta, Boquete and La Cuesta units). For the Mid-Miocene basalts, slab fluids are produced at relatively high pressures (1.6-2.0 GPa), while in the Late-Miocene-Pliocene basalts were produced at lower pressures (1.0-1.4 GPa) (Figure 4.8a). Moreover, the degree of partial melting of the mantle peridiotite (F(%)) is predicted by our modeling to have been greater during the Mid-Miocene (F=20-23%) and smaller afterwards (10-15%). The F (%) parameter is directly correlated to the H_2O

% in the mantle periodiotite (XFlux in Figure 4.8). This water content is greater in the mantle source for the Respingo basalts (0.8-1.5%) in comparison with the mantle source for the more recent basalts (0.2-1%). Finally, the estimated H_2O contents in primary magmas (X H_2O bas, in Figure 4.8) are consistently high (3.5-6%) for the Mid-Miocene basalts, while during the Late-Miocene to Pliocene primary magmas may have variable amounts of dissolved H_2O (2-5%).

5.4 Origin of the adakite signal

The origin of adakite-like magmas remains controversial. Initially, the term adakite had petrogenetic significance, implying an origin by direct melting of the eclogitized subducting oceanic crust (Defant, 1990; Defant et al., 1991a; Kay, 1978; Kay and Kay, 2002; Kay et al., 1993). In this model, the subducting edge of the slab is undergoing melting caused by being in contact with mafic magmas (not necessarily cogenetic) that are derived from adiabatic decompression of mantle material. From this model, the resulting melts should be hot and relatively dry (≤0.7 wt. % H_2O) as the subducting slab has undergone dehydration in the forearc before achieving melting (Obara, 2002; Kohut et al., 2006).

The somewhat lower water content of parental mafic melts during the Late-Miocene to Pliocene period, is clearly more hydrous than melts generated by slab melting processes (<0.7 % H_2O; Kohut et al., 2006). The decrease in water content from the Mid-Miocene to the Late-Miocene to Pliocene, might be related to loss of water in the forearc due to shallow subduction of the Nazca Plate (Dzierma et al., 2011) or dilution of hydrous wedge mantle with dry mantle derived from the back-arc, or a combination of these processes.

A decrease fluid content in the parental melts is also supported by key trace element ratios. The Pb/Ce has been used an indicator of slab-derived fluid addition to the mantle peridotite basalt source because Pb is more fluid mobile whereas Ce is relatively compatible in melts but not in hydrous fluids (Pearce et al., 2005; Zellmer, 2008). Hence this ratio can evaluate the fluid component in our units across time. In our data suit, Pb/Ce (Figure 4.5) tends to extend towards lower ratios in the Boquete unit (Figure 4.5) than in Cerro Punta and Respingo units. This may be consistent with a progressive decrease in the fluid component towards the Quaternary.

Water content is extremely important during deep to shallow fractionation of arc magmas. In arcs, amphibole is a major component of the fractionation assemblage (Davidson et al., 2007). Müntener et al. (2001) and Alonso-Perez et al. (2009) have shown that at moderate pressures (12 kbar, pressure expected at lower crust levels at Baru volcano) and high water contents (8% H_2O) crystallization is dominated by amphibole, and as a consequence the amount of garnet is limited. As amphibole crystallization progresses, garnet stability increases at the expense of amphibole with decreasing water contents (< 3-6% H_2O) (Alonso-Perez et al., 2009) and generation of an adakitic signature is possible. It is for this reason, that Zellmer (2009) argues that

H_2O variations may modulate adakite signature at normal arc crustal thicknesses: garnet being favored at lower H_2O contents (3-6%) while, amphibole is favored at higher water contents, consistent with the model results that show a lower water content in the more adakitic mid-miocene-pliocene magmas.

The absence of an adakitic signal prior to the late-Miocene might not only be related to an increase magmatic water content in this period but also to the arc crust architecture. Hidalgo and Rooney (2010) have theorized that prior to the arrival of the Cocos and Coiba ridges to the Middle America Trench, magma ascent was rapid. Expedited magma ascent promotes the crystallization of anhydrous phases, which are favored during decompression and degassing (Annen et al., 2006). Mid-Miocene magmas (Respingo unit) are characterized by abundant anhydrous minerals (ol+cpx) which is consistent with this observation. The widespread role of amphibole in the Western Panamanian magmas from Late-Miocene to present may have its origin in the arrival of the Cocos and Coiba ridges to the Middle American Trench. This event may have generated significant perturbations of the crustal and upper mantle structure of the region. Specifically, enhanced plate coupling, crustal shortening, changes in the stress conditions of the overlying plate, and arc-parallel movement of material have been invoked (Hoernle et al., 2008; LaFemina et al., 2009).

During the initial stages of the ridge collision magma ascent is impeded due to the sealing of usual crustal transfer structures, causing stalling and differentiation of magmas at lower crustal levels e.g. (Chiaradia et al., 2009; Rooney et al., 2010).

Magma stalling impedes the crystallization of anhydrous phases, and cooling promotes the widespread precipitation of amphibole in hydrated magmas (e.g. Carmichael, 2002). Furthermore, magma stalling and fractionation at deeper crustal levels within the garnet stability field at reduced water contents (3-6 %) successfully explains the origin of adakite signature in the Western Panamanian arc.

Our results are difficult to reconcile with models that propose that the origin of the adakite signature in the region is a product of variable contributions of slab melts across time (e.g. Defant et al., 1991). Adakitic magmas from Baru volcano have temperatures and water contents that are similar to the non-adakitic Respingo unit basalts but carry less H_2O, this would favor the absence of slab melting, and would imply that the adakites signatures in Baru volcano lavas may be related to liquid lines of descend of a somewhat less hydrous mantle melts in the lower arc's crust in the presence of residual garnet. Our results are consistent with models that explain the adakitic signature by lower crust fractionation of mantle derived magmas (e.g., Macpherson et al., 2006; Hidalgo and Rooney, 2010).

We have shown that the trace element variations in primary magmas from the mid-miocene to present can be explained by subtle variations in the subduction parameters and do not require the introduction of exotic slab melting processes. Increasing, La/Yb and Sr/Y ratios (Figures. 4.5 and 4.6) during the Late-Miocene to present are related to decreasing water contents in associated magmas (Figure 4.8).

5.5 Concluding remarks

The outcome of our modeling allows us to understand the evolution of magmatic sources that contribute to magmatism in the Western Panamaina Arc and ultimately result in the generation of an adakitic signature during the Mid-Miocene to Quaternary. Our findings highlight that melting of the subducting oceanic crust is not responsible for the generation of the adakite signature in the Panamanian arc like it has been proposed for this area. Our results join other studies (Sisson and Grove, 1993, Shelnutt and Zelmer, 2010 and Zellmer 2012) that have concluded that small variations in H_2O content have a determining role in the chemical evolution of arc magmas at crustal levels. In addition, the generation of the adakite signal in the Western Panamanian arc, may have been aided by the arrival of the Cocos and Coiba ridges to the subduction zone, which enhanced magma stalling in the lower crust and the crystallization of hydrous phases and garnet.

6. Appendices

6.1 Appendix one: Figure Captions and Table captions

Figure 4.1. For interpretation of the references to color in this and all other figures, the reader is referred to the electronic version of this thesis (or dissertation).Map of Costa Rica and Panama showing the tectonic setting of the region and the subduction of the Galapagos hotspot Seamount province beneath Costa Rica (Hoernle et al, 2008). Other features of the subduction zone include the Cocos and Coiba ridges impacting the Middle America Trench, and the temporal evolution of the arc through time. Positions of the arc are shown from Oligocene (34-23 Myr ago) to the Early Miocene (11-23 Myr ago) to the Late Miocene (6-12 Myr ago) to the Quaternary (represented by the solid triangles). In Panama, the Quaternary volcanism is represented by voluminous adakite-like magmas that were erupted in a short period of time. The inset shows the location of the type localities sampled for this study (refer to text for complete explanation).

Figure 4.2. $^{40}Ar/^{39}$ age spectra for the studied units. Composite isochron ages based on 2 runs for each of the samples. Full data is available in the online resource 1.

Figure 4.3. Bulk rock geochemistry of selected major element variation versus SiO_2. In the K_2O vs SiO_2; subdivision of subalkaline rocks is after Rickwood (1989). Complete composition and standard deviations for major- and trace-elements for analysis of lava samples are provided in table 4.2. Samples with totals lower than 96% are excluded because it was assumed that these samples were secondarily hydrated or altered. All major elements have been normalized to 100%.

Figure 4.4. Primitive mantle (PM) normalized spider diagrams (Sun and McDonough, 1995) for the distinct arc units sampled in this study: Respingo (~15 Ma), Cerro Punta (~10-9 Ma) and Boquete (~0.77 Ma).

Figure 4.5. Incompatible trace element ratios of lavas from the Baru volcano region during the period from ~15 Ma to ~6 Ma. (X/Y)n indicates primitive mantle normalized element ratios where (X/Y)n = 1 using the primitive mantle (PM) estimate of Sun and

McDonough (1995). All trace element concentrations are normalized to primitive mantle values (Sun and McDonough, 1995), except for the Sr/Y diagram. Thin lines are primitive mantle ratios.

Figure 4.6. A. MgO and B. TiO_2 vs. SiO_2. C. and D. La, Yb and Dy concentrations are normalized to chondrite concentrations of Sun and McDonough (1995) (C) Garnet vs amphibole crystallization. This diagram includes a dotted field that corresponds with La Cuesta Lavas described in Hidalgo and Rooney (2010). The involvement of garnet is evident in the Boquete lavas while amphibole is more apparent during the Miocene in the Cerro Punta lavas. (D) This diagram includes the La Cuesta lavas as a dotted field. This diagram indicates that amphibole might be responsible for the chemical variation observed during the Miocene in MREE (F) Nb/La–Sr/Nd (after Rudnick, 1995) and (E) Rb/Sr–Sr/Nd, illustrating the composition of average oceanic island arc basalts (Hawkesworth and Kent, 2006), ocean island basalts (OIB) (Sun and McDonough, 1989), selected crustal reservoirs (upper crust, UC; bulk crust, BC) and MORB and primitive mantle (Sun and McDonough, 1989). These diagrams indicate that some of the Miocene lavas from Baru volcano (Cerro Punta) have similar chemical composition as bulk upper continental crust.

Figure 4.7. Fitting calculation results from Arc Basalt Simulator version 3 (Kimura et al., 2010) model calculations for primitive basalts from different periods of acr activity at the Baru volcano region. We include primitive basalts from the recent activity of Baru volcano (La Cuesta unit), that have been dated at ~0.213 Ma (Hidalgo et al., in prep). Solid lines with circles denotes estimated primary basalt composition, blue thin lines denote calculated melt/fluid compositions, and thin purple lines denote calculated source mantle compositions. Depleted MORB mantle (Workman and Hart, 2005) is shown for reference (DMM). The parameters used are included in Tables 4.3 and 4.4.

Figure 4.8. Intensive and extensive parameter intervals that reproduce the trace element of the primitive basalts from Baru volcano. A. Pressure of melt generation P(GPa) vs. Temperature of melt generation T(C). Respingo unit basalts are skewed towards higher temperature and pressure of melting, while the rest of the units present similar systematics. B. Melt fraction in the source peridiotite (F%) vs. Temperature of melting. Respingo samples could be reproduced if high melt fractions are present in the mantle source in comparison with the rest of the units. C. Melt fraction in the source peridiotite (F%) vs. H_2O % in peridiotite (Xflux (%)=X H_2O (%)) following the definition by Kelley et al. (2006). Samples from Respingo are derived from high degrees of melting enhanced by high water contents. D. Water content in Primitive Basalts ((X H_2O)(Bas)(%)) vs H_2O % in peridiotite (Xflux (%)). Respingo primitive basalts have consistently high water contents (4-6%) while a broad range is observed in the rest of the primitive basalts (2-6).

6.2 APPENDIX TWO: Figures

Figure 4.1

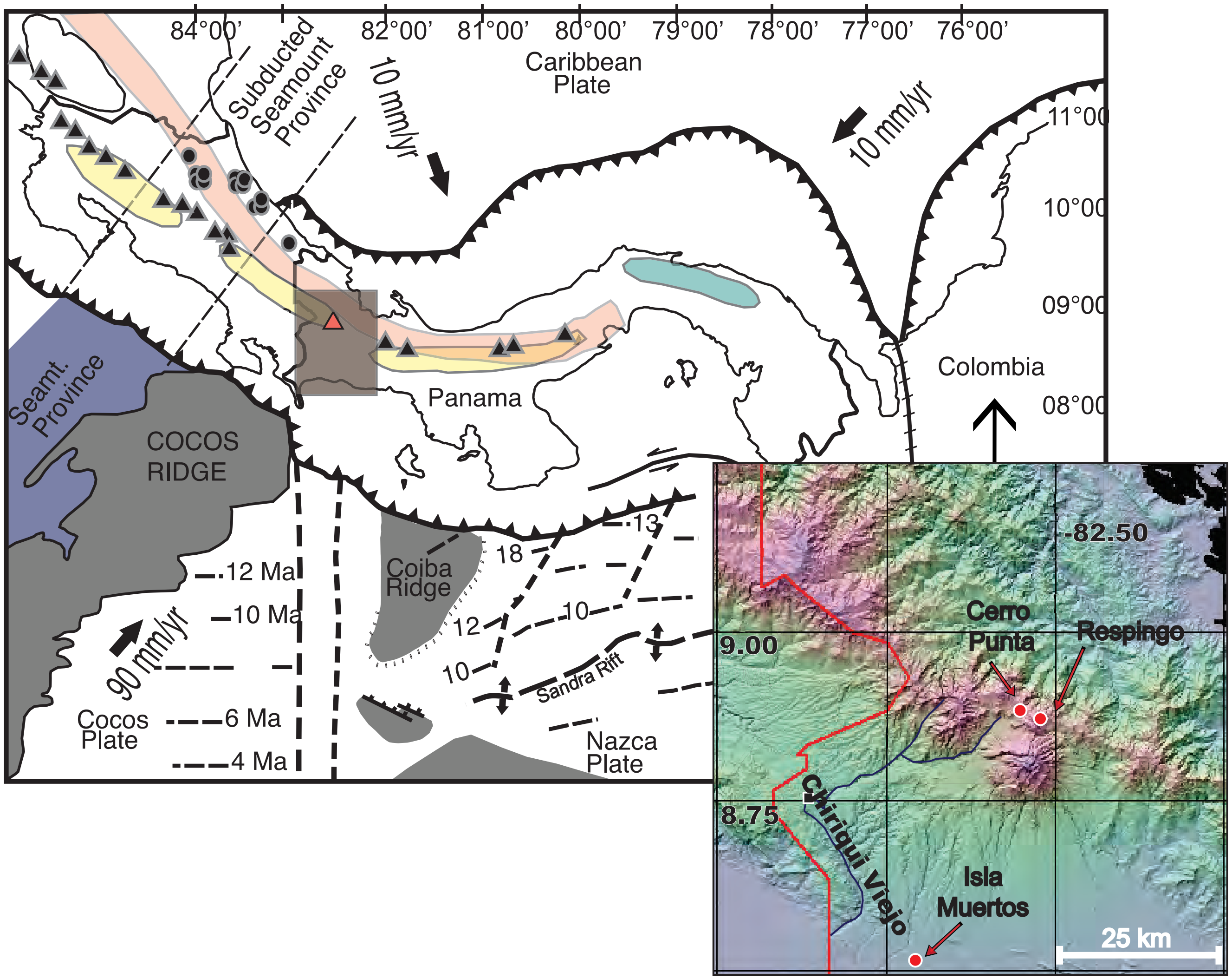

Figure 4.2

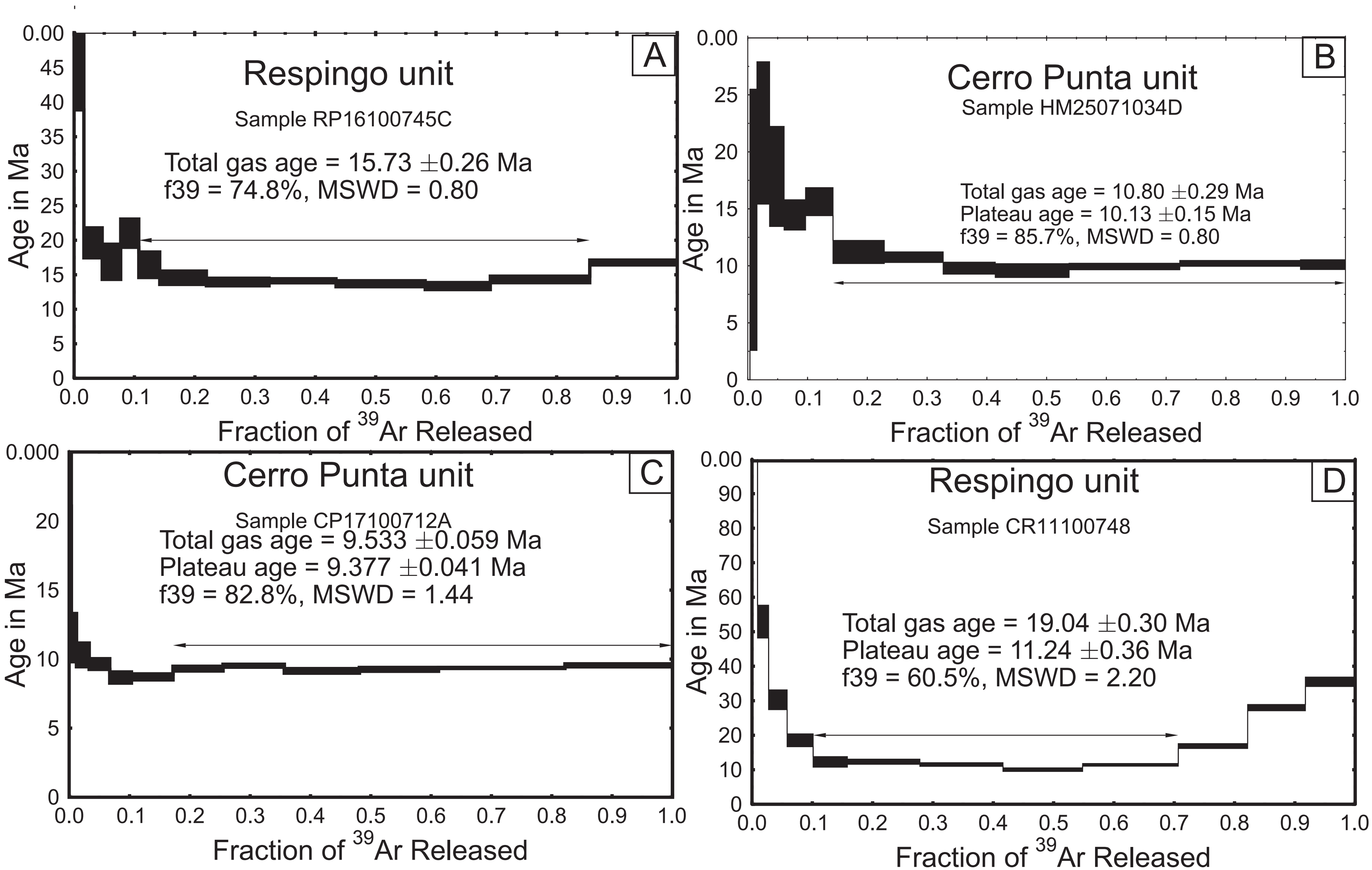
A
Respingo unit
Sample RP16100745C
Total gas age = 15.73 ±0.26 Ma
f39 = 74.8%, MSWD = 0.80
Age in Ma
Fraction of 39Ar Released
B
Cerro Punta unit
Sample HM25071034D
Total gas age = 10.80 ±0.29 Ma
Plateau age = 10.13 ±0.15 Ma
f39 = 85.7%, MSWD = 0.80
Age in Ma
Fraction of 39Ar Released
C
Cerro Punta unit
Sample CP17100712A
Total gas age = 9.533 ±0.059 Ma
Plateau age = 9.377 ±0.041 Ma
f39 = 82.8%, MSWD = 1.44
Age in Ma
Fraction of 39Ar Released
D
Respingo unit
Sample CR11100748
Total gas age = 19.04 ±0.30 Ma
Plateau age = 11.24 ±0.36 Ma
f39 = 60.5%, MSWD = 2.20
Age in Ma
Fraction of 39Ar Released

Figure 4.3

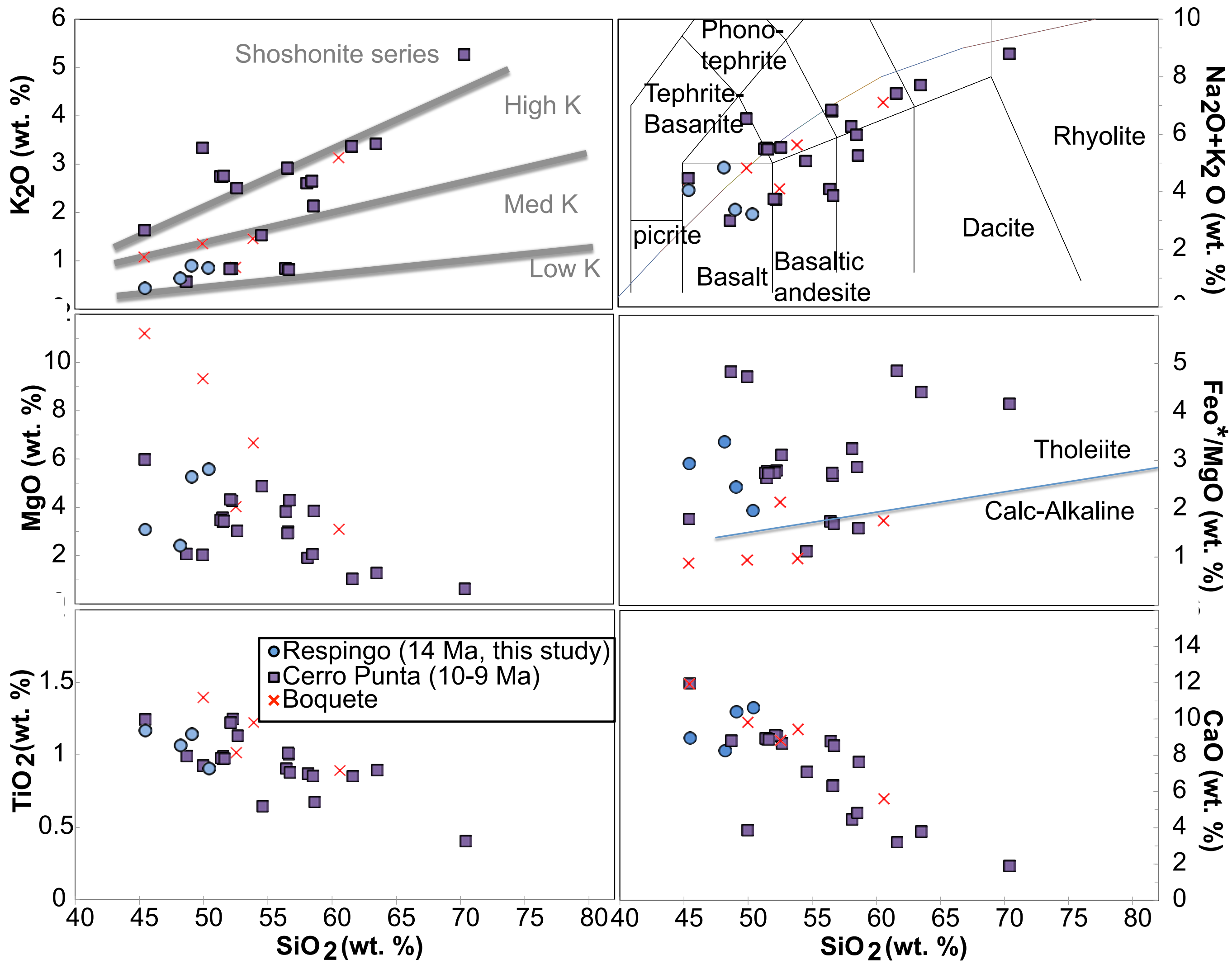

Shoshonite series
High K
Med K
Low K
K2O (wt. %)
Phono-tephrite
Tephrite-Basanite
picrite
Basalt
Basaltic andesite
Dacite
Rhyolite
Na2O+K2O (wt. %)
MgO (wt. %)
Tholeiite
Calc-Alkaline
Feo*/MgO (wt. %)
TiO2(wt. %)
Respingo (14 Ma, this study)
Cerro Punta (10-9 Ma)
Boquete
CaO (wt. %)
SiO2 (wt. %)
SiO2 (wt. %)

Figure 4.4

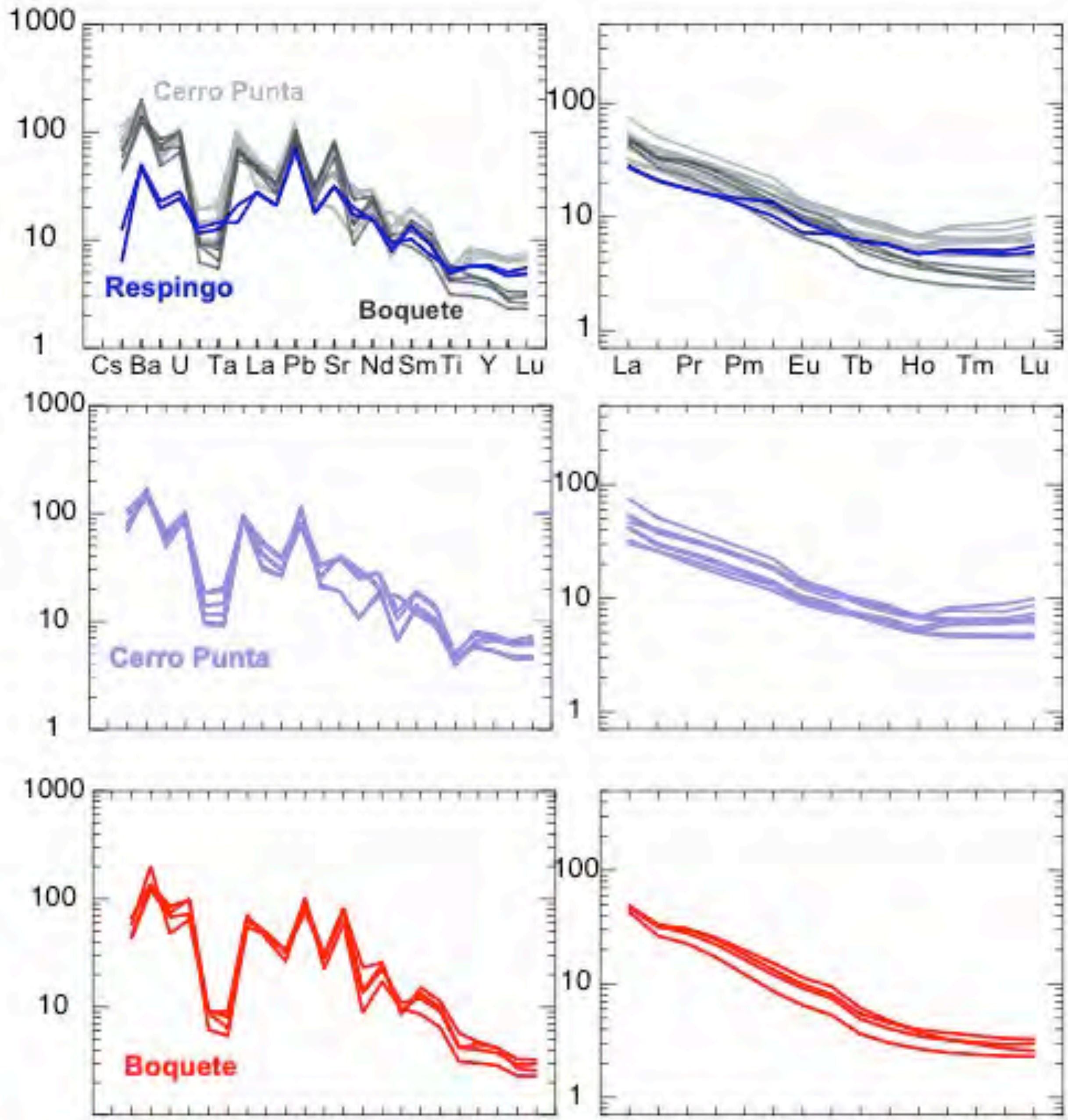

1000
100
10
1
Cerro Punta
Respingo
Boquete
Cs Ba U Ta La Pb Sr Nd Sm Ti Y Lu
100
10
1
La Pr Pm Eu Tb Ho Tm Lu
1000
100
10
1
Cerro Punta
100
10
1
1000
100
10
Boquete
100
10
1

Figure 4.5

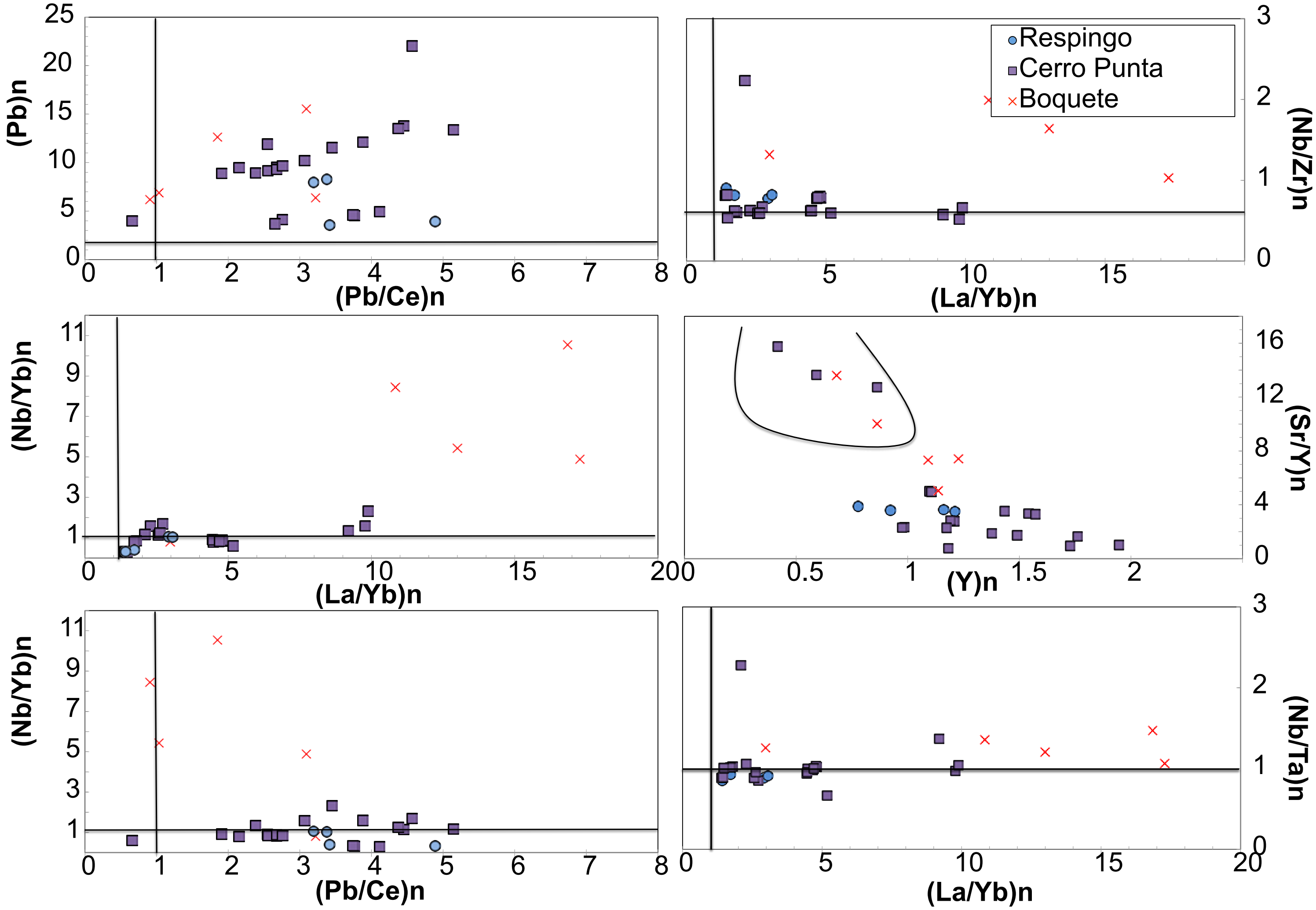
Respingo
Cerro Punta
Boquete
(Pb)n
(Pb/Ce)n
(Nb/Zr)n
(La/Yb)n
(Nb/Yb)n
(La/Yb)n
(Sr/Y)n
(Y)n
(Nb/Yb)n
(Pb/Ce)n
(Nb/Ta)n
(La/Yb)n

Figure 4.6

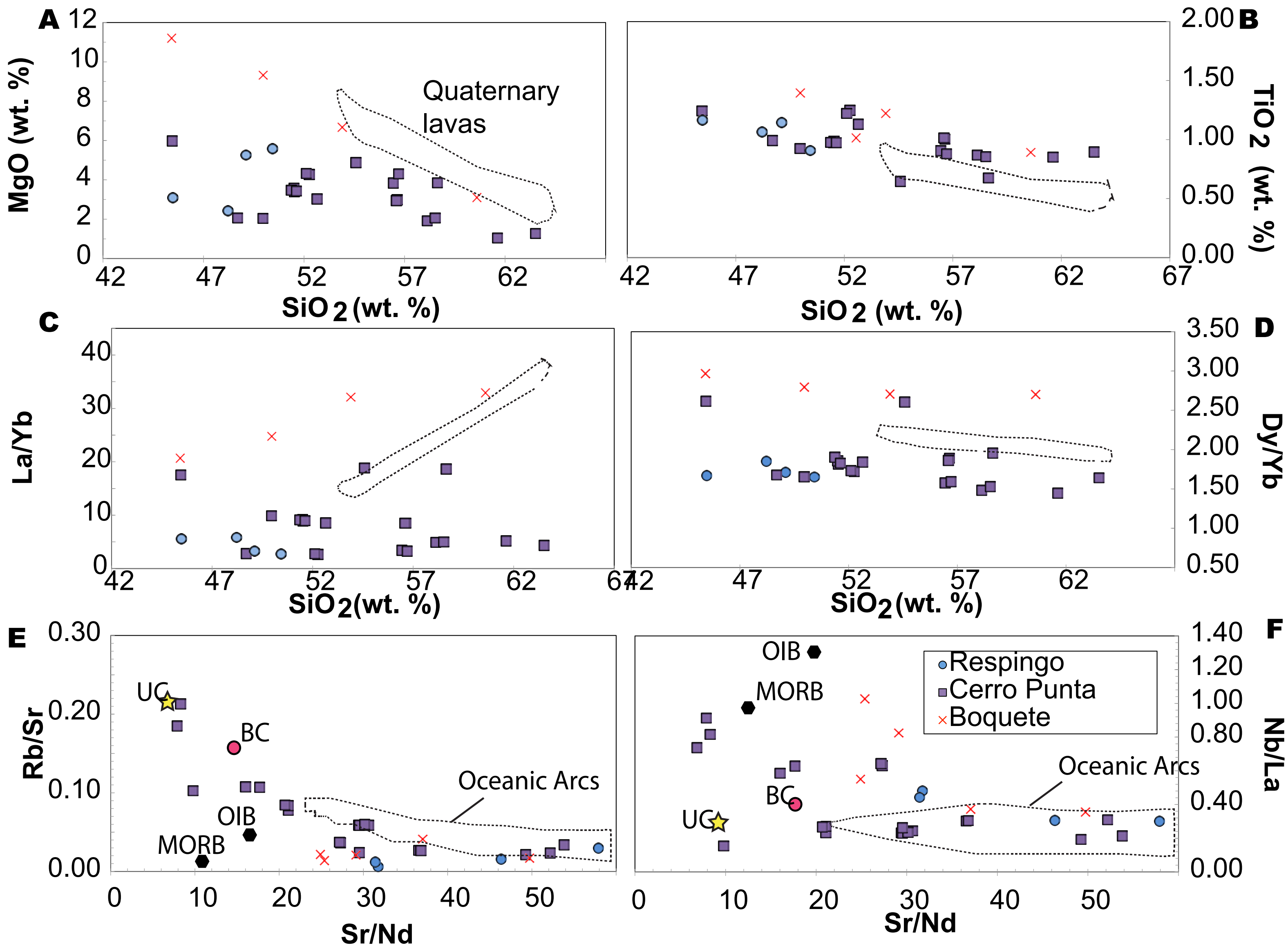
A
B
C
D
E
F
MgO (wt. %)
TiO2 (wt. %)
La/Yb
Dy/Yb
Rb/Sr
Nb/La
SiO2 (wt. %)
Sr/Nd
Quaternary lavas
Oceanic Arcs
UC
BC
OIB
MORB
Respingo
Cerro Punta
Boquete

Figure 4.7

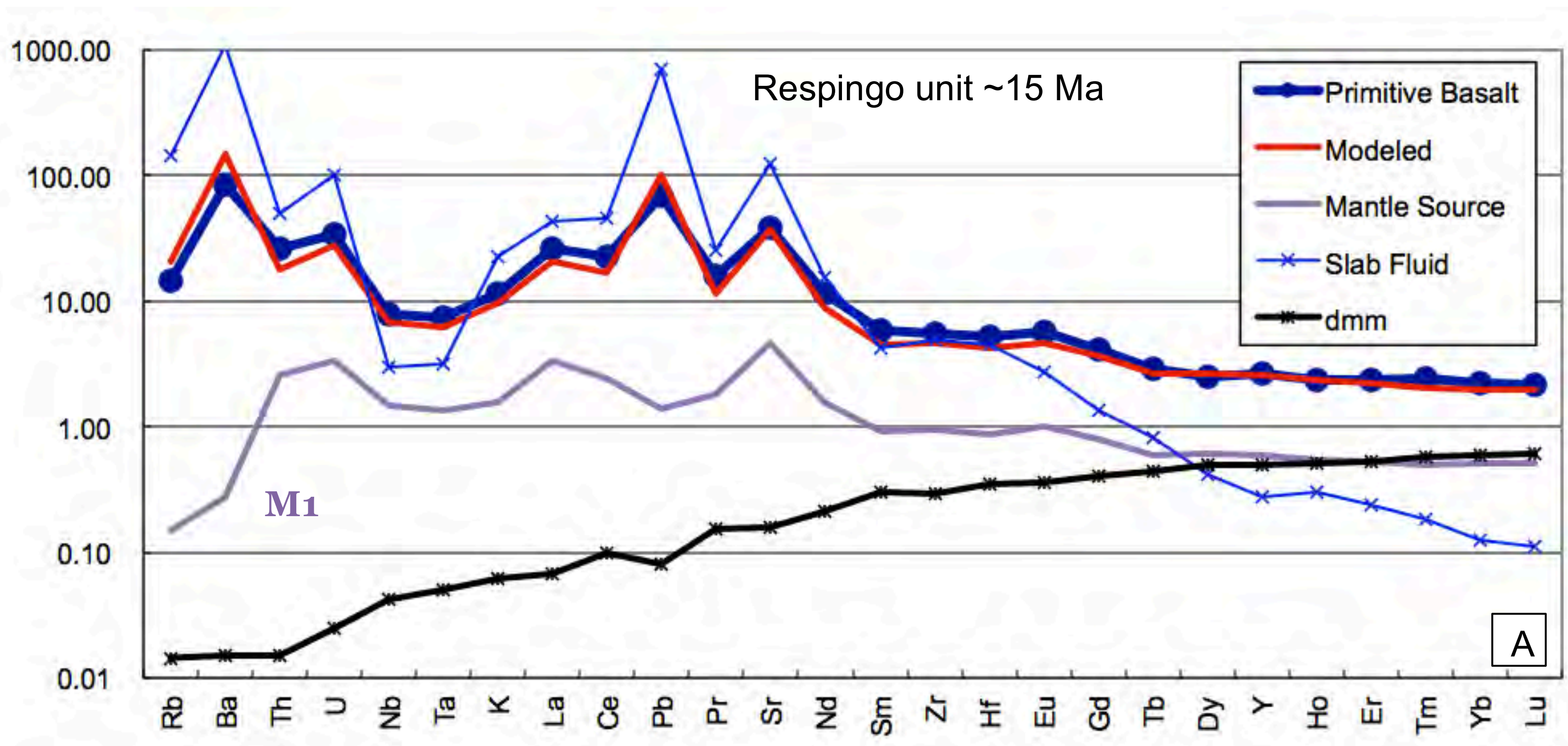

Respingo unit ~15 Ma
Primitive Basalt
Modeled
Mantle Source
Slab Fluid
dmm
M1
A
1000.00
100.00
10.00
1.00
0.10
0.01
Rb Ba Th U Nb Ta K La Ce Pb Pr Sr Nd Sm Zr Hf Eu Gd Tb Dy Y Ho Er Tm Yb Lu

Cont. Figure 4.7

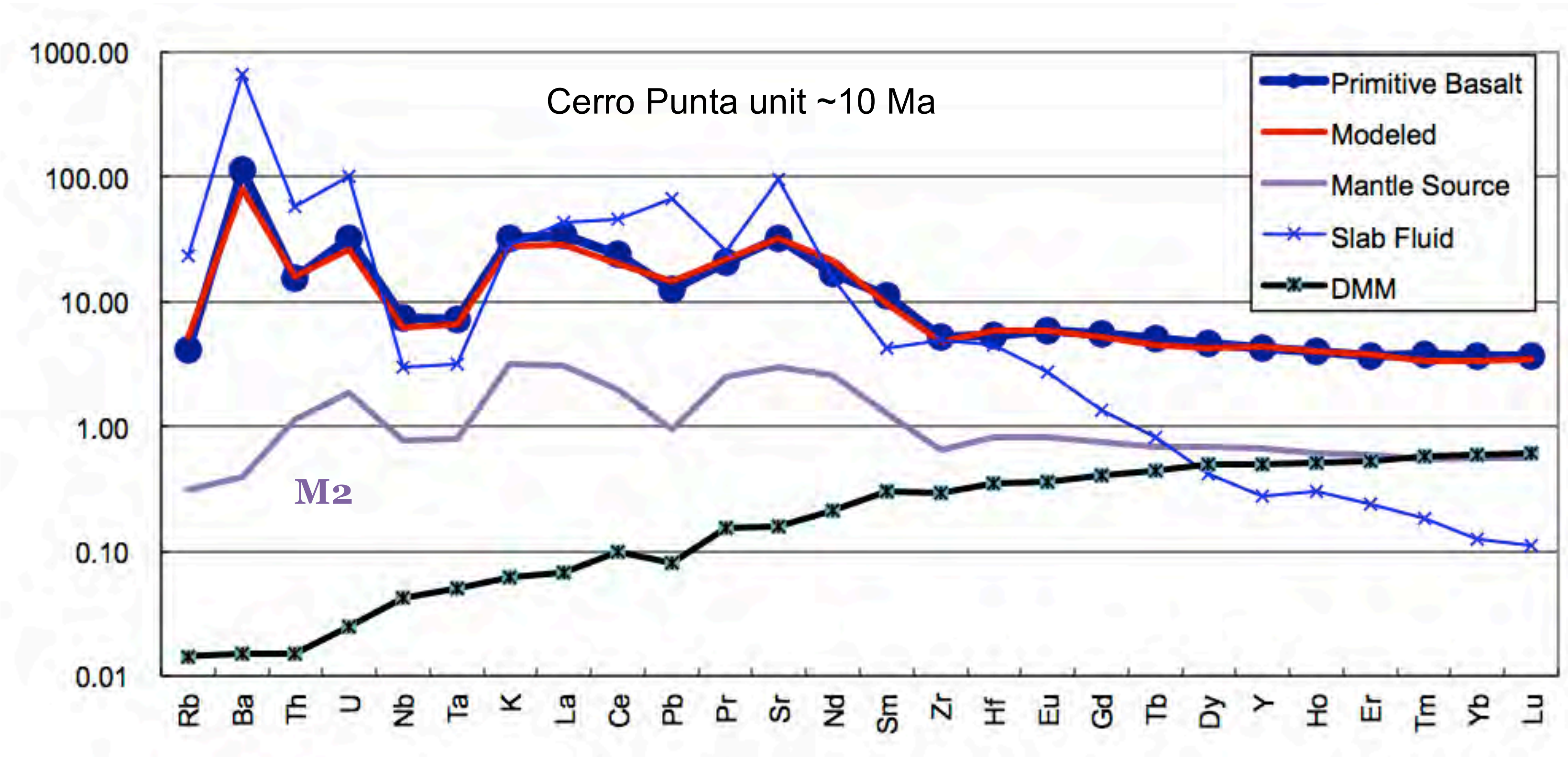

Cont. Figure 4.7

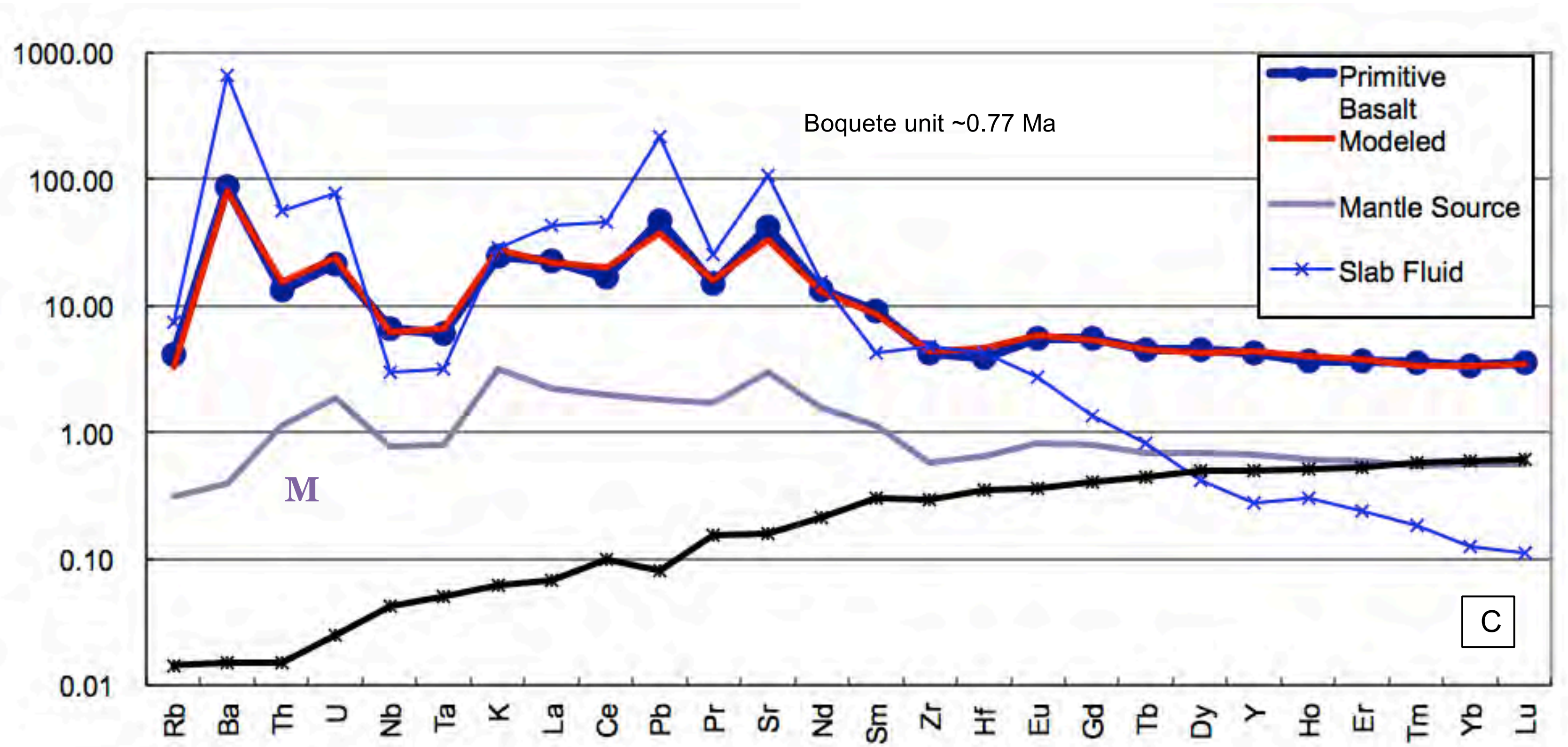

Cont. Figure 4.7

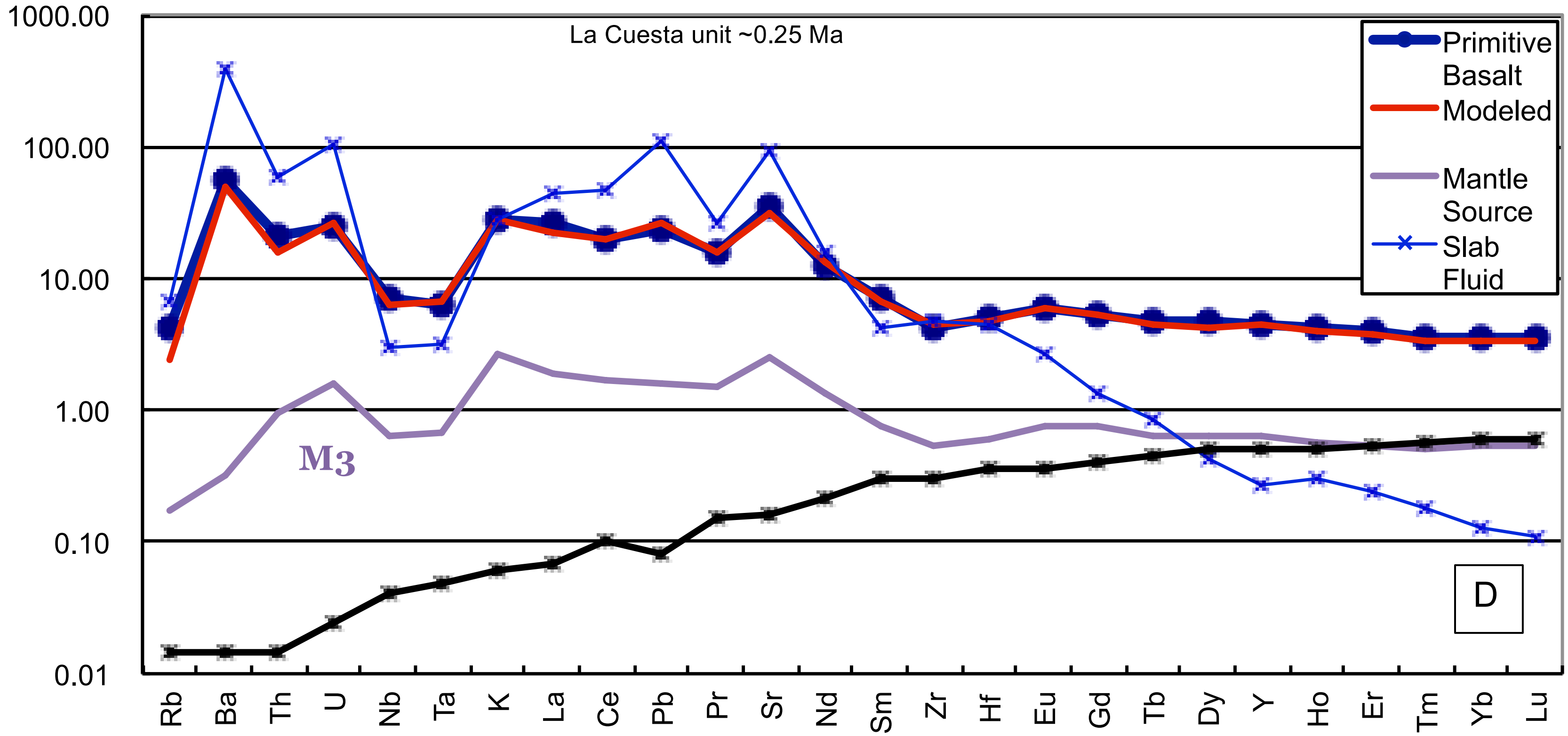

Figure 4.8

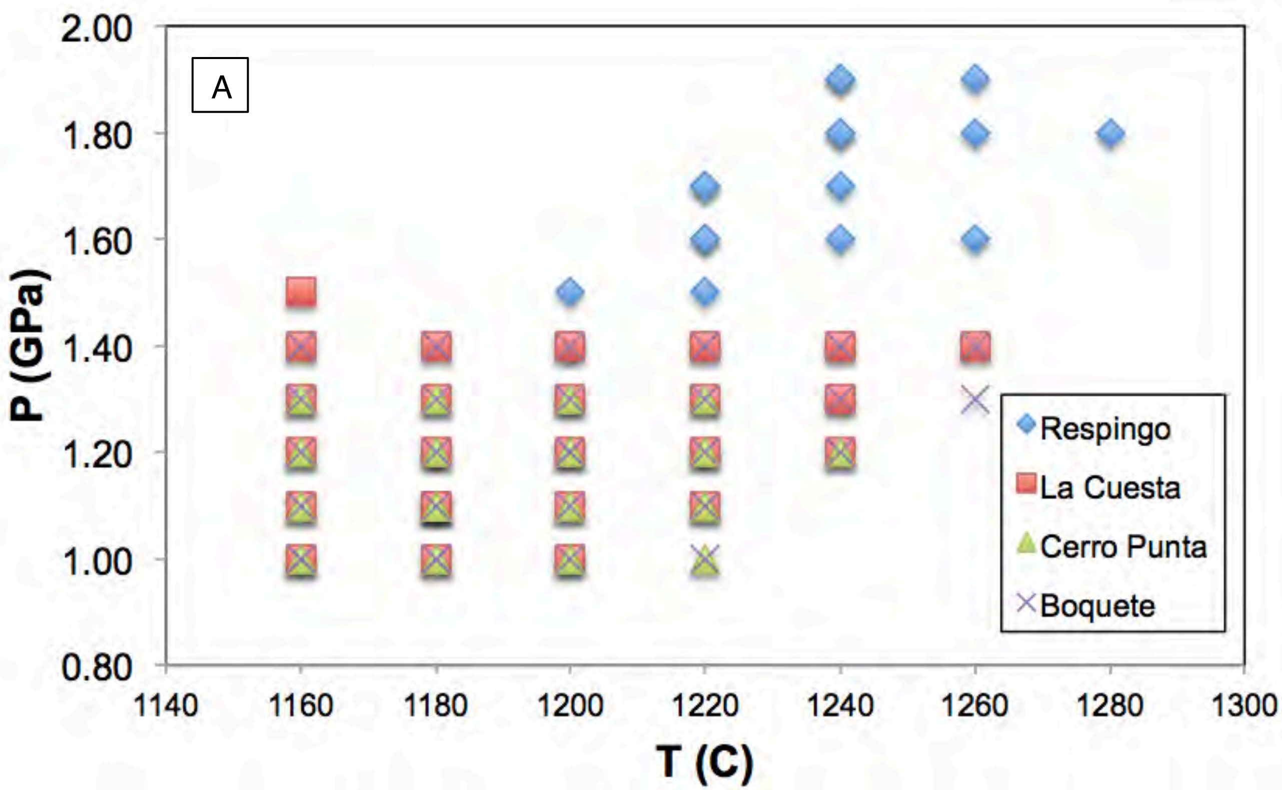
A
2.00
1.80
1.60
1.40
1.20
1.00
0.80
P (GPa)
1140
1160
1180
1200
1220
1240
1260
1280
1300
T (C)
Respingo
La Cuesta
Cerro Punta
Boquete

Cont. Figure 4.8

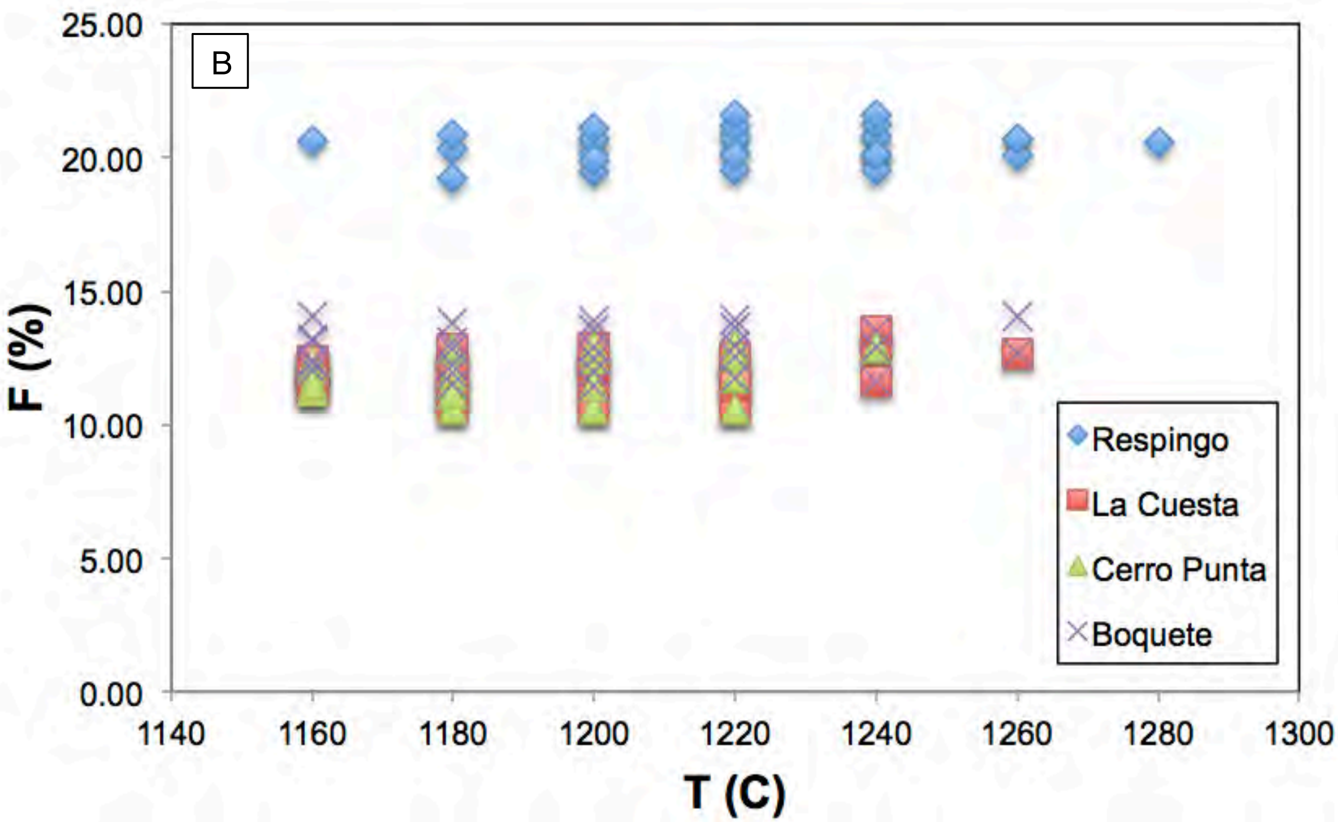

Cont. Figure 4.8

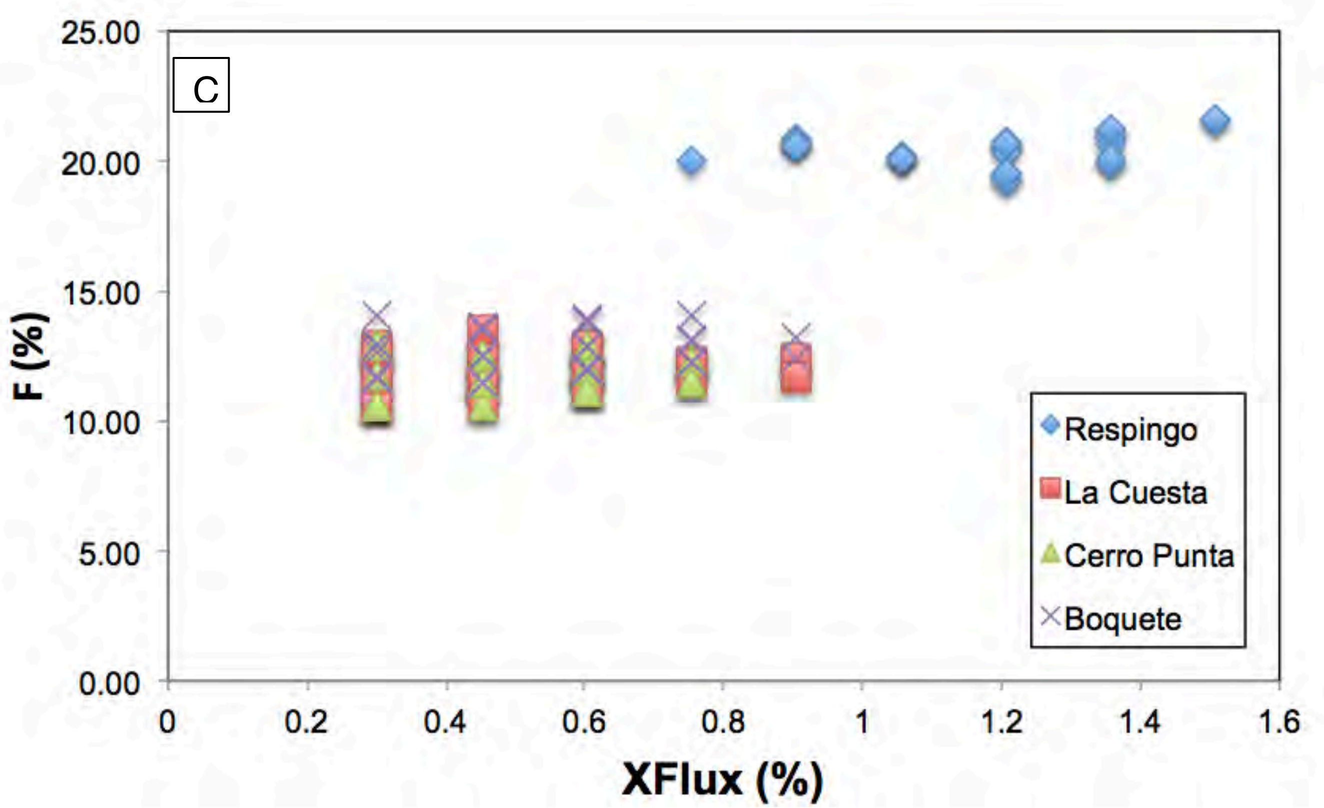

Cont. Figure 4.8

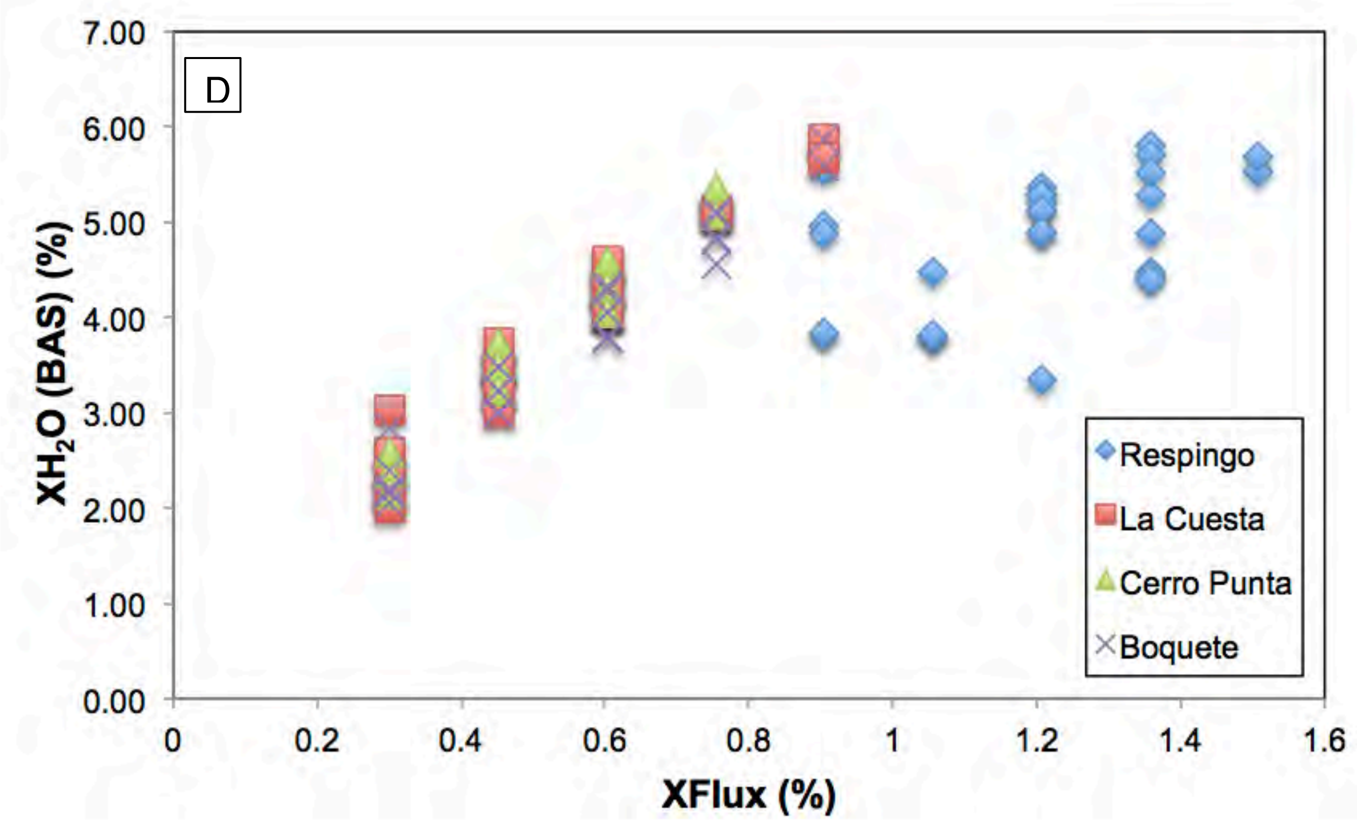

6.2 APPENDIX THREE: TABLES

Table 4.1: Summary of dates calculated in this study.

Sample	Irradiation	Packet	Run	TGA	+/-
CR11100748	mc29	L9	a	22.029	0.377
			b	19.043	0.304
		Avg.		20.220	1.459
CP17100712A	mc29	L10	a	9.533	0.059
			b	9.768	0.066
		Avg.		9.637	0.117
RP1610076B	mc29	T19	a	14.907	0.187
			b	15.734	0.256
		Avg.		15.195	0.394
HM25-07-10 34D	mc27	T12	a	10.797	0.288
			b	10.613	0.386
		Avg.		10.731	0.231

Table 4.1 cont.

MSWD	EWP	+/-	Fracs	f39%	MSWD
	10.979	0.371	6-10	59.0	1.45
	11.244	0.362	6-10	60.5	2.20
38.01	11.115	0.259			0.26
	9.360	0.038	8-12	65.0	1.12
	9.149	0.085	6-10	52.4	2.19
7.05	9.325	0.079			0.51
	NA				
	9.490	0.370	6-12	74.8	0.80
6.80					
	10.131	0.150	7-13	85.7	0.80
	10.555	0.205	7-12	79.5	0.86
0.15	10.279	0.202			2.79

Table 4.1 cont.

Combined Isochron						Preferred Age
n	MSWD	40Ar/36Ar	+/-	Age	+/-	
26	25.52	390.3	14.1	7.467	1.495	11.115
26	7.80	307.1	3.1	9.134	0.100	9.134
26	8.34	328.8	7.9	12.462	0.527	9.490
26	3.46	296.6	0.9	10.216	0.244	10.279

Table 4.2: Major and trace element composition of lava samples. Major elements are giving in weight %, while trace elements are given in ppm.

Sample	BO-06-21-07	BO-06-34-07	BO-06-39-07
unit	Boquete	Boquete	Boquete
	XRF Analyses (wt.%)		
SiO_2	52.54	60.60	45.42
TiO_2	1.01	0.89	2.45
Al_2O_3	19.45	16.05	12.82
Fe_2O_3T	9.57	6.04	10.90
MnO	0.15	0.09	0.16
MgO	4.03	3.10	11.20
CaO	8.82	5.60	11.95
Na_2O	3.25	3.97	3.05
K_2O	0.86	3.14	1.08
P2O5	0.33	0.51	0.97
	Laser ablation ICP-MS analyses (ppm)		
Ni	13	37	264
Zn	78	82	127
Rb	15.03	59.15	19.9
Zr	37	152	235
Sr	889	1439	1412
Ba	607	1223	829
La	15.57	47.76	51.84
Ce	29.67	75.48	102.47
Pr	4.17	10.49	14.20
Nd	17.88	38.85	55.67
Sm	4.09	6.30	10.14
Eu	1.40	1.74	2.89
Gd	4.21	4.93	8.60
Tb	0.64	0.56	1.04
Y	25.00	15.00	27.00
Dy	3.81	2.81	5.34
Ho	0.78	0.50	0.95
Er	2.22	1.18	2.23
Yb	1.97	1.04	1.80
Lu	0.29	0.15	0.25
Nb	5.55	17.81	53.22
Hf	0.93	3.80	5.25

Table 4.2 cont.

Ta	0.25	0.95	2.22
Pb	3.82	9.33	3.72
Th	1.15	8.03	6.72
U	0.32	2.59	1.94

Sample	BO-06-64-07	BO-06-40-07	PAN-06-147
unit	Boquete	Boquete	Cerro Punta
SiO_2	49.97	53.90	63.51
TiO_2	1.39	1.22	0.90
Al_2O_3	14.09	14.98	16.09
Fe2O3T	9.74	7.20	6.28
MgO	9.32	6.67	1.28
CaO	9.81	9.44	3.79
Na_2O	3.47	4.18	4.29
K_2O	1.35	1.46	3.43
P2O5	0.69	0.84	0.26
Ni	229	108	4
Zn	98	85	86
Rb	27.05	28.03	47.34
Zr	156	167	328
Sr	1238	1341	256
Ba	747	1152	1241
La	52.86	60.90	25.54
Ce	99.90	102.40	49.90
Pr	13.26	12.65	7.78
Nd	49.72	46.06	32.47
Sm	8.28	7.52	7.31
Eu	2.32	2.10	1.75
Gd	7.07	6.35	7.18
Tb	0.83	0.73	1.14
Y	24.00	19.00	38.00
Dy	4.28	3.68	6.91
Ho	0.78	0.66	1.45
Er	1.89	1.59	4.36
Yb	1.53	1.36	4.21
Lu	0.22	0.20	0.65

Table 4.2 cont.

Nb	29.10	50.20	23.32
Hf	3.68	3.77	7.43
Ta	1.37	1.93	1.25
Pb	4.13	7.58	6.12
Th	6.47	9.20	4.81
U	1.98	2.42	1.80

Sample	PAN-06-019	PAN-06-022	PAN-06-157
unit	Cerro Punta	Cerro Punta	Cerro Punta
SiO_2	58.64	45.44	70.40
TiO_2	0.68	1.24	0.40
Al2O3	16.79	18.29	14.77
Fe2O3T	6.84	11.90	2.95
MnO	0.12	0.20	0.07
MgO	3.85	5.98	0.64
CaO	7.64	11.97	1.89
Na_2O	3.12	2.84	3.53
K_2O	2.14	1.64	5.27
P2O5	0.19	0.51	0.08
Ni	22	20	3
Zn	64	108	39
Rb	42.47	36.25	101
Zr	108	96	65
Sr	1249	1703	142
Ba	952	1399	1775
La	29.63	32.52	22.40
Ce	46.90	56.42	39.00
Pr	6.26	8.40	5.57
Nd	23.21	34.58	20.80
Sm	3.81	6.72	4.43
Eu	1.09	1.91	0.68
Gd	3.17	5.63	4.71
Tb	0.39	0.66	0.74
Y	13.00	19.00	26.00
Dy	2.23	3.48	4.86
Ho	0.44	0.62	1.06

Table 4.2 cont.

Er	1.19	1.56	3.50
Yb	1.14	1.33	4.03
Lu	0.17	0.19	0.61
Nb	6.35	6.28	16.50
Hf	2.88	2.32	2.13
Ta	0.37	0.26	0.41
Pb	7.28	5.37	8.03
Th	6.34	4.06	13.70
U	2.09	1.36	3.27

Sample	HM-25-10-07-34B	TL-1710-07-741	TL-10-17-10-07-Ty1A
unit	Cerro Punta	Cerro Punta	Cerro Punta
SiO_2	51.53	56.44	56.71
TiO_2	0.99	0.91	0.88
Al2O3	18.28	18.19	17.29
Fe2O3T	10.52	7.43	8.10
MnO	0.20	0.14	0.15
MgO	3.40	3.84	4.31
CaO	8.89	8.78	8.53
Na_2O	2.77	3.26	3.05
K_2O	2.75	0.84	0.82
P2O5	0.66	0.17	0.16
Ni	0	3	3
Zn	84	61	61
Rb	50.00	13.00	13.00
Zr	77	93	89
Sr	849	357	349
Ba	1024	344	341
La	29.17	10.05	9.75
Ce	53.53	22.39	20.92
Pr	7.06	3.03	2.91
Nd	28.86	13.08	12.85
Sm	6.25	3.22	3.26
Eu	1.75	1.08	1.03
Gd	5.40	3.19	3.20
Tb	0.75	0.55	0.54
Y	24.33	21.66	21.46

Table 4.2 cont.

Dy	4.27	3.33	3.41
Ho	0.84	0.68	0.71
Er	2.31	1.98	2.01
Yb	2.35	2.11	2.14
Lu	0.35	0.31	0.30
Nb	6.77	6.33	6.27
Hf	2.60	2.04	2.09
Ta	0.39	0.35	0.35
Pb	5.73	2.47	2.22
Th	5.00	0.85	0.86
U	1.82	0.40	0.37

Sample	IM-25-10-07-33	GU26-1007-37A	GU26-1007-37B
unit	Cerro Punta	Cerro Punta	Cerro Punta
SiO_2	52.65	52.26	52.11
TiO_2	1.13	1.25	1.22
Al2O3	17.71	15.67	15.75
Fe2O3T	10.49	13.25	13.23
MnO	0.19	0.26	0.25
MgO	3.03	4.27	4.33
CaO	8.66	9.05	9.11
Na_2O	3.04	2.89	2.91
K_2O	2.51	0.84	0.84
P2O5	0.60	0.24	0.24
Ni	0	0	0
Zn	88	102	101
Rb	61.00	14.00	14.00
Zr	116	32	32
Sr	785	520	523
Ba	1057	660	657
La	35.51	9.80	9.81
Ce	66.23	18.08	18.44
Pr	8.88	2.92	2.92
Nd	37.26	14.22	14.21
Sm	8.03	3.99	4.08
Eu	2.16	1.35	1.37
Gd	6.76	3.94	3.99

Table 4.2 cont.

Tb	0.95	0.71	0.70
Y	31.54	26.59	26.22
Dy	5.49	4.54	4.42
Ho	1.09	0.95	0.93
Er	3.02	2.61	2.60
Yb	2.98	2.64	2.55
Lu	0.45	0.39	0.38
Nb	8.28	2.96	2.99
Hf	3.53	1.60	1.63
Ta	0.47	0.19	0.19
Pb	5.70	2.72	2.76
Th	5.49	0.99	1.03
U	1.89	0.34	0.35

Sample	Pb-25-10-07-35A	Pb-25-10-07-35B	HM-25-10-07-34A
unit	Cerro Punta	Cerro Punta	Cerro Punta
SiO_2	56.63	56.59	51.50
TiO_2	1.00	1.01	0.97
Al2O3	16.56	16.59	18.24
Fe2O3T	8.92	8.96	10.47
MnO	0.21	0.21	0.20
MgO	2.99	2.94	3.57
CaO	6.34	6.31	8.91
Na2O	3.89	3.93	2.75
K_2O	2.91	2.92	2.74
P2O5	0.54	0.54	0.65
Ni	0	0	0
Zn	92	99	82
Rb	67.00	68.00	50.00
Zr	140	141	75
Sr	801	805	852
Ba	1121	1136	984
La	36.68	37.39	29.02
Ce	69.92	70.15	53.79
Pr	9.25	9.29	7.07
Nd	37.99	38.90	28.85
Sm	8.21	8.42	6.16
Eu	2.30	2.35	1.68

Table 4.2 cont.

Gd	6.88	7.14	5.10
Tb	1.01	1.03	0.75
Y	33.91	34.58	24.16
Dy	5.86	5.87	4.22
Ho	1.14	1.16	0.82
Er	3.16	3.16	2.23
Yb	3.10	3.15	2.27
Lu	0.46	0.47	0.34
Nb	9.92	9.96	6.66
Hf	3.99	4.11	2.57
Ta	0.60	0.59	0.37
Pb	5.34	7.15	5.50
Th	5.55	5.84	4.92
U	2.11	2.15	1.72

Sample	HM-25-10-07-34C	HM-25-10-07-34D	CP13100713A
unit	Cerro Punta	Cerro Punta	Cerro Punta
SiO_2	51.37	51.62	61.62
TiO_2	0.98	0.97	0.85
Al2O3	18.32	18.25	14.75
Fe2O3T	10.58	10.47	5.66
MnO	0.20	0.20	0.12
MgO	3.47	3.44	1.05
CaO	8.93	8.89	3.21
Na2O	2.75	2.72	4.05
K_2O	2.75	2.76	3.37
P2O5	0.65	0.66	0.24
Ni	0	0	9
Zn	82	82	60
Rb	50.00	51.00	65.00
Zr	76	75	341
Sr	850	852	305
Ba	999	1002	1332
La	28.34	28.50	31.78
Ce	52.13	52.47	72.32
Pr	6.86	6.91	9.39
Nd	27.75	28.27	36.78

Table 4.2 cont.

Sm	5.92	6.01	8.05
Eu	1.68	1.68	2.07
Gd	5.05	5.12	6.02
Tb	0.75	0.74	1.08
Y	24.15	24.33	42.80
Dy	4.25	4.17	6.37
Ho	0.81	0.82	1.12
Er	2.24	2.28	3.94
Yb	2.23	2.28	4.40
Lu	0.33	0.35	0.73
Nb	6.91	6.72	25.95
Hf	2.56	2.63	6.98
Ta	0.38	0.38	1.73
Pb	5.58	5.79	13.22
Th	4.98	4.92	5.34
U	1.80	1.76	3.10

Sample	CP1700712A	CR1100747	CR1100748
unit	Cerro Punta	Respingo	Respingo
SiO_2	58.12	49.96	48.69
TiO_2	0.87	0.93	0.99
Al2O3	14.88	15.72	14.98
Fe2O3T	6.89	10.71	11.11
MnO	0.14	0.14	0.17
MgO	1.91	2.04	2.07
CaO	4.47	3.87	8.82
Na2O	3.66	3.21	2.42
K_2O	2.61	3.34	0.57
P2O5	0.23	0.45	0.19
Ni	11	18	15
Zn	68	36	74
Rb	43.00	46.00	10.00
Zr	194	118	41
Sr	399	448	416
Ba	1166	2904	535
La	22.34	51.76	9.49
Ce	46.42	91.10	18.00
Pr	6.12	11.54	2.86

Table 4.2 cont.

Nd	24.92	45.76	14.09
Sm	5.76	9.87	3.85
Eu	1.58	2.45	1.36
Gd	4.82	6.64	3.85
Tb	0.80	1.06	0.59
Y	32.79	38.74	25.81
Dy	4.87	6.23	4.06
Ho	0.90	1.10	0.77
Er	3.02	3.75	2.45
Yb	3.28	3.76	2.42
Lu	0.54	0.64	0.39
Nb	13.09	7.98	2.49
Hf	4.34	3.59	1.53
Ta	0.84	0.68	0.14
Pb	8.27	2.40	2.96
Th	4.29	3.07	1.15
U	1.84	2.25	0.37

Sample	CP17100712B	CP26100738B	RP1610076B
unit	Respingo	Respingo	Respingo
SiO_2	58.52	54.58	45.47
TiO_2	0.86	0.65	1.17
Al2O3	14.85	15.80	17.54
Fe2O3T	6.58	6.10	10.06
MnO	0.14	0.10	0.18
MgO	2.07	4.88	3.08
CaO	4.83	7.08	8.96
Na2O	3.33	3.55	3.62
K_2O	2.65	1.53	0.44
P2O5	0.24	0.25	0.44
Ni	13	86	21
Zn	71	66	72
Rb	43.00	24.00	4.00
Zr	192	93	105
Sr	402	1018	660
Ba	1211	875	349
La	20.70	22.61	19.21
Ce	46.35	50.25	37.37

Table 4.2 cont.

Pr	5.69	5.41	4.92
Nd	22.76	19.51	20.79
Sm	5.19	3.23	4.52
Eu	1.50	1.08	1.22
Gd	4.54	3.47	4.22
Tb	0.75	0.46	0.66
Y	30.29	9.17	26.66
Dy	4.56	2.24	4.14
Ho	0.84	0.42	0.77
Er	2.78	1.01	2.45
Yb	2.98	0.86	2.48
Lu	0.50	0.10	0.41
Nb	13.00	6.99	9.24
Hf	3.99	2.23	2.85
Ta	0.77	0.38	0.59
Pb	8.11	6.93	4.77
Th	4.10	3.72	1.93
U	1.93	1.66	0.59

Sample	RP1610076C	WP-18-3003	WP-17-3003
unit	Respingo	Respingo	Respingo
SiO2	48.22	49.11	50.43
TiO_2	1.06	1.14	0.91
Al2O3	17.35	16.01	16.62
Fe2O3T	9.12	14.30	12.21
MnO	0.14	0.22	0.26
MgO	2.43	5.26	5.58
CaO	8.25	10.41	10.64
Na2O	4.21	2.48	2.37
K_2O	0.63	0.90	0.86
P2O5	0.37	0.16	0.11
Ni	19	0	0
Zn	62	89	80
Rb	8.00	8.00	14.00
Zr	88	30	19
Sr	658	515	469
Ba	322	652	561
La	18.56	9.11	6.48

Table 4.2 cont.

Ce	36.86	15.66	12.01
Pr	4.87	2.36	1.70
Nd	20.94	11.11	8.10
Sm	5.96	3.06	3.04
Eu	1.52	1.06	0.85
Gd	4.28	3.03	2.33
Tb	0.67	0.54	0.43
Y	25.55	20.30	17.12
Dy	4.22	3.41	2.84
Ho	0.77	0.70	0.58
Er	2.38	1.94	1.74
Yb	2.28	1.99	1.72
Lu	0.36	0.30	0.26
Nb	8.21	2.78	1.95
Hf	2.44	1.43	1.01
Ta	0.51	0.17	0.13
Pb	4.98	2.14	2.35
Th	1.66	1.62	1.01
U	0.51	0.44	0.37

Table 4.3: Average incompatible element abundance for the calculated primitive basalts.

	Primitive Basalts compositions				
Element (ppm)	**Oligocene**	**Respingo PB**	**Cerro Punta PB**	**Boquete PB**	**La Cuesta PB**
Rb	40.00	19.20	40.00	15.00	6.40
Ba	560.00	700.00	787.20	607.00	345.60
Th	4.80	2.98	3.94	1.15	1.71
U	1.60	1.33	1.38	0.32	0.64
Nb	5.04	5.59	5.33	5.55	4.22
Ta	0.20	0.30	0.30	0.25	0.22
K	11444	2890	18191	7141	6326
La	20.24	18.09	23.22	15.57	15.27
Ce	36.08	40.20	43.03	29.67	32.70
Pb	1.80	5.54	1.01	3.82	1.77
Pr	4.40	4.33	5.66	4.17	3.81
Sr	608.00	814.40	681.60	889.00	646.40
Nd	19.76	15.61	23.08	17.88	14.94
Sm	3.76	2.58	4.93	4.09	4.18
Zr	72.00	74.40	60.00	37.00	46.40
Hf	1.30	1.78	2.06	0.93	1.50
Eu	1.11	0.86	1.34	1.40	0.90
Gd	3.44	2.78	4.08	4.21	2.82
Tb	0.48	0.37	0.60	0.64	0.38
Dy	2.96	1.79	3.38	3.81	2.07
Y	16.00	8.20	19.33	26.00	9.22
Ho	0.58	0.30	0.66	0.95	0.38
Er	1.76	0.81	1.78	2.50	0.98
Tm	0.22	0.12	0.28	0.42	0.16
Yb	1.44	0.80	1.82	2.60	0.98
Lu	0.23	0.12	0.27	0.37	0.15

Table 4.3 cont.

Subducting Sediment [a]	Altered oceanic crust [b]	Galapagos component [c]	DM [d]	M1	M2	M3
1640.00	1.87	100.72	0.05	0.6	0.9	0.6
3941.00	33.9	1098.27	0.563	12.3	12.3	12.3
4.295	0.5	12.14	0.0079	1.6	0.5	0.5
4.461	0.1	6.042	0.0032	0.5	0.2	0.2
5.7	18	35.19	0.1485	6.1	2.3	2.3
0.35	1.13	1.84	0.0096	0.3	0.13	0.13
34503	3320	3040	2000	2343	3403	3403
25.3	9.7	88.77	0.192	11.3	7.3	5.3
3.2	31	167.33	0.55	15.3	9.3	9.3
50	0.88	4.745	0.018	0.35	0.18	0.35
3	4.36	23.09	0.107	1.43	1.5	1.02
2936	68	1330	7.664	250	125.3	120.3
9.982	18.9	59.23	0.581	4.8	6.4	3.8
2.151	4.97	5.2	0.239	0.8	0.9	0.6
104	140	151.09	5.082	17.5	10.2	9.3
1.5	3.47		0.157	0.41	0.35	0.27
1.097	1.66	1.307	0.096	0.29	0.2	0.2
2.343	5.38		0.358	0.778	0.63	0.66
1	0.9		0.07	0.1	0.1	0.1
2.7	5.35		0.505	0.65	0.65	0.65
21.177	30		3.2	3.99	3.99	3.99
1	1.1		0.115	0.13	0.13	0.13
1.9	2.97		0.348	0.36	0.36	0.36
0.4	0.42		0.055	0.05	0.05	0.05
1.5	2.55		0.365	0.33	0.33	0.33
0.25	0.37		0.058	0.05	0.05	0.05

Table 4.4: Initial intensive and extensive parameters used in ABS 3.

Initial Parameters	Respingo	Cerro Punta	Boquete	La Cuesta
Slab Sediment liquid fraction (FLiq(SED))	0.4	0.4	0.35	0.35
Slab depth parameter Slab P(Gpa)	1.5	3.0	3.0	3.0
Melting Pressure P (Gpa)	1.5	1.5	1.5	1.5
Melting Temperature T(C)	1260	1200	1180	1190
Slab liquid fraction added Fslb liq %	3	2.5	2	2

7. REFERENCES

7.REFERENCES

Abratis, M., 1998. Geochemical variations in magmatic rocks from southern Costa Rica as a consequence of Cocos Ridge subduction and uplift of the Cordillera de Talamanca, Mathematisch-Naturwissenschaftlichen Fakultäten. Georg-August-Universität zu Göttingen, Göttingen, p. 148.

Abratis, M., Worner, G., 2001. Ridge collision, slab-window formation, and the flux of Pacific asthenosphere into the Caribbean realm. Geology 29, 127-130.

Alonso-Perez, R., Muntener, O., Ulmer, P., 2009. Igneous garnet and amphibole fractionation in the roots of island arcs: experimental constraints on andesitic liquids. Contributions to Mineralogy and Petrology 157, 541-558.

Alvarado, G.E., Kussmaul, S., Chiesa, S., Guillot, P.Y., Appel, H., Wörner, G., Rundle, C., 1992. Cuadro cronoestrátigrafico de las rocas ígneas de Costa Rica basado en dataciones radiométricas K-Ar y U-Th. Journal of South American Earth Sciences 6, 151-168.

Atherton, M.P., Petford, N., 1993. Generation of sodium-rich magmas from newly underplated basaltic crust. . Nature 362, 144-146.

Bachmann, O. and G. W. Bergantz (2003). "Rejuvenation of the Fish Canyon magma body; a window into the evolution of large-volume silicic magma systems." Geology **31**(9): 789-792.

Camacho, E., Hutton, W., Pacheco, J.F., 2010. A New Look at Evidence for a Wadati-Benioff Zone and Active Convergence at the North Panama Deformed Belt. Bulletin of the Seismological Society of America 100, 343-348.

Carmichael, I.S.E., 2002. The andesite aqueduct: perspectives on the evolution of intermediate magmatism in west-central (105-99 degrees W) Mexico. Contributions to Mineralogy and Petrology 143, 641-663.

Carr, M.J., Feigenson, M.D., Patino, L.C., Walker, J.A., 2003. Volcanism and Geochemistry in Central America: Progress and Problems, in: Eiler, J.M. (Ed.), Inside the Subduction Factory. American Geophysical Union, Washington, pp. 153-174.

Carr, M., I. Saginor, Alvarado, G. E., Bolge, L. L. (2007) Element fluxes from the volcanic front of Nicaragua and Costa Rica. Geochemistry Geophysics Geosystems **8**, Q06001 DOI: doi:10.1029/2006GC001396

Castillo, P.R., 2006. An Overview of adakite petrogenesis. Chinese Science Bulletin 51, 257-376.

Castillo, P.R., Janney, P.E., Solidum, R.U., 1999. Petrology and geochemistry of Camiguin Island, southern Philippines: insights to the source of adakites and other lavas in a complex arc setting. Contributions to Mineralogy and Petrology 134, 33-51.

Clark, L.F., 1989. The Geology, Geochemistry, and Petrogenesis of El Valle volcano, Panama., Geological Sciences. University of South Florida, Tampa, Florida, p. 150.

Coates, A.G., Aubry, M.-P., Berggren, W.A., Collins, L.S., Kunk, M., 2003. Early Neogene history of the Central American arc from Bocas del Toro, western Panama. GSA Bulletin 115, 271-287.

Coates, A.G., Jackson, J.B.C., Collins, L.S., Cronin, T.M., Dowsett, H.J., Bybell, L.M., Jung, P., Obando, J.A., 1992. Closure of the Isthmus of Panama; the near-shore marine record of Costa Rica and western Panama, Geological Society of America Bulletin, pp. 814-828.

Collins, L.S., Coates, A.G., Berggren, W.A., Aubry, M.-P., Zhang, J., 1996. The late Miocene Panama isthmian strait. Geology 24, 687-690.

Davies, J., Stevenson, D., 1992. Physical model of source region of subduction zone volcanics. Journal of Geophysical Research-Solid Earth 97.

de Boer, J.Z., Defant, M.J., Stewart, R.H., Bellon, H., 1991. Evidence for active subduction below western Panama. Geology 19, 649-652.

de Boer, J.Z., Drummond, M.S., Bordelon, M.J., Defant, M.J., Bellon, H., Maury, R.C., 1995. Cenozoic magmatic phases of the Costa Rican island arc (Cordillera de Talamanca). Special Paper Geological Society of America, Boulder, CO.

Deering, C.D., Cole, J.W., Vogel, T.A., 2008. A Rhyolite Compositional Continuum Governed by Lower Crustal Source Conditions in the Taupo Volcanic Zone, New Zealand. Journal of Petrology 49, 2245-2276.

Defant, M., Kepezhinskas, P., Xu, J., Wang, Q., Zhang, Q., Xiao, L., 2002. Adakites: some variations on a theme. Acta Petrologica Sinica 18, 129-142.

Defant, M.J., 1990. Derivation of some modern arc magmas by melting of young subducted lithosphere. Nature 347, 662-665.

Defant, M.J., Clark, L.F., Stewart, R.H., Drummond, M.S., de Boer, J.Z., Maury, R.C., Bellon, H., Jackson, T.E., Restrepo, J.F., 1991a. Andesite and dacite genesis via contrasting processes: The geology and geochemistry of El Valle volcano, Panama. Contributions to Mineralogy and Petrology 106, 309-324.

Defant, M.J., Jackson, T.E., Drummond, M.S., Deboer, J.Z., Bellon, H., Feigenson, M.D., Maury, R.C., Stewart, R.H., 1992. The Geochemistry of Young Volcanism Throughout Western Panama and Southeastern Costa-Rica - an Overview. Journal of the Geological Society 149, 569-579.

Defant, M.J., Richerson, P.M., Deboer, J.Z., Stewart, R.H., Maury, R.C., Bellon, H., Drummond, M.S., Feigenson, M.D., Jackson, T.E., 1991b. Dacite Genesis Via Both Slab Melting and Differentiation - Petrogenesis of La-Yeguada Volcanic Complex, Panama. Journal of Petrology 32, 1101-1142.

DeMets, C., 2001. A New Estimate for Present-Day Cocos-Caribbean Plate Motion: Implications for Slip Along the Central American Volcanic Arc. Geophysical Research Letters 28, 4043-4046.

DePaolo, D.J., 1981. Trace element and isotopic effects of combined wallrock assimilation and fractional crystallization. Earth and Planetary Science Letters 53, 189-202.

Drummond, M.S., Bordelon, M., Deboer, J.Z., Defant, M.J., Bellon, H., Feigenson, M.D., 1995. Igneous Petrogenesis and Tectonic Setting of Plutonic and Volcanic-Rocks of the Cordillera De Talamanca, Costa-Rica Panama, Central-American Arc. American Journal of Science 295, 875-919.

Drummond, M.S., Defant, M.J., 1989. A model for trondhemite- tonalite-dacite genesis and crustal growth via slab melting: Archean to modern comparisons Journal of Geophysical Research 95, 21503-21521.

Drummond, M.S., Defant, M.J., 1990. A model for trondhjemite-tonalite-dacite genesis and crustal growth via slab melting; Archean to modern comparisons Journal of Geophysical Research 95, 21503-21521.

Duque-Caro, H., 1990. The Choco Block in the northwestern corner of South America: structural, tectonostratigraphic, and paleogeographic implications. Journal of South American Earth Sciences 3, 71-84.

Dzierma, Y., Thorwart, M.M., Rabbel, W., Flueh, E.R., Alvarado, G.E., Mora, M.M., 2010. Imaging crustal structure in south central Costa Rica with receiver functions. Geochem. Geophys. Geosyst. 11, Q08S26.

Elkins-Tanton, L., Grove, T., Donnelly-Nolan, J., 2001. Hot, shallow mantle melting under the Cascades volcanic arc. Geology 29, 631-634.

Feigenson, M.D., Carr, M., Maharaj, S., Juliano, S., Bolge, L.L., 2004. Lead isotope composition of Central American volcanoes: Influence of the Galapagos plume, Geochemistry Geophysics Geosystems.

Fisher, D.M., Gardner, T.W., Sak, P.B., Sanchez, J.D., Murphy, K., Vannucchi, P., 2004. Active thrusting in the inner forearc of an erosive convergent margin, Pacific coast, Costa Rica. Tectonics 23, DOI: 10.1029/2002tc001464.

Forneris, J., Holloway, J., 2003. Phase equilibria in subducting basaltic crust: implications for H_2O release from the slab. Earth and Planetary Science Letters 214, 187-201.

Frey, H.M., Lange, R.A., Hall, C.M., Delgado-Granados, H., Carmichael, I.S.E., 2007. A Pliocene ignimbrite flare-up along the Tepic-Zacoalco rift: Evidence for the initial stages of rifting between the Jalisco block (Mexico) and North America. Bulletin of the Geological Society of America 119, 49.

Gazel, E., Carr, M., Hoernle, K., Feigenson, M., Szymanski, D., Hauff, F., van den Bogaard, P., 2009. Galapagos-OIB signature in southern Central America: Mantle refertilization by arc–hot spot interaction, Geochemistry Geophysics Geosystems, p. Q02S11.

Goff, J., Cochran, J., 1996. The Bauer scarp ridge jump: A complex tectonic sequence revealed in satellite altimetry. Earth and Planetary Science Letters 141, 21-33.

Grove, T.L., Parman, S.W., Bowring, S.A., Price, R.C., Baker, M.B., 2002. The role of an H_2O -rich fluid component in the generation of primitive basaltic andesites and andesites from the Mt. Shasta region, N California. Contributions to Mineralogy and Petrology 142, 375-396.

Hasegawa, A., Nakajima, J., 2004. Geophysical constraints on slab subduction and arc magmatism. Geophysical monograph 150, 81-93.

Hauff, F., Hoernle, K., Schmincke, H.U., Werner, R., 1997. A Mid Cretaceous origin for the Galapagos hotspot: Volcanological, petrological and geochemical evidence from Costa Rican oceanic crustal segments. Geologische Rundschau 86, 141-155.

Hauff, F., Hoernle, K., van den Bogaard, P., Alvarado, G., Garbe-Schönberg, D., 2000. Age and geochemistry of basaltic complexes in western Costa Rica: Contributions to the geotectonic evolution of Central America. Geochemistry, Geophysics, Geosystems 1, 1009.

Hidalgo, P.J., Rooney, T.O., 2010. Crystal fractionation processes at Baru volcano from the deep to shallow crust. Geochemistry Geophysics Geosystems 11, Q12S30.

Hidalgo, P.J., Rooney, T.O., Hall, C., in preparation. Petrogenesis a voluminous Quaternary adakitic volcano: The case of Baru volcano.

Hidalgo, P.J., Vogel, T.A., Rooney, T.O., Currier, R.M., Layer, P.W., 2011. Origin of silicic volcanism in the Panamanian arc: evidence for a two-stage fractionation process at El Valle volcano. Contributions to Mineralogy and Petrology, 1-24.

Hoernle, K., Abt, D.L., Fischer, K.M., Nichols, H., Hauff, F., Abers, G.A., van den Bogaard, P., Heydolph, K., Alvarado, G., Protti, M., Strauch, W., 2008. Arc-parallel flow in the mantle wedge beneath Costa Rica and Nicaragua. Nature 451, 1094-1097.

Hoernle, K., van den Bogaard, P., Werner, R., Lissina, B., Hauff, F., Alvarado, G.E., Garbe-Schoenberg, C.D., 2002. Missing history (16-71 Ma) of Galapagos hotspot; implications for the tectonic and biological evolution of the Americas. Geology 30, 795-798.

Jarrard, R.D., 1986. Terrane Motion by Strike-Slip Faulting of Fore-Arc Slivers. Geology 14, 780-783.

Johnston, S.T., Thorkelson, D.J., 1997. Cocos-Nazca slab window beneath Central America. Earth and Planetary Science Letters 146, 465-474.

Katz, R.F., Spiegelman, M., Langmuir, C.H., 2003. A new parameterization of hydrous mantle melting. Geochem. Geophys. Geosyst 4, 1073.

Kay, R.W., Kay, S.M., 2002. Andean adakites: Three ways to make them. Acta Petrologica Sinica 18, 303-311.

Kellogg, J., Vega, V., 1995. Tectonic development of Panama, Costa Rica, and the Colombian Andes: constraints from global positioning system geodetic studies and gravity, in: Mann, P. (Ed.), Geologic and Tectonic Deelopment of he Caribbean PLate Boundary in Southern Central America. Geological Society of America, Boulder, Colorado, pp. 75-75.

Kessel, R., Schmidt, M.W., Ulmer, P., Pettke, T., 2005. Trace element signature of subduction-zone fluids, melts and supercritical liquids at 120-180 km depth. Nature 437, 724-727.

Kimura, J.-I., Kent, A.J.R., Rowe, M.C., Katakuse, M., Nakano, F., Hacker, B.R., van Keken, P.E., Kawabata, H., Stern, R.J., 2010. Origin of cross-chain geochemical variation in Quaternary lavas from the northern Izu arc: Using a quantitative mass balance approach to identify mantle sources and mantle wedge processes. Geochem. Geophys. Geosyst. 11, Q10011.

Kolarsky, R.A., Mann, P., 1995. Structure and neotectonics of an oblique-subduction margin, southwestern Panama, in Geologic and Tectonic Development of the Caribbean Plate Boundary in Southern Central America. Geological Society of America Special Paper 295, 131-158.

Lee, C.T.A., Luffi, P., Plank, T., Dalton, H., Leeman, W.P., 2009. Constraints on the depths and temperatures of basaltic magma generation on Earth and other terrestrial planets using new thermobarometers for mafic magmas. Earth and Planetary Science Letters 279, 20-33.

Lissinna, B., Hoernle, K., Hauff, F., van den Bogaard, P., Sadofsky, S., 2006. The Panamanian island arc and Gal·pagos hotspot: A case study for the long-term evolution of arc/hotspot interaction. Geophysical Research Abstracts.

Lonsdale, P., 2005. Creation of the Cocos and Nazca plates by fission of the Farallon plate. Tectonophysics 404, 237-264.

Macpherson, C.G., 2008. Lithosphere erosion and crustal growth in subduction zones: Insights from initiation of the nascent East Philippine Arc. Geology 36, 311-314.

Macpherson, C.G., Dreher, S.T., Thirlwall, M.F., 2006. Adakites without slab melting: High pressure differentiation of island arc magma, Mindanao, the Philippines. Earth and Planetary Science Letters 243, 581-593.

Mann, P., Kolarsky, R.A., 1995. East Panama deformed belt: Age, structure, neotectonic significance, in: Mann, P. (Ed.), Geologic and Tectonic development of the Caribbean plate boundary in southern Central America. Geological Society of America Special Paper Geological Society of America, Boulder, pp. 111-129.

Maury, R., Defant, M., Bellon, H., De Boer, J., 1995. Early Tertiary arc volcanics from eastern Panama. SPECIAL PAPERS-GEOLOGICAL SOCIETY OF AMERICA, 29-29.

Morell, K.D., Fisher, D.M., Gardner, T.W., 2008. Inner forearc response to subduction of the Panama Fracture Zone, southern Central America. Earth and Planetary Science Letters 265, 82-95.

Patino, L.C., Carr, M.J., Feigenson, M.D., 2000. Local and regional variations in Central American arc lavas controlled by variations in subducted sediment input. Contributions to Mineralogy and Petrology 138, 265-283.

Pearce, J., Thirlwall, M., Ingram, G., Murton, B., Arculus, R., van der Laan, S., 1992. 13. Isotopic evidence for the origin of boninites and related rocks drilled in the Izu-Bonin (Ogasawara) forearc, Leg 125, pp. 237-261.

Pearce, J.A., Stern, R.J., Bloomer, S.H., Fryer, P., 2005. Geochemical mapping of the Mariana arc-basin system: Implications for the nature and distribution of subduction components. Geochemistry, Geophysics, Geosystems 6.

Rapp, R.P., Long, X., Shimizu, N., 2002. Experimental constraints on the origin of potassium-rich adakites in eastern China. Acta petrologica Sinica 18, 293-302.

Rickwood, P.C., 1989. Boundary lines within petrologic diagrams which use oxides of major and minor elements. Lithos 22, 247-263.

Rooney, T.O., Franceschi, P., Hall, C., 2011. Water Saturated Magmas in the Panama Canal Region – A Precursor to Adakite-Like Magma Generation? Contributions to Mineralogy and Petrology Volume 161, 373-388.

Rudnick, R.L., Gao, S., 2005. Composition of the Continental Crust, in: Rudnick, R.L. (Ed.), The Crust. Elsevier, Kidlington, UK, pp. 1-64.

Schmidt, M., Poli, S., 1998. Experimentally based water budgets for dehydrating slabs and consequences for arc magma generation. Earth and Planetary Science Letters 163, 361-379.

Sempere, T., Hérail, G., Oller, J., Bonhomme, M., 1990. Late Oligocene-early Miocene major tectonic crisis and related basins in Bolivia. Geology 18, 946-949.

Sigurdsson, H., Kelley, S., Leckie, R.M., Carey, S.N., Browing, J.M., Rogers, R.D., 2000. History of Circum-Caribbean explosive volcanism: Ar/Ar dating of tephra layers, in: Leckie, R.M., Sigurdsson, H., Acton, G.D., Draper, G. (Eds.), Proceeding of the Ocean Drilling Program, pp. 299-314.

Sisson, T., Bronto, S., 1998. Evidence for pressure-release melting beneathmagmatic arcsfrom basalt at Galunggung, Indonesia. Nature 391, 883.

Sun, S., McDonough, W.F., 1989. Chemical and isotopic systematics of oceanic basalts: implications for mantle compositions and processes., in: Saunders, A.D., Norry, M.J. (Eds.), Magmatism in the Ocean Basins. Geological Society Special Publications, pp. 313-345.

Syracuse, E.M., Abers, G.A., 2006. Global compilation of variations in slab depth beneath arc volcanoes and implications. Geochemistry, Geophysics, Geosystems 7.

Tatsumi, Y., 1989. Migration of fluid phases and genesis of basalt magmas in subduction zones. J. Geophys. Res 94, 4697-4707.

Tatsumi, Y., Eggins, S., 1995. Subduction zone magmatism. Blackwell Publishing.

Trenkamp, R., Kellogg, J.N., Freymueller, J.T., Mora, H.P., 2002. Wide plate margin deformation, southern Central America and northwestern South America, CASA GPS observations. Journal of South American Earth Sciences 15, 157-171.

Ulmer, P., 2001. Partial melting in the mantle wedge -- the role of H_2O in the genesis of mantle-derived arc-related' magmas. Physics of The Earth and Planetary Interiors 127, 215-232.

Vogel, T.A., Flood, T.P., Patino, L.C., Wilmont, M.S., Maximo, R.P.R., Arpa, C.B., Arcilla, C.A., Stimac, J.A., 2006. Geochemistry of silicic magmas in the Macolod Corridor, SW Luzon Philippines: evidence of distinct, mantle-derived, crustal sources for silicic magmas. Contributions to Mineralogy and Petrology 151, 267-281.

Wegner, W., Worner, G., Harmon, R.S., Jicha, B.R., 2011. Magmatic history and evolution of the Central American Land Bridge in Panama since Cretaceous times. Geological Society of America Bulletin 123, 703-724.

Wilson, D.S., 1996. Fastest known spreading on the Miocene Cocos-Pacific plate boundary. Geophysical Research Letters 23.

Workman, R., Hart, S., 2005. Major and trace element composition of the depleted MORB mantle (DMM). Earth and Planetary Science Letters 231, 53-72.

Xu, J.-F., Shinjo, R., Defant, M.J., Wang, Q., Rapp, R.P., 2002. Origin of Mesozoic adakitic intrusive rocks in the Ningzhen area of east China: Partial melting of delaminated lower continental crust? Geology 30, 1111-1114.

Yogodzinski, G.M., Kelemen, P.B., 1998. Slab melting in the Aleutians: implications of an ion probe study of clinopyroxene in primitive adakite and basalt. Earth and Planetary Science Letters 158, 53-65.

Zellmer, G.F., 2008. Some first-order observations on magma transfer from mantle wedge to upper crust at volcanic arcs. Geological Society, London, Special Publications 304, 15.